THE DE HAAS-VAN ALPHEN EFFECT IN ARSENIC

OBSERVATIONS OF THE

DE HAAS-VAN ALPHEN EFFECT

IN

ARSENIC

by

JOHN VANDERKOOY, B. ENG.

A Thesis

Submitted to the Faculty of Graduate Studies
in Partial Fulfilment of the Requirements

for the Degree

Doctor of Philosophy

McMaster University

May 1967

DOCTOR OF PHILOSOPHY (1967)   McMASTER UNIVERSITY
(Physics)   Hamilton, Ontario.

TITLE: Observations of the de Haas-van Alphen
                  effect in Arsenic

AUTHOR: John Vanderkooy, B. Eng. (McMaster University)

SUPERVISOR: Dr. W. R. Datars

NUMBER OF PAGES: x , 168

SCOPE AND CONTENTS:

Semimetallic arsenic has been studied by magneto-resistance methods and measurement of the de Haas-van Alphen effect using torque and magnetothermal measurements. Several modifications have been made in the conventional torque techniques. An important cause of nonlinear effects in the torque experiments is presented and compared to other mechanisms for nonlinearities. The Fermi surface of arsenic as determined experimentally is shown to be in good agreement with recent theoretical calculations which were partially guided by the experiments.

ABSTRACT

The de Haas-van Alphen effect of arsenic has been studied using a self-balancing torque magnetometer. Techniques were used employing detection of torque, first derivative of torque and torque with vector magnetic field modulation. An effect that showed hysteresis and a discontinuity in each de Haas-van Alphen oscillation was observed. The effect is explained in terms of the finite angular compliance of the magnetometer coupled with the periodicity of the torque vs reciprocal magnetic field and orientation. The de Haas-van Alphen periods are reported for the magnetic field in the trigonal-bisectrix, trigonal-binary and binary-bisectrix planes. Long periods are from necks of hyperboloidal shape tipped - $10^{\circ} \pm 1^{\circ}$ from the trigonal direction. Short periods are from carriers of two sets of pockets with tilt angles of minimum area from the trigonal direction of + $38^{\circ} \pm 1^{\circ}$ for the α carriers and $86^{\circ} \pm 1^{\circ}$ for the β carriers. The data support the topology of Lin and Falicov's model of the Fermi surface of arsenic. Magnetothermal experiments were done and oscillations were observed in accord with the torque measurements. Magnetoresistance experiments showed that arsenic is semimetallic and has an anomalous $H^{1.8}$ behaviour of the steady magnetoresistance. Short period Shubnikov-de Haas oscillations were observed with amplitudes in reasonable agreement with theory but long period oscillations were absent.

ACKNOWLEDGEMENTS

Mrs. Kennelly has skillfully typed this thesis and managed to insert most of the Greek symbols with her new machine. My wife has been patient and has kept me in suspended animation during the compilation of the thesis.

TABLE OF CONTENTS

LIST OF FIGURES

LIST OF TABLES

CHAPTER I

INTRODUCTION

The de Haas-van Alphen effect (hereafter called dHvA effect) is a low temperature phenomenon in metals that was discovered by W. J. de Haas and P. M. van Alphen[1] in bismuth single crystals. The effect is characterized by the oscillatory magnetic susceptibility which is periodic in reciprocal magnetic field. Landau had predicted an oscillatory field variation of susceptibility of conduction electrons in his paper[2] on diamagnetism in metals, but he concluded that field inhomogeneities would cause averaging of oscillations and prevent observation of the effect for electrons. He was unaware that field inhomogeneities could be vastly improved by proper magnet design and smaller sample size, and did not realize that carriers of very low effective mass could exist. Many metal single crystals have since exhibited the dHvA effect, and a good understanding of the effect has developed over the years. Peierls[3], Blackman[4] and Landau[5] have worked on the theory using free electron models with introduction of small effective masses to explain the bismuth results. As more materials were studied[6], it became obvious that effective masses in a free electron type of model would not properly interpret the observed dHvA oscillations. The proper interpretation was advanced by Onsager[7]

and Lifshitz[8], who realized that the area of an electron orbit in momentum space in a plane perpendicular to the magnetic field was quantized for an arbitrary Fermi surface, whereas the energy of the levels had no simple condition. As a result, the dHvA frequencies F in the variable 1/H were given by

$$F = \frac{cA}{eh} \qquad\qquad (I-1)$$

where A is the extremal area of the Fermi surface perpendicular to the magnetic field. The extremal areas emerge as the measured quantities since only at extrema does a band of electrons exist all of which have the same area, and these electrons act in consort to give an oscillatory magnetization with field because of the field dependent area between energy levels. Understanding of the effects of collisions on the oscillatory behaviour was given by Dingle[9] for the effective mass approximation. The major effect was shown to be a decrease in the amplitude of oscillations by the factor exp (- h/$\tau \beta$H), where β = e$\hbar$/m*c and τ is closely related to the collision time. In their very important paper Lifshitz and Kosevich[10] have calculated the dHvA effect for an arbitrary Fermi surface which has proved Onsager's relation (I-1) and showed that the temperature dependence would yield the cyclotron effective mass. Cohen and Blount[11] showed that the splitting of the electron energy levels due to spin would cause a factor cos (Π g m*/2m) to appear in the dHvA ampli-

tude, where g is the effective splitting factor and m* is the cyclotron mass. Under appropriate conditions this factor can reduce the amplitude of the dHvA effect to zero.

Recently several other important features of the dHvA effect have been brought out. Shoenberg[12] has measured large harmonic content for dHvA oscillations in the noble metals, and he conjectures that this was due to the magnetization of the sample itself. The formula for the magnetization should be written so that $\vec{H} + 4\pi\vec{M}$ is substituted for the magnetic field $\vec{H}$. As a result the oscillations are distorted from their more or less sinusoidal shape. Kittel[13] has justified theoretically the conjecture of Shoenberg, as well as Pippard[14], who goes into details of Shoenberg's pulsed field techniques and the role of eddy currents induced in the sample. Plummer and Gordon[15] have observed mixing of two oscillations which they attribute to the effects of magnetic interaction. The discovery of magnetic breakdown in magnesium by Priestley, Falicov and Cohen[16], and the explanation by the above authors and Blount[17] means that for small band gaps the representative point in k-space may "tunnel" its way to a different Fermi surface orbit. This destroys the Onsager relation (equation I-1) linking one specific extremal area to one dHvA frequency and a number of interesting consequences can result. As the magnetic field increases dHvA oscillations change character when the breakdown appears.

Williamson, Foner and Smith[18] have shown that Dingle's treatment of Landau level broadening could be extended by the method of Lifshitz and Kosevich to Fermi surfaces of arbitrary shape, for systems of non-interacting fermions. The effective mass entering the Dingle factor is now found to be $(1/2_\pi)$ $(\partial A/\partial E)$, the cyclotron effective mass. This fact has actually been realized before the formal derivation of the result.

Finally, several new methods have been introduced at various stages of dHvA effect studies to measure the effect. As well as torque experiments, Shoenberg used differential techniques employing pick-up coils and pulsed high field magnets[19]. Radio frequency techniques[20] have been used in which the second harmonic can be observed due to the non-linear variation of the magnetization as a function of field. Differential techniques using low-frequency modulation were first employed by Goldstein, Williamson and Foner[21]. Kunzler, Hsu and Boyle[22] have measured oscillatory changes in temperature as a function of field of an adiabatically isolated sample. As the field is varied the entropy of the system is constant and the sample changes temperature because the magnetic entropy is changing.

Almost any low temperature property of a metal will be affected by the dHvA effect. The ultrasonic attenuation[23] has oscillations which are practically identical to the dHvA

effect. Oscillations of the specific heat occur since the number of electrons at the Fermi surface changes with field. Electron transport properties such as electrical[24] and thermal conductivities will also undergo oscillations. These processes are fundamentally different than the dHvA effect, but the oscillations will have the same frequencies because the effects depend on the electron distributions in k-space.

Our own dHvA experiments[25] have pointed out that all compliant crystal mounts, especially torque magnetometer mounts, cause a nonlinearity in the dHvA effect which is virtually indistinguishable from the magnetic interaction proposed by Shoenberg. An analysis shows that it can dominate the other effects unless care is taken to mount the sample quite rigidly.

In summary, then, the dHvA effect is an aesthetically pleasing phenomenon due to quantum effects of the conduction electrons. The oscillations in susceptibility, torque or temperature enable us to determine extremal areas of the Fermi surface. A detailed study of temperature and magnetic field dependences of the oscillation amplitudes can yield important parameters such as the cyclotron effective mass, the carrier relaxation time, and the effective spin g-factor of the conduction electrons. Such data enable us to compare band structure calculations to experiment and hence predict much information about metals.

PURPOSE

This thesis contains a description and analysis
of experimental research on the dHvA effect of arsenic using
torque, differential modulation and magnetothermal experi-
ments to determine the Fermi surface. Some magnetoresistance
or Shubnikov-de Haas experiments are also described. Chap-
ter II contains a short survey and summary of the present
theory for the dHvA effect. This is followed by a chapter
on the crystal and band structure of arsenic. The torque
dHvA experiments and differential modulation experiments are
described and analyzed in Chapter IV. Magnetothermal and
magnetoresistance experiments are discussed in Chapter V.
The Fermi surface as determined experimentally is compared
to theory in Chapter VI, followed by a conclusion.

CHAPTER II

THEORY OF THE DE HAAS VAN-ALPHEN EFFECT

THEORY

A truly accurate determination of the properties of conduction electrons would require that they be treated as a system of interacting fermions under the mediation of an ionic lattice held together by forces that are almost harmonic. This approach has hitherto been impossible and it is necessary to make approximations from even the beginnings of almost any calculation. It is fortunate that in the case of the de Haas-van Alphen effect, the assumptions necessary to make the problem tractable also seem to be valid as far as present day observations go. The dynamics of conduction electrons are usually done in a semi-classical way, ignoring the interactions between electrons and approximating the interaction of the electrons with the lattice by the band structure. In this chapter a physical, simple account of the dHvA effect is given and guidelines are shown to the current theories of the effect.

When a magnetic field is applied along the z-axis to a metal, the momentum $\vec{p}$ in the Hamiltonian must be replaced by $\vec{p} + \frac{e}{c} \vec{A}$, where $\vec{A}$ is the vector potential. The vector potential for this situation is $\vec{A} = Hx\vec{j}$ in the Landau gauge. For free electrons and neglecting spin

$$\mathcal{H} = \frac{1}{2m} (\vec{p} + \frac{e}{c} \vec{A})^2 = \frac{1}{2m} [p_x^2 + p_z^2 + (p_y + m\omega_c x)^2]$$

7

where $\omega_c = \dfrac{eH}{mc}$ is the cyclotron frequency. If we define $x_o = -\dfrac{Py}{m\omega_c}$, $\mathcal{H}$ can be written as

$$\mathcal{H} = \frac{1}{2m}[p_x^2 + m^2\omega_c^2(x-x_o)^2] + \frac{\hbar^2 k_z^2}{2m}$$

which is recognized as the Hamiltonian of a harmonic oscillator centred at x_o, plus the energy term along the magnetic field direction. The eigenvalues are

$$E_n = (n + \tfrac{1}{2})\,\hbar\omega_c + \frac{\hbar^2 k_z^2}{2m} \qquad (II-1)$$

where $n = 0,1,2 \ldots$. Physically the field has split up the parabolic band structure into a series of oscillator levels which we can associate with the circular motion of the electron about the magnetic field direction. The one dimensional parabolic term remains because the magnetic field has no effect for velocity components along the field. These oscillator levels are called Landau levels, and each is highly degenerate. The degeneracy is estimated by box normalization of states and the requirement that the centre position of the oscillator x_o fall within the crystal. The degeneracy then becomes $\dfrac{eHV}{4\pi^2\hbar c}\,\Delta k_z$ per level for a slice Δk_z of $\vec{k}$-space perpendicular to the magnetic field, where V is the volume of the crystal. The average density of states is unaffected but the field pulls together many states into a single level. This is true because the magnetic field does not allow the electrons to act like plane waves but now circular orbits exist. We are not saying that more than one

fermion occupies the same state, even though it has a degener-
ate energy, because the centre of the orbit is different for
each electron. Each orbit can be interpreted as a quantization
of the flux which passes through it in units of hc/e. Physical-
ly, the magnetic field causes a Lorentz force on the electrons
which causes them to spiral about the field direction. Only
certain orbits are allowable since the wave functions must be
single-valued as a boundary condition. As a result, there are
tubes of levels which are allowable (Landau levels) and the
area in momentum space between levels perpendicular to the
field is linearly dependent on field. As the field is increas-
ed, levels that attain an energy greater than E_F, the Fermi
energy, are depopulated and distributed to lower levels, whose
degeneracy increases with field. Periodic changes in the en-
ergy will result whenever levels pass out of the Fermi surface
and contributions from different slices of momentum space will
only be additive if the area of the Fermi surface is stationary.
The oscillatory effects will then depend only on the extremal
area of the Fermi surface.

The upper portion of Figure II-1 shows the Landau levels
drawn for free electrons, and a free electron Fermi surface
appears as a sphere. All the levels, which form concentric cylin-
ders, are populated inside, but not outside the sphere. The
lower diagram shows the energy of the states as a function of
the momentum p_z along the magnetic field direction. It is easy
to visualize that the level n=5 has the largest change in the

FERMI SURFACE

P = O

n = 5
4
3
2
1

P_z

0
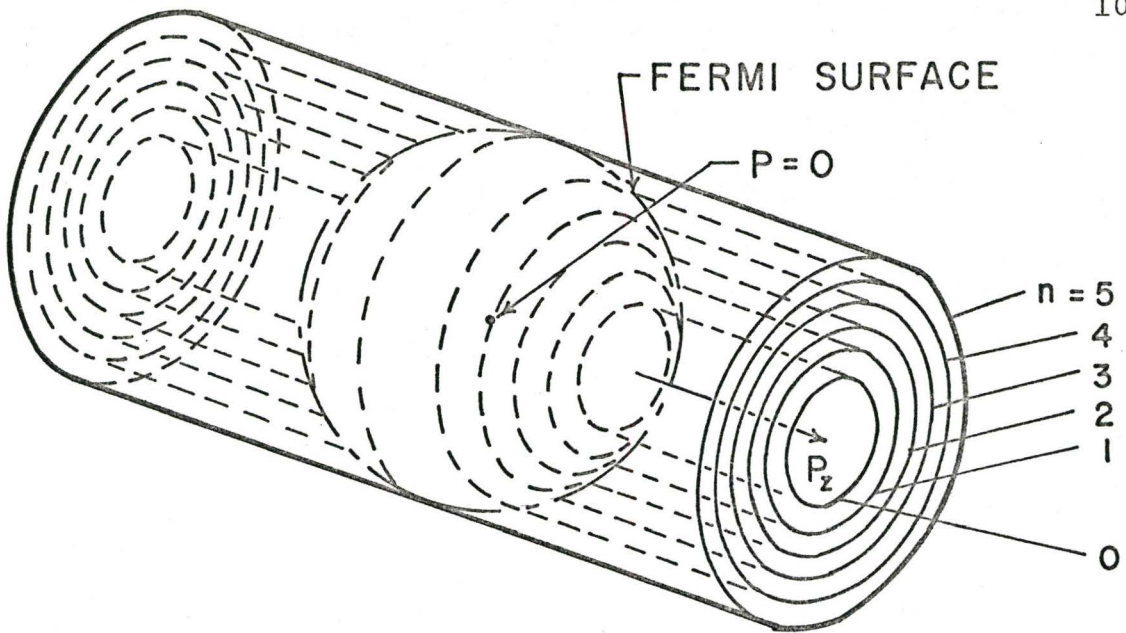
P — SPACE

FREE ELECTRON LANDAU LEVELS

E n = 5, 4, 3, 2, 1, 0

FERMI ENERGY

$\hbar \omega_c$

$\hbar \omega_c / 2$

P_z

ENERGY LEVEL DIAGRAM
FOR FREE ELECTRONS
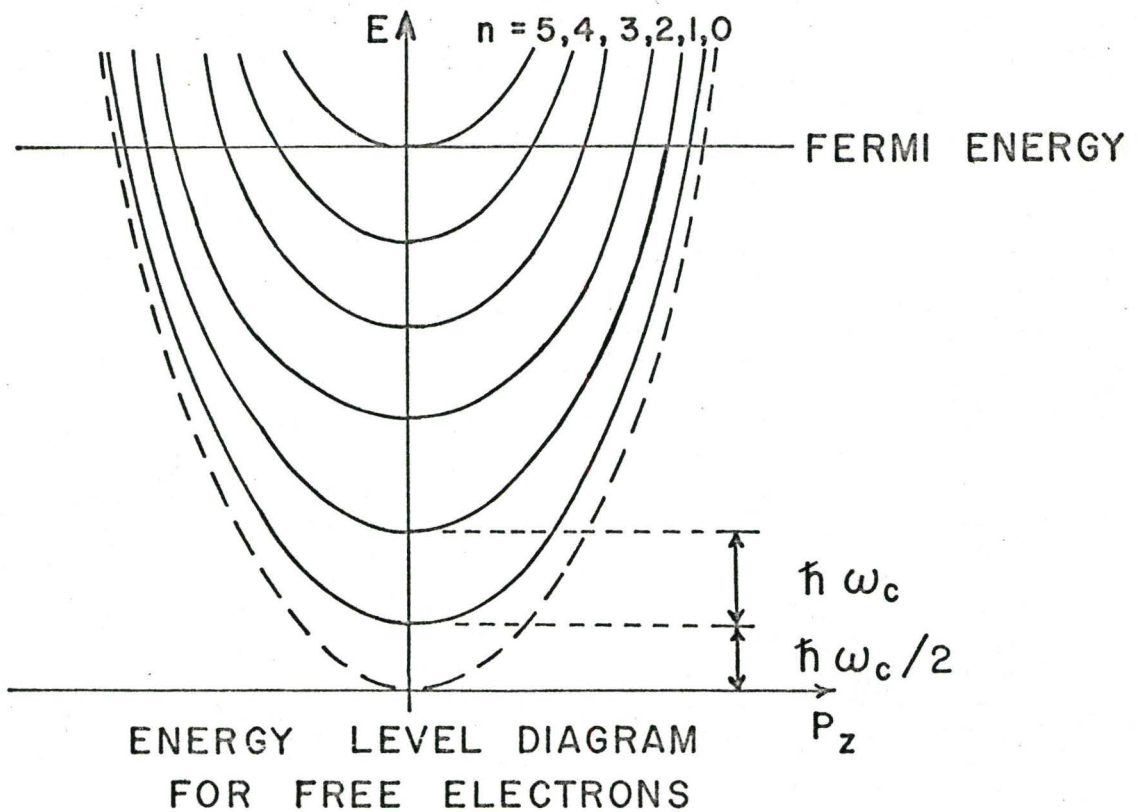
FIGURE II-1

range of p_z that is occupied as the field is increased, since
this level has just left the Fermi surface. This will happen
each time a level passes through the Fermi surface. Since the
spacing between levels is directly proportional to the field,
the number that exist inside the Fermi sphere at $p_z = 0$ will be
inversely proportional to the field H. Thus the oscillations
in energy are periodic in 1/H.

The intrinsic spin of the electron has a corresponding
dipole moment, which will change the energy eigenvalues of
equations (II-1) by an amount

$$\pm \frac{1}{2} \left\{ \frac{e\hbar}{2mc} g \ H \right\}$$

where g is the effective g-factor of the electron. For free el-
ectrons, g = 2 and the term can be written as

$$\pm \frac{1}{2} \hbar \omega_c \quad .$$

The positive sign is for a spin parallel to the field, while the
negative sign is for the opposite spin direction. We note that
the spin-up electron in the $(n-1)^{th}$ Landau level has the same
energy as the spin-down electron of the nth level. In consequence
the spin moment for free electrons does not much influence the
dHvA effect, but it will of course account for the spin para-
magnetism.

For an arbitrary band structure $E(\vec{k})$, the treatment must
be semi-classical.[7] The rate of change of momentum is given

by[26]

$$\hbar \dot{\vec{k}} = - \frac{e}{c} \vec{v} \times \vec{H} \qquad (II-2)$$

giving a constant k_z wavevector component parallel to $\vec{H}$. Since $\vec{v}_k \propto \vec{\nabla}_k E(\vec{k})$, the velocity is normal to a constant energy surface. Hence $\vec{k}$ moves such that it stays along a orbit of constant energy with constant k_z. We see that the orbit in real space (perpendicular to the magnetic field) is derived from the one in $\vec{k}$-space by multiplying the latter by $\frac{\hbar c}{eH}$ and rotating by $\pi/2$. The semi-classical Bohr-Sommerfeld quantization condition is

$$\oint \vec{p} \cdot d\vec{q} = 2\pi(n + \gamma)\hbar \qquad (II-3)$$

where n is an integer and γ is a phase factor constant. For free electrons, $\gamma = \frac{1}{2}$. Let us consider integrating about a contour of constant energy perpendicular to the magnetic field. Evaluating integrals using the relation $\vec{p} = \hbar\vec{k} - \frac{e\vec{A}}{c}$

$$\int \vec{H} \cdot d\vec{a} = (\text{area}) \, H = \int (\vec{\nabla} \times \vec{A}) \cdot d\vec{a} = \oint \vec{A} \cdot d\vec{q}$$

$$\oint \hbar\vec{k} \cdot d\vec{q} = \frac{eH}{c} \oint r_\perp \, dq = 2\frac{eH}{c} \, (\text{Area of orbit})$$

Thus $\qquad \frac{eH}{c} \, (\text{Area of orbit}) = 2\pi(n + \gamma)\hbar \qquad (II-4)$

and we see that the area of an orbit is quantized, rather than the energy spacing between levels. The area in $\vec{p}$-space is more important, because the areas that will decide whether or not a level is populated at low temperatures will be the cross-sectional areas of the Fermi surface which are perpendicular to the magnetic

field.

$$A = \frac{2\pi eH}{c} (n + \gamma)\hbar \qquad\qquad \text{(II-5)}$$

is the quantum condition on the area in momentum space. At large n, the energy spacing between levels will be $\hbar\omega_c$, where ω_c is the cyclotron frequency. Thus

$$\frac{dE}{dn} = \hbar\omega_c . \qquad\qquad \text{(II-6)}$$

If we differentiate the expression for A, we obtain

$$\omega_c = \frac{2\pi eH}{c} \left(\frac{dA}{dE}\right)^{-1}$$

which is the usual definition for the cyclotron frequency.

Continuing with the dHvA effect, we consider a slice of the Fermi surface Δk_z perpendicular to the magnetic field, assuming that the Fermi surface stays perfectly fixed. The degeneracy of each Landau level even for an arbitrary band structure will still be the same since the energies of these levels are not involved in the degeneracy calculation. At absolute zero the highest level occupied is the one which satisfies the inequality

$$S \geqslant \frac{2\pi eH}{c} (n' + \gamma)\hbar \qquad\qquad \text{(II-7)}$$

where S is the cross-sectional area of the Fermi surface. When an equals sign obtains, the level n' is just at the Fermi surface and there will be a discontinuous jump in total energy as the level is depopulated. This will occur at fields such that

$$\frac{cS}{2\pi e\hbar} \frac{1}{H} = n' + \gamma \qquad\qquad \text{(II-8)}$$

The energy will oscillate in saw-tooth fashion with a frequency $\frac{c\,S_{kz}}{eh}$ in the variable $1/H$. This could be expanded as a Fourier series in the functions $\sin\left(\frac{2\pi pc\,S_{kz}}{e\,h\,H} - 2\pi p\gamma\right)$ for $p = 1,2,3\ldots$. All these contributions must be summed over the k_z direction along the magnetic field. For ordinary magnetic fields the phase $\frac{c\,S_{kz}}{ehH}$ is very large, and the functions will oscillate rapidly since S varies with k_z. Only at extremal areas of the Fermi surface, where $\frac{\partial S}{\partial k_z} = 0$, will there be a contribution that is not negligible. Then

$$S = S_o \mp \frac{1}{2}\left|\frac{\partial^2 S}{\partial k_z^2}\right|\hbar^2(k_z - k_o)^2 + \ldots \qquad \text{(II-9)}$$

depending on whether S_o is a maximum (−) or minimum (+) area, and integrals of a type

$$I = \int_{-\infty}^{\infty} \sin\left\{\frac{2\pi p\ c\ (S_o \mp \frac{1}{2}\left|\frac{\partial^2 S}{\partial k_z}\right|\hbar^2(k_z - k_o)^2)}{e\,h\,H} - 2\pi p\gamma\right\}\cdot dk_z \qquad \text{(II-10)}$$

will occur for the total energy. When the sine function is expanded, Fresnel integrals of the type $\int_{0}^{\infty} \cos\left(\frac{\pi}{2}x^2\right)\,dx = \frac{1}{2}$ will occur. The integral II-10 will be proportional to

$$\left|\frac{\partial^2 S}{\partial k_z^2}\right|^{-\frac{1}{2}} \sin\left(\frac{2\pi p\ c\ S_o}{ehH} \mp \frac{\pi}{4} - 2\pi\,p\gamma\right). \qquad \text{(II-11)}$$

The upper sign of the phase factor $\frac{\pi}{4}$ is for a maximum, and the lower for a minimum area of the Fermi surface. At a finite temperature, the analysis must include the fuzziness of the Fermi surface, and it is found that in general all terms are greatly

reduced in magnitude by a factor $\frac{x}{\sin h\ x}$, where $x = \frac{2\pi^2 pk\ T}{\beta\ H}$,

$\beta = (e\hbar/m^* c)$, and m^* is the cyclotron mass describing the

Landau level energy spacing at the Fermi surface. The term

for $p = 1$ is most dominant. The important points are that

the energy of the electronic system will oscillate with recip-

rocal magnetic field having a frequency

$$F = \frac{c\ S_o}{e\hbar} \qquad\qquad (II-12)$$

where S_o is an extremal area of the Fermi surface in p-space.

Relation II-12 is recognized as the Onsager-Lifshitz formula.

The amplitude of the oscillations is inversely proportional

to the square root of the Fermi surface curvature at the ex-

tremum. Torque, susceptibility and a host of other properties

are related closely to the distribution of electrons in $\vec{k}$-space

and will have similar oscillatory behaviour.

The broadening of the Landau levels by collisions has

been considered by Dingle[9] using the effective mass approx-

imation for free electrons. Each Landau level is considered to

have a width that can be described by the normalized Lorentzian

$$dN = \frac{\hbar}{\tau\ \pi} \frac{dE}{(E-E_n)^2 + \hbar^2/\tau^2} \qquad\qquad (II-13)$$

where τ is the mean collision time and E_n is the energy of

the level if collisions were not taken into account. It is

found that the p'th harmonic of the dHvA free energy is multi-

plied by $\exp(- \frac{hp}{\tau\beta H})$. This means physically that the energy

levels can only be distinguished if the separation βH is greater

than their broadening h/τ.

Lifshitz and Kosevich[10] calculate the free energy of the dHvA effect for an arbitrary dispersion law. Their quantization scheme is the same as the one described above. The cyclotron mass $m_c^* = \frac{1}{2\pi} (\frac{\partial S}{\partial E})$ occurs in a natural way in the description of the Landau level structure near the Fermi surface. The free energy is obtained from

$$F = - kT \sum_{\lambda} \ell n \ (1 + e^{\frac{\xi - E(\lambda)}{kT}}) - \xi N \qquad (II-14)$$

where $E(\lambda)$ is the energy of an electron in the state λ, ξ is the Fermi energy, and the summation is performed over all possible states λ of an individual electron. In working out the free energy, the infinite sum over Landau levels n is reduced to a number integration by Poisson's formula. There are two integrals which turn up, of which one is due to the spin paramagnetism of the conduction electrons and leads to well known formulas. The second is due to diamagnetic effects and contributions come from two regions of interest on the Fermi surface. As before, stationary points where $\frac{\partial S}{\partial p_z} = 0$ are important, as well as regions near S = 0. The latter result in the steady diamagnetism of the electrons and since the points near S = 0 will occur for the lowest Landau levels, we see that the fact that the lowest energy level increases in energy with field (as in the free electron case) causes the steady dimagnetism. The magnetization is opposite to the field, causing a positive interaction energy $- \vec{M} \cdot \vec{H}$. The stationary points result in the dHvA effect when

the Fermi surface is expanded as

$$S = S_o + (\frac{\partial S}{\partial E})\ (E - \xi) + \frac{1}{2}\ |\frac{\partial^2 S}{\partial p_z^2}|\ (p_z - p_z^o)^2 + .. \quad (II\text{-}15)$$

The method results in some Fresnel integrals for the variable p_z and the oscillatory part of the free energy becomes, after an energy integration

$$F_{osc} = 2VkT\ (\frac{eH}{hc})^{3/2}\ |\frac{\partial^2 S}{\partial p_z^2}|^{-1/2} \quad x$$

$$\sum_{p=1}^{\infty} \frac{\cos(\frac{2\pi pc\ S_o}{ehH} - 2\pi p\gamma \mp \frac{\pi}{4})}{p^{3/2}\ \sinh\ (2\pi^2 pkT/\beta H)}\ \cos(\frac{qp\pi m^*}{2m_o}). \quad (II\text{-}16)$$

where $\beta = \frac{eh}{m^* c}$ and $m^* = \frac{1}{2\pi}\ (\frac{\partial S}{\partial E})_{S_o}$

As before, the upper sign is for a maximum, and the lower for a minimum area of the Fermi surface.

This formula is the one commonly used in dHvA work, and only minor changes have been proposed by Cohen and Blount[11] and by Williamson et al[18]. The former discuss spin-orbit coupling and show that the spin effective mass m_o should be replaced by 2 m_e/g, where m_e is the true electron mass and g is the effective splitting factor. The latter authors show that by using Dingle's treatment of Landau level broadening and the method of Lifshitz and Kosevich[10], each term of the summation should be multiplied by exp($- 2\pi^2$ p k $T_D/\beta H$), where T_D is called

the Dingle temperature and is related to the collision time by $k\,T_D = \hbar/\tau$. Finally, then, the formal expression for the oscillatory free energy can be written as

$$F_{osc} = 2VkT \left(\frac{eH}{hc}\right)^{3/2} \left|\frac{\partial^2 S}{\partial p_z^2}\right|^{-1/2} \sum_{p=1}^{\infty} \frac{\exp(-2\pi^2 pkT_D/\beta H)}{p^{3/2}\, \sinh(2\pi^2 pkT/\beta H)} \; x$$

$$\cos\left[\frac{2\pi pF}{H} - 2\pi p\gamma \mp \frac{\pi}{4}\right] \cos\left(\frac{\pi pgm^*}{2m_e}\right). \qquad (II-17)$$

where the dHvA frequency $F = \dfrac{c\,S_o}{eh}$ and all quantities such as the curvature $\left(\dfrac{\partial^2 S}{\partial p_z^2}\right)$ and m^* are defined at the Fermi surface extremal area.

Let us again recall that the above formulation was for non-interacting fermions, whereas in reality we know that Coulomb forces give large interactions. In a real metal there may not be a sharp momentum distribution, but Luttinger[27] has shown that a well-defined discontinuity can exist if the inter- actions have certain analytic properties. A possible picture of the distribution function would be:
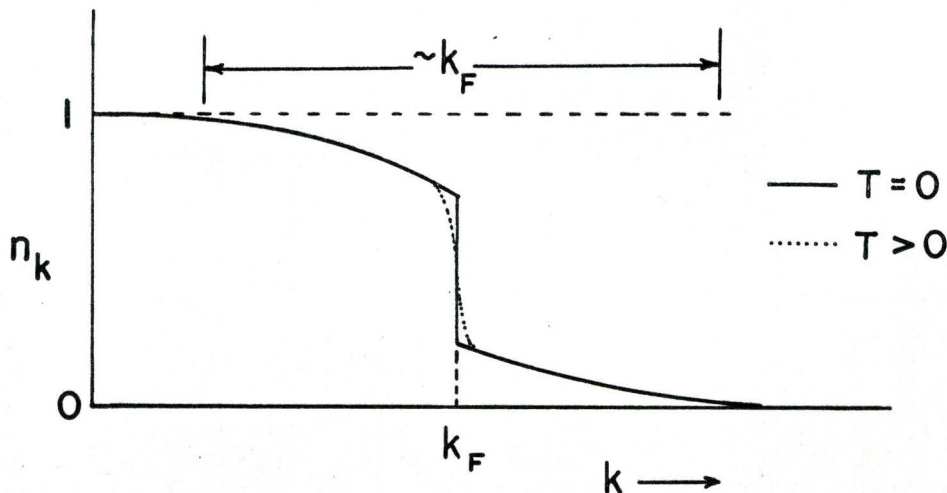
A possible result of interactions is that the temperature and field dependences of amplitude may differ from those of the theory presented earlier. Luttinger discounts this but concludes that the phases could be quite different in the presence of interactions. The presence of interactions changes the shape of the Fermi surface, but does not change its total volume from the case in which interactions are not considered. Areas in momentum space of the true Fermi surface will occur in the dHvA effect and total carrier densities will be preserved. Simple properties such as the specific heat and spin paramagnetism, which depend on the density of states near the Fermi surface, are not affected by electron-electron interactions except to the extent in which the interactions influence the energies of the single particle states at the Fermi surface.

Another point of departure between theory and experiment is that the Fermi level does not stay constant, especially in a semimetal which has a small number of carriers. The number of carriers must be constant and this determines the dependence of the Fermi energy on magnetic field[28]. It will have oscillatory behaviour similar to the dHvA effect and several indications of this behaviour can be expected in actual experiments. If there is one dominant oscillation which causes oscillatory variation of the Fermi energy, it will cause all other dHvA frequencies to oscillate in the same manner. If the dominant frequency, F_D, causes a change in Fermi energy, we can write

$$\xi \cong \xi_o + \Delta\xi \, \cos \frac{2\pi F_D}{H} \; . \qquad \text{(II-18)}$$

This means that the extremal area for the ith carrier can be written

$$S_m^{\ i} = S_o^{\ i} + (\frac{\partial S}{\partial E}) \ \Delta \xi \ \cos \frac{2\pi F_D}{H} \qquad \text{(II-19)}$$

As a consequence, the dHvA oscillations of the ith carrier will have a form given by

$$F_{osc} = A_i(H,T) \ \cos \ [\frac{2\pi c}{ehH}(S_o^{\ i} + \frac{\partial S_i}{\partial E} \ \Delta \xi \ \cos \frac{2\pi F_D}{H}) - 2\pi\gamma \mp \frac{\pi}{4}] \qquad \text{(II-20)}$$

where $A_i(H,T)$ gives the field and temperature dependence of the amplitude. If the effect is large it may be possible to measure $\frac{\partial S_i}{\partial E} \Delta \xi$ and determine the change in Fermi level, if the cyclotron effective mass $m_i^* = \frac{1}{2\pi} \cdot \frac{\partial S_i}{\partial E}$, is known. In any event, if i denotes the dominant oscillation F_D, itself, the harmonic content of the oscillations will be altered. If i is another carrier, then the free energy for it is basically a frequency modulated wave, and frequencies $\frac{c \ S_o^{\ i}}{eh} \pm nF_D = F_i \pm nF_D$ will occur (where n = 0,1,2,.... .) as a result of the modulation provided by an oscillatory Fermi energy. Other mechanisms for non linear behaviour are more conveniently discussed later.

In conclusion, it may be well to point out that in a two dimensional electron gas the dHvA effect would not occur, since as the field increases the Fermi energy will change such that the energy of the gas increases monotonically (diamagnetism). The variation of energies in the third dimension is necessary to stabilize the Fermi energy.

CHAPTER III

CRYSTAL AND BAND STRUCTURE OF ARSENIC

CRYSTAL STRUCTURE OF ARSENIC

Arsenic, Antimony and Bismuth are group -V semimetals all possessing the same crystal structure[29] of which the unit cell and also the primitive cell is rhombohedral, containing 2 atoms. The simplest specification of this cell is to give the length of one of the primitive vectors, a, and the angle between any two of them, usually denoted by α. If α were 60°, then this cell would be the primitive cell for the face-centred cubic (F.C.C.) structure. The two atoms in each cell are symmetrically placed and the coordinates of an atom are given as (u,u,u) in the system of axes which uses the three basic primitive vectors of the cell. $\alpha = 60^O$ and $u = 1/4$ would specify exactly a simple cubic lattice. Falicov and Golin[30] indicate the arsenic structure as derived from the F.C.C. structure by a shear along the body diagonal of the primitive cell and a displacement of one of the interpenetrating rhombohedral lattices with respect to the other, along the three-fold rotation symmetry axes. The resulting structure has one three-fold axis, three two-fold axes with mirror planes perpendicular to each axis, and an inversion centre. For arsenic, the numerical values for the crystal constants are

$$a = 4.131 \ \overset{O}{A}$$
$$\alpha = 54^O 10'$$
$$u = 0.226$$

21

at room temperature. These parameters will probably change at helium temperatures and the rhombohedral angle α should increase, (as it does in Sb[31]) making the crystal more cubic.

H. Jones[73] gives the algebra used for the construction of the Brillouin zone for a rhombohedral lattice. Instead of Jones' notation, we define the three primitive translation vectors $\vec{a}_1, \vec{a}_2$ and $\vec{a}_3$ as in the diagram below .
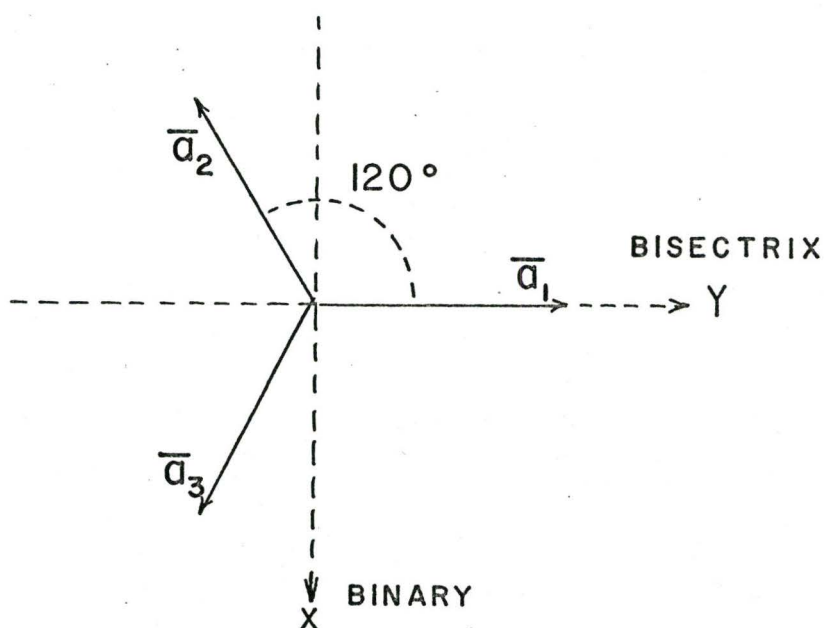
The x-axis is one of the binary or two-fold symmetry axes, while the z-axis is the three-fold or trigonal axis. The y-axis is called the bisectrix axis, but it has no special symmetry.

The matrix which specifies any lattice vector $n_1\vec{a}_1 + n_2\vec{a}_2 + n_3\vec{a}_3$, where the n_i's are integers, is

$$\vec{\vec{A}} = \begin{pmatrix} 0 & -\frac{\sqrt{3}}{2} a \sin \theta & \frac{\sqrt{3}}{2} a \sin \theta \\ a \sin \theta & -\frac{1}{2} a \sin \theta & -\frac{1}{2} a \sin \theta \\ a \cos \theta & a \cos \theta & a \cos \theta \end{pmatrix} \quad \text{(III-1)}$$

Here θ is the angle that each of the primitive vectors makes with the z-axis (trigonal). If $\vec{n} = \begin{pmatrix} n_1 \\ n_2 \\ n_3 \end{pmatrix}$ denotes a column vector of the lattice, its cartesian coordinates are $\vec{L} = \vec{\vec{A}} \cdot \vec{n}$. The angle between two primitive vectors is found easily by the scalar product and gives

$$\cos \theta = [\frac{1 + 2 \cos \alpha}{3}]^{1/2}$$

The reciprocal lattice is specified by a similar matrix $\vec{\vec{B}}$ such that

$$\vec{\vec{B}} \cdot \vec{\vec{A}} = 2\pi \, \vec{\vec{I}} \tag{III-2}$$

where $\vec{\vec{I}}$ is the unit matrix. Then

$$\vec{\vec{B}} = \begin{pmatrix} 0 & b \sin \phi & b \cos \phi \\ -\frac{\sqrt{3}}{2} b \sin \phi & -\frac{1}{2} b \sin \phi & b \cos \phi \\ \frac{\sqrt{3}}{2} b \sin \phi & -\frac{1}{2} b \sin \phi & b \cos \phi \end{pmatrix} \tag{III-3}$$

Any vector of the reciprocal lattice $\vec{G}$ is found in cartesian coordinates from its oblique row vector $\vec{\ell} = (\ell_1, \ell_2, \ell_3)$. by the relation

$$\vec{G} = \vec{\ell} \cdot \vec{\vec{B}} \quad , \tag{III-4}$$

where ℓ_1, ℓ_2 and ℓ_3 are integers. By using equation (III-2) it can be shown that

$$\tan \theta = 2 \cot \phi . \tag{III-5}$$

The angle β between primitive reciprocal lattice vectors is given by

$$\cos \beta = \frac{- \cos \alpha}{1 + \cos \alpha} \tag{III-6}$$

The length of the primitive reciprocal vectors is given by

$$\frac{2\pi}{ab} = [\frac{(1 + 2 \cos \alpha)(1 - \cos \alpha)}{(1 + \cos \alpha)}]^{1/2} \qquad \text{(III-7)}$$

The Brillouin zone is constructed by bisecting the line joining the origin to the nearest reciprocal lattice points with planes which interact to produce the zone. It is shown in Figure III-1, with the notation of the symmetry points and lines chosen to conform to those of Falicov and Golin[30] who have done the recent band structure calculations of As and Sb. The ΓL direction lies in the quadrant between the positive y and z axes. Rotations will be labelled positive in the three planes from x → y, y → z and z → x. In the trigonal-bisectrix plane, rotations are labelled starting from the trigonal axis towards the negative bisectrix axis. This quadrant contains the direction ΓX. The directions ΓX and ΓL are respectively $58°17'$ and $- 72°50'$ from the ΓT or trigonal direction.

The volume of the Brillouin zone can be shown to be given by

$$V = \vec{b}_1 \cdot \vec{b}_2 \times \vec{b}_3$$

$$= \frac{3\sqrt{3}}{2} b^3 \sin^2 \phi \cos \phi \qquad . \qquad \text{(III-8)}$$

Numerical values for the reciprocal lattice constants are given below.

$$\theta = 31° \ 30'$$
$$\phi = 72° \ 50'$$

BRILLOUIN ZONE FOR ARSENIC STRUCTURE
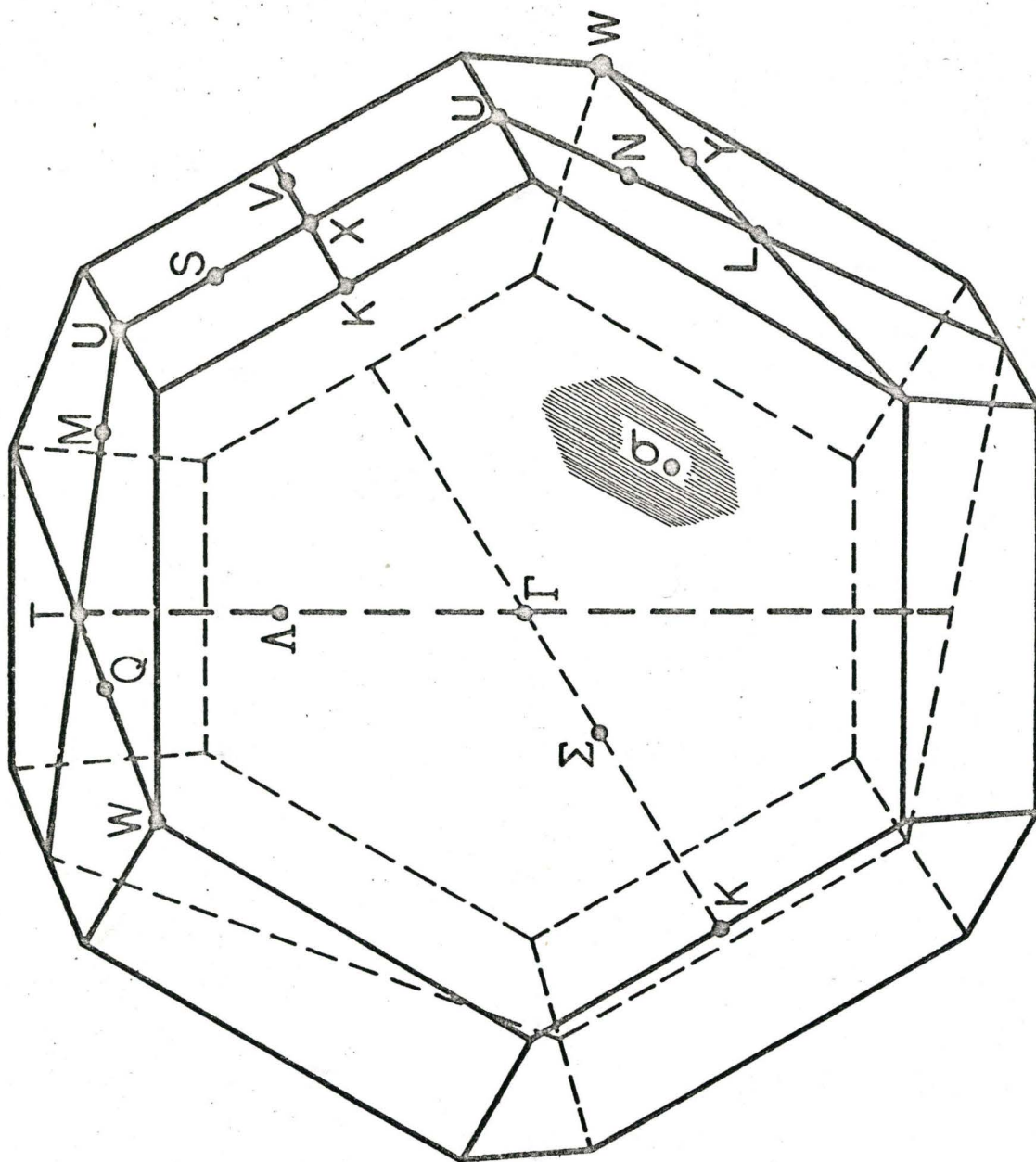
FIGURE III-1

$$\beta = 111^\circ \ 41'$$

$$\frac{2\pi}{ab} = 0.8490$$

$$\frac{3\sqrt{3}}{2} \sin^2\Phi \cos\Phi = 0.6955$$

FREE ELECTRON THEORY

Our initial work on arsenic considered the free electron theory to see if any sense could be made of the Fermi surface as observed by Berlincourt[32]. There are five valence electrons per atom and two atoms per unit cell, hence the volume of occupied $\vec{k}$-space is five complete Brillouin zones, since the true Brillouin zone always holds two electrons per atom. A free electron model immediately predicted a multitude of segments to the Fermi surface, contrary to the earlier work[32], as well as ours. Many zone boundaries were within the Fermi sphere of occupied states. Electrical conductivity of arsenic[33] as represented by a resistivity of $\rho \simeq 30 \times 10^{-6}$ ohm-cm shows that the carrier density must be low. A typical metal such as copper has a resistivity at room temperature of 1.8×10^{-6} ohm-cm. There are thus only a few available carriers and this approach must be abandoned.

A second approach is indicated by Jones[73]. Since Bi, Sb and As are poor conductors and have the properties of semi-metals with almost filled energy bands, we try to find a large zone which is bounded by planes with a non-vanishing energy gap, such that it has a volume equal to five times that of the Bril-

louin zone. This large zone turns out to be bounded by six

vertical planes whose indices in the oblique coordinate system

are $(01\bar{1})$, $(10\bar{1})$, $(1\bar{1}0)$, $(0\bar{1}1)$, $(\bar{1}01)$, $(\bar{1}10)$ and by six planes

inclined to the trigonal axis with indices (221), (212), (122),

$(\bar{2}\bar{2}\bar{1})$, $(\bar{2}\bar{1}\bar{2})$, $(\bar{1}\bar{2}\bar{2})$. Drawing in a Fermi sphere such that its

volume is equal to that of the large "Jones"zone, we are in a

position to make general comments on the Fermi surface of arsen-

ic. Figures (III-2) and (III-3) show two sections in the y-z

and x-z planes of the large zone. One figure has the primitive

vector $\vec{b}_1$ labelled. The small circles represent reciprocal

lattice points. The free electron Fermi sphere is drawn in

both planes, having a radius of 0.94b, which just gives it a

volume equivalent to five true Brillouin zones. The sections

of the true Brillouin zone are drawn in for comparison. Notat-

ion of the large zone corresponds to that found in Jones[73].

In the absence of any more detailed information, we may assume

that the electron Fermi surface will correspond to the section

in the zone which is closest to the centre Γ, since the energy

will probably be lowest at this point. Thus we expect the el-

ectron Fermi surfaces to be centred at B or C points, which map

back to X or L points of the Brillouin zone. The holes of the

highest energy band are expected to be centred at points such

as A_1, which map to T points of the reduced zone. Bi, Sb,

and As, in order of decreasing spin-orbit coupling, are not ex-

pected to have Fermi surfaces resembling those suggested by the

Jones zone, but the general directives as to where we may expect
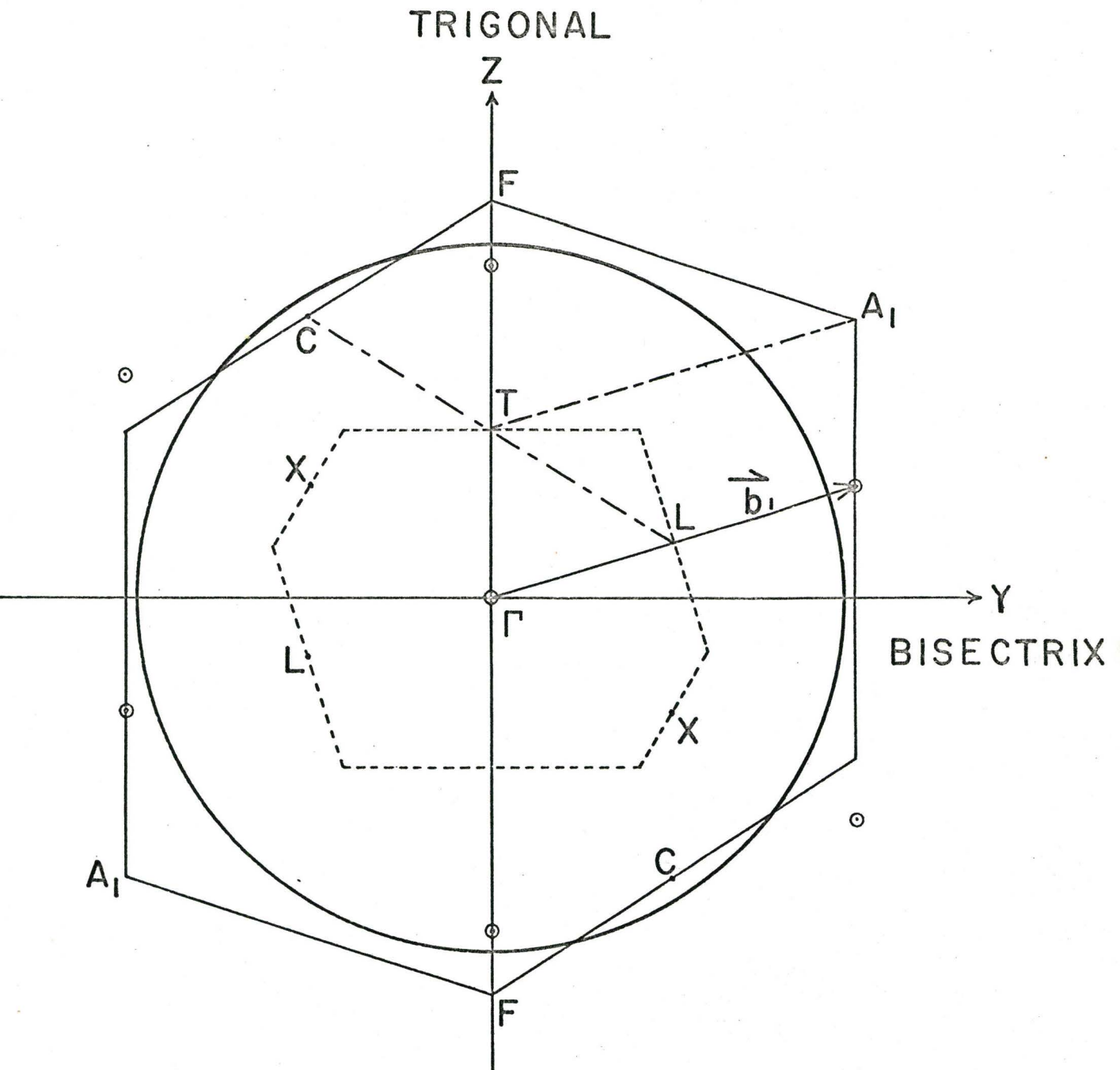
FIGURE III-2
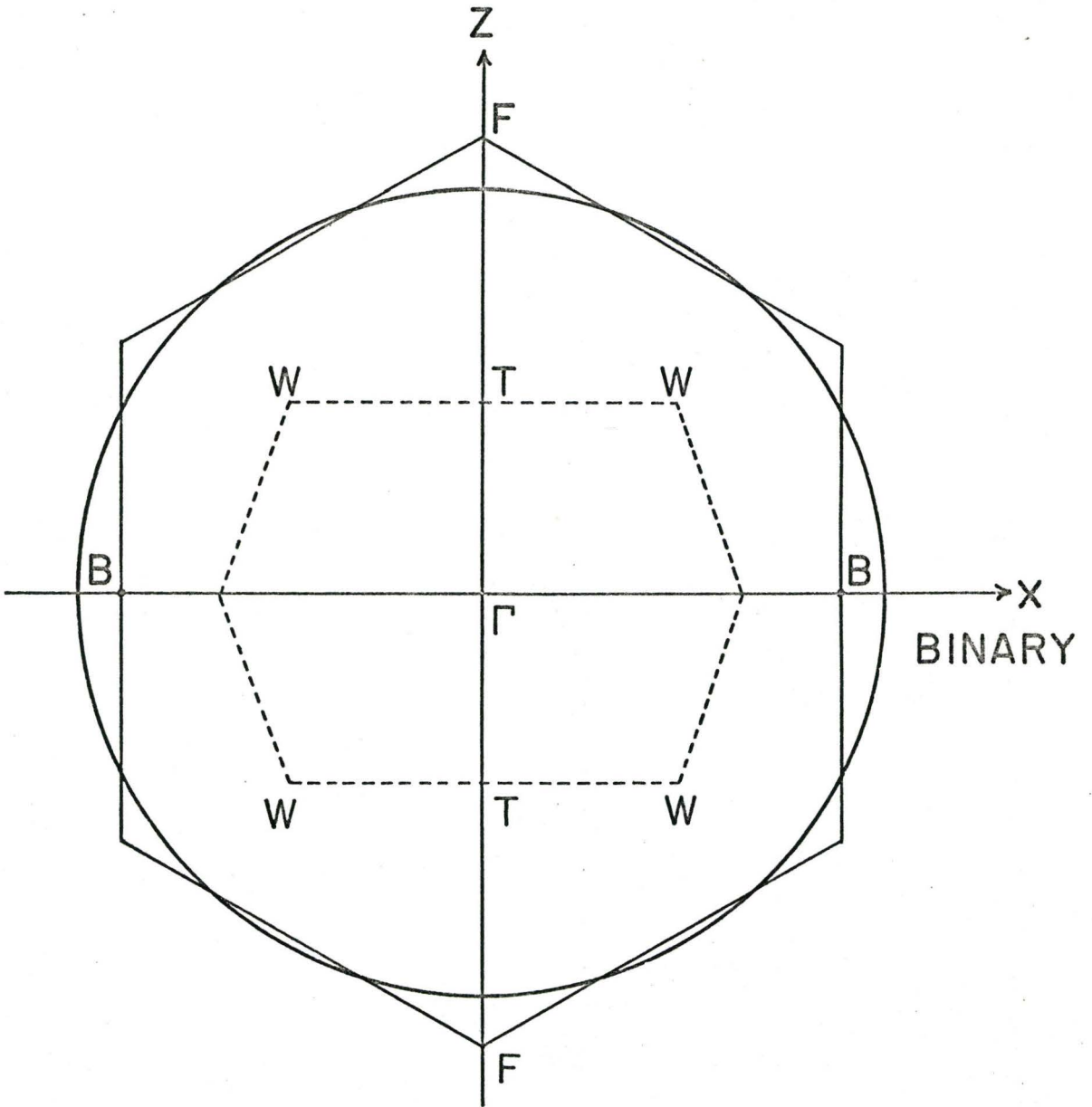
FIGURE III-3

hole and electron surfaces will be found to be reasonably correct. Of these three semi-metals, arsenic can be best expected to follow the picture as outlined above since spin-orbit coupling is less and more confidence may be placed on the crystal structure itself to determine the Fermi surface.

BAND STRUCTURE CALCULATIONS

The first realistic band structure calculations were done for the group V semimetals by Cohen, Falicov and Golin[34], by determining the basic energies which the A7 crystal structure should produce. The semi-metallic nature of As, Sb and Bi was shown to be a consequence of their crystal structure and it was expected that they would have many common features in their band structure. Experimentally, arsenic had been least studied of these three, but theoretically it should be the easiest to handle, for several reasons. As has the smallest atomic number (Z = 33), and in the periodic table it is next to germanium, which has very well-known properties. Thus a calculation by Falicov and Golin[30] using the pseudopotential approach has appeared for the band structure of arsenic.

Pseudopotential methods are based on the idea that the one-electron Schrodinger equation for the perfect crystal

$$[\frac{\hbar^2}{2m} \nabla^2 + V(\vec{r})] \; \psi_{n\vec{k}}(\vec{r}) \; = \; E_n(\vec{k}) \; \psi_{n\vec{k}}(\vec{r}) \qquad (III-9)$$

can be rewritten[35] as

$$[\frac{\hbar^2}{2m} \nabla^2 + V_P] \; \phi_{n\vec{k}}(\vec{r}) \; = \; E_n(\vec{k}) \; \phi_{n\vec{k}}(\vec{r}) \qquad (III-10)$$

having the same eigenvalues for the band structure $E_n(\vec{k})$. V_p is a non-local integral operator, and $\Phi_{n\vec{k}}$ is a smooth wave-function which does not have the rapid atomic core oscillation of the true wave function $\Psi_{n\vec{k}}$. As a consequence an expansion of Φ into plane waves converges rapidly to a good solution. The matrix elements $<\vec{k}|V_p|\vec{k}'>$ are non-zero only for $\vec{k}-\vec{k}' = \vec{G}$, where $\vec{G}$ is a reciprocal lattice vector. These matrix elements depend on $\vec{k}$ as well as $\vec{G}$, but for the case of silicon and germanium[36][37] quantitative agreement with the band structure is obtained even if two greatly simplifying assumptions are made.

(a) V_p is a superposition of atom-like pseudopotentials centred about each ion site

$$V_p = \sum_i U_i \qquad\qquad \text{(III-11)}$$

i = ion sites

(b)   The U_i are taken to be local, simple functions of the position

$$U_i = U_i(|\vec{r} - \vec{r}_i|) \qquad\qquad \text{(III-12)}$$

rather than integral operators. If these assumptions are used, the matrix elements of V_p can be written as a product of a structure factor $S(\vec{G})$ and the Fourier transform $U(\xi)$ of the atomic-like pseudopotential, for $\xi = |\vec{G}| = |\vec{k} - \vec{k}'|$. Thus the set of numbers $\{U(|\vec{G}|)\}$ specify the band structure. Falicov and Golin[30] used the pseudopotential points of Brust[37] for Ge, smoothed the curve, and, to their amazement, a semi-metallic structure resulted for arsenic. The matrix

element can be written as a product

$$< \vec{k} | V_p | \vec{k}' > = S(\vec{G}) \; U(\vec{G}) \quad . \qquad \text{(III-13)}$$

This means that the A7 structure of arsenic is mainly responsible for its semimetallic properties. The parameter u described in the first section has a great effect on the structure factor. If $u = 1/4$ (simple cubic structure) or $1/8$ (diamond structure) many matrix elements will vanish, but not for the semimetals, in which u is irrational. The $\{U(|\vec{G}|)\}$ do not depend on the internal displacement u, nor do they depend much on the shear distortion in arsenic, since this only slightly changes the vectors G. The shear does change the kinetic energy terms at different points in the zone with respect to others, whereas the parameter u does not affect the kinetic energy at all.

Group theory arguments are used to determine points of accidental degeneracy and also for connecting the various energy levels that were numerically obtained at different points. The four parameters in the pseudopotential were varied and for nine cases it was found that the resulting band structure was much the same. This confirms that the kinetic energy is more important than the pseudopotential and that the matrix elements $<\vec{k} | V_p | \vec{k}' >$ depend mostly on the structure factor. Figure III-4 shows the overall band structure for the pseudopotential finally used. The free electron Fermi energy has been drawn in to facilitate a visualization of the Fermi surface, which is what concerns us here. It is seen immediately that electrons exist
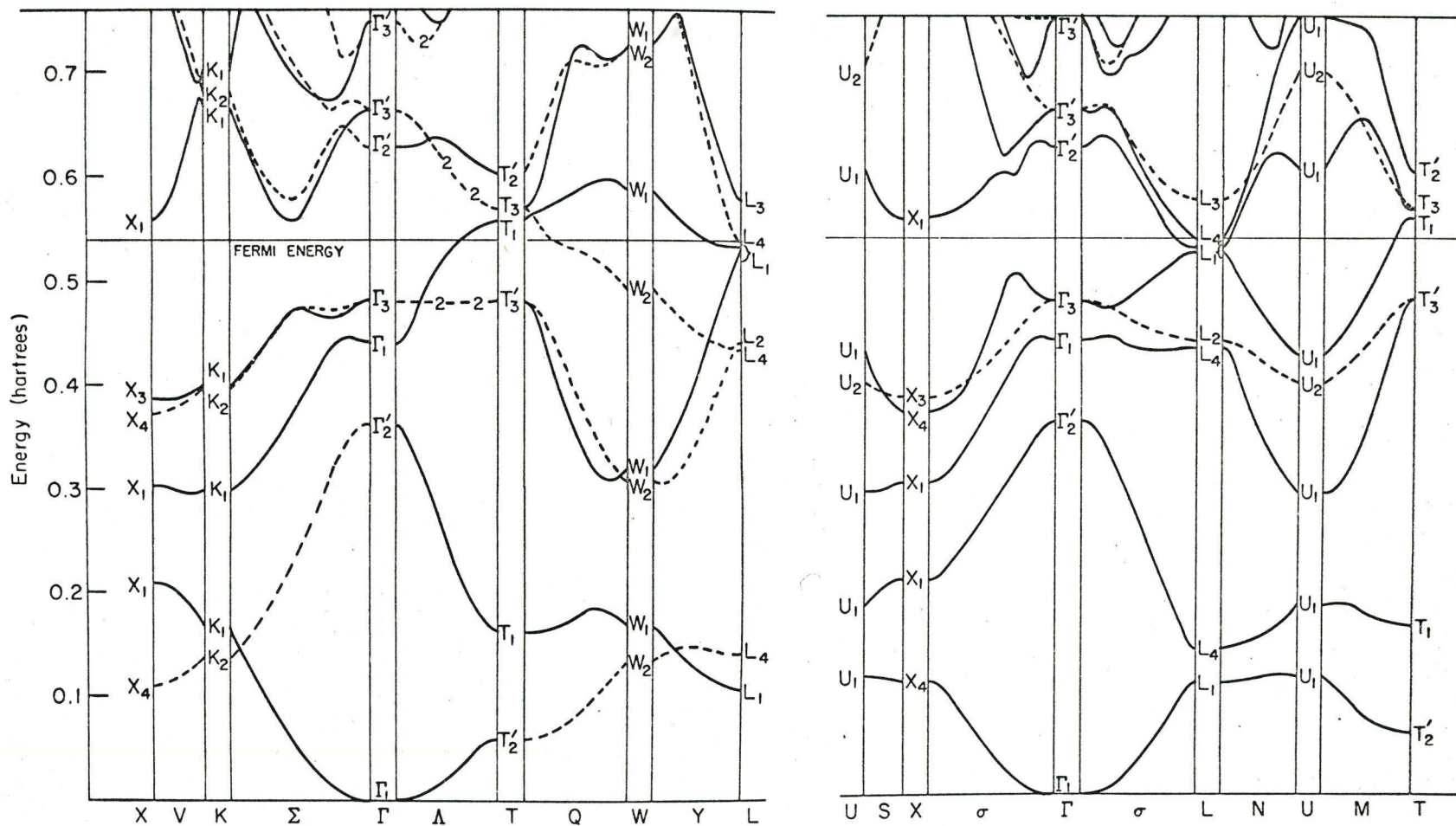
OVERALL BAND STRUCTURE OF ARSENIC

FIGURE III-4

at L points of the Brillouin zone and holes occur at the point T. Figures III-5 and III-6 show enlarged diagrams of the areas of interest both with (b,d) and without (a,c) spin-orbit coupling for two different pseudopotentials. The Fermi energies are not drawn in since it is permissible to make slight changes to fit the Fermi surface. This can be arranged by small pseudopotential changes.

Spin-orbit coupling is included in the band structure calculation after the pseudopotential calculation only in the neighborhood of points L and T, where it will be important for the determination of the Fermi surface. The $J = 1/2, 3/2$ splitting of the As III $4p^2$ P ground state is 0.36 eV. For Ge II it is 0.22 eV but since rhombohedral structures (As) have only about 2/3 the spin splitting of cubic (Ge) structures, it is expected that a spin-splitting of ~ 0.3 eV will exist at points of high symmetry. This is fairly small in comparison with Sb (0.6 eV) or Bi (1.5 eV), and a tight-binding approach is used for the spin-orbit corrections. The approximations made are that the real crystal potential is assumed to be spherically symmetric about each ion and constant in regions between ions, and that the conduction electron wave functions ψ_{nk} have a definite S,P,D ... character about each ion and close to the ion they are like 4s and 4p wave functions. The spin orbit Hamiltonian can then be written

$$H = \lambda \sum_{\alpha} \vec{L}_{\alpha} \cdot \vec{S} \qquad \text{(III-14)}$$
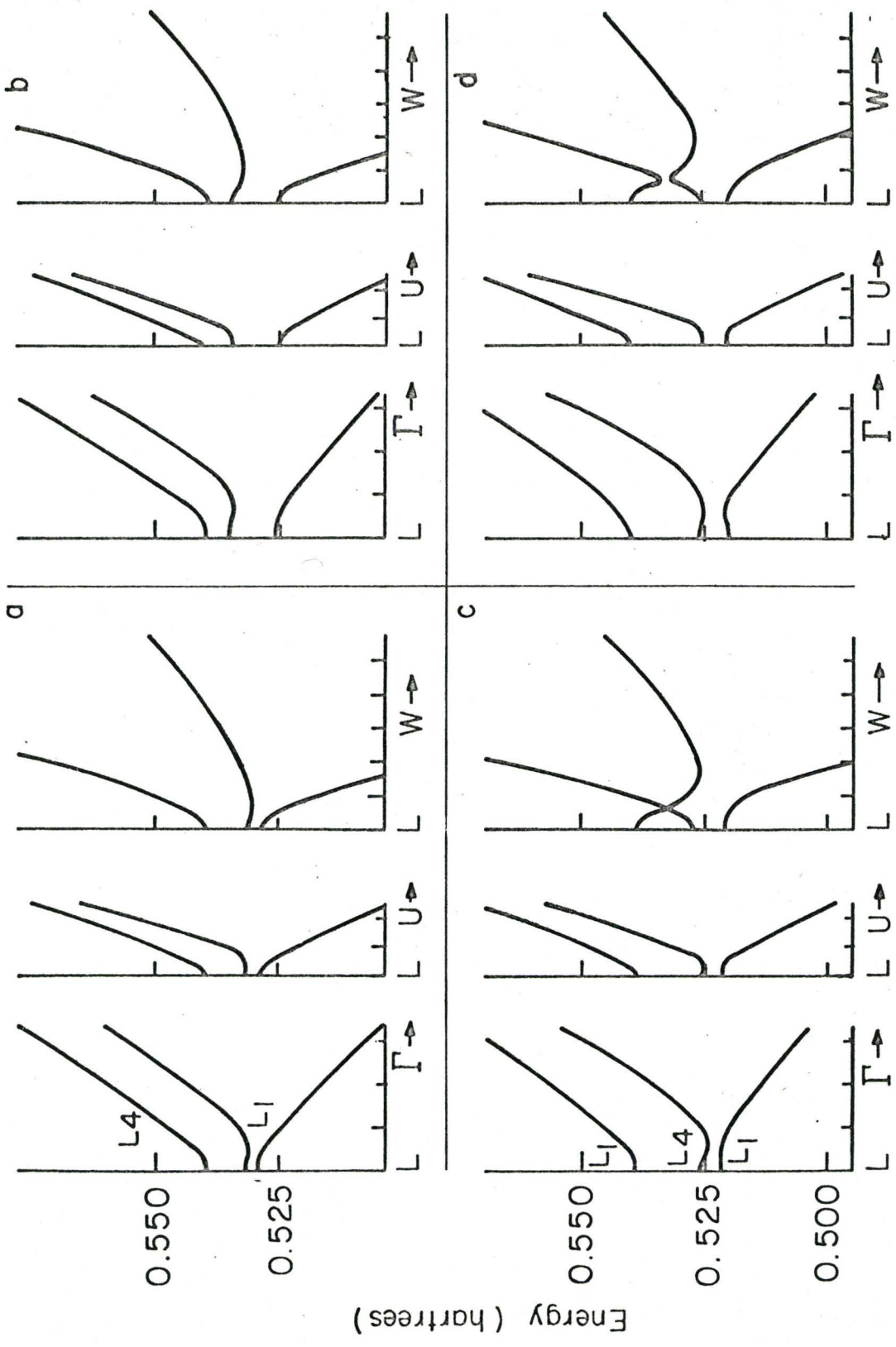
ELECTRONS

FIGURE III-5
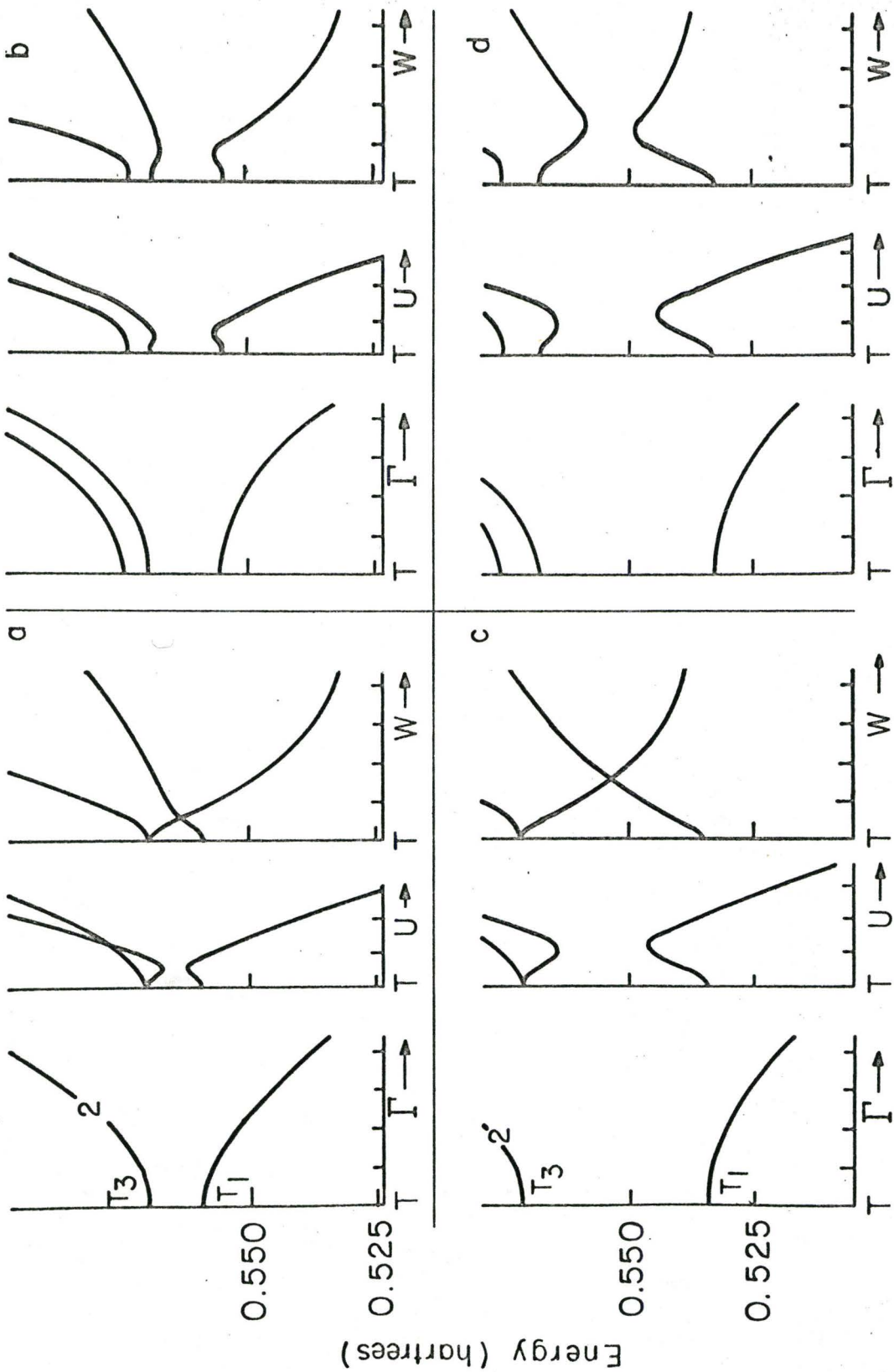
HOLES

FIGURE III-6

where $\vec{L}_\alpha$ is an angular momentum operator which acts only on atomic-like functions centred around site α, and λ is chosen to reproduce the 4p state splitting. As well the character of an energy level near a symmetry point is assumed to have the same character as the point (T or L). The analysis of the level ordering and energy shifts due to spin-orbit coupling are evident in Figures III-5 and III-6 and it is seen that close to T the situation is much simpler, with all the degeneracies lifted. At L there are no important changes caused by the splitting. From the band structure calculation the only positive facts are that there are electrons at or near L in the sixth band and holes are close to T in the fifth band. Some guide lines are drawn as to what the Fermi surface must be, but a more accurate determination of the pseudopotential parameters is necessary.

More information has in the past few years come to light about the Fermi surface of arsenic. Shapira and Williamson[38] have observed a second major part of the Fermi surface in addition to the "ellipsoids" seen by Berlincourt[32]. Our observations also included both segments of the Fermi surface. In addition, many discrepancies occurred in the explanation of the long periods in arsenic. Ketterson and Eckstein[39] also reported three carriers and measured a tilt angle in their long periods of about 5°. A possible interpretation of our data at the time was that the long periods could be connecting cylinders. This was not understood until the results of Priestley et al[40]

and our preliminary results[41] confirmed the final theoretical determination of the Fermi surface by Lin and Falicov[42]. Better determination of the pseudopotential parameters is possible only by a direct comparison with the experiments.

Pseudopotential parameters of As were determined as in the case of antimony[43] by adding to the atomic pseudopotential of Ge[37] one half of that for Ga As[44] and renormalizing according to the unit cell volumes.

$$U^{As} = \left\{ U^{Ge} + \frac{1}{2} U^{Ga\ As} \right\} \frac{\Omega\ Ga\ As}{\Omega\ As} \qquad (III-15)$$

The Fermi energies at the points T and L were altered slightly to satisfy two experimental observations. The cross-sectional area of the cylinders (to be described later) was fitted to the dHvA measured values, and the minimum area of the electron ellipsoids in the trigonal bisectrix plane was fitted also by dHvA measurements. The resulting Fermi surface is to be compared with experiment.

The overall band structure is very similar to the original calculation shown in Figure III-4. Enlarged details near points L and T are shown in Figure III-7. Levels were expected from the Sb results to be ordered $L_1 < L_4 < L_1$ for the 5th to 7th bands at L and $T_1 < T_3' < T_2$ or $T_1 < T_2'' < T_3$ for the 5th to 8th bands at T. The maximum of the fifth band occurs at the points H on the mirror planes, one of which is given in trigonal co-ordinates as [0.2043, 0.3758, 0.2043]. Along the T-W line an accidental degeneracy occurs which is removed if spin-orbit coup-
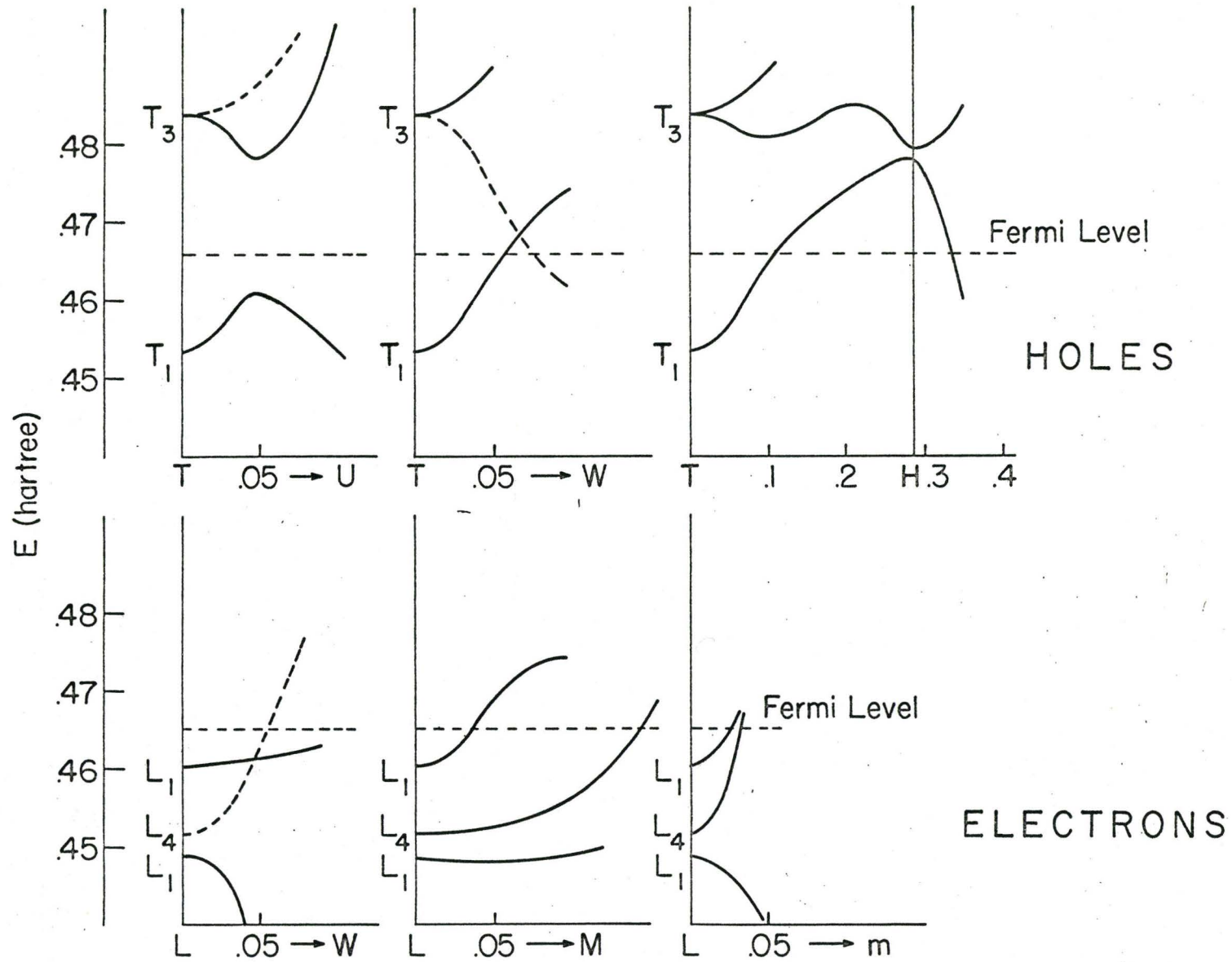
ENLARGED DETAILS OF THE BAND STRUCTURE

FIGURE III-7

39

ling is included. One of the six equivalent cross-over points
B has trigonal coordinates [0.4617, 0.5, 0.5383]. Holes, then,
will probably occur near both H and B points. For electrons two
levels L_4 and L_1 (sixth and seventh bands) are below the Fermi
energy chosen to fit the dHvA results of the surface caused by
L_4. Since no new segments to the Fermi surface have been
detected (nor are likely to be), the level L_1 must be above
the Fermi energy. There are several plausible explanations.
Spin-orbit interactions will tend to repel the two L_1 levels
but not the L_4, pushing the upper L_1 above the Fermi energy.
Also, if the rhombohedral angle between primitive cell vectors
increases at low temperatures, as is expected, the levels at
L will increase in energy relative to those at T. In any
event, the L_1 level is ignored since the agreement obtained
for the L_4 electrons and the holes is very good.

The actual Fermi surface determined from Lin and Falicov's
calculation is that of three electron ellipsoids at L points
and a multiply connected hole surface around the T point in the
Brillouin zone. Electron surfaces show slight deviation from
true ellipsoidal shape. Details of the surface are shown in
Table III-1. The tilt angle is measured from the trigonal axis,
with a rotation from ΓT to ΓX being defined as positive. This
angle is sensitive to changes in the pseudopotential parameters
and the experimental value is not considered to violate the
theory. If L_1 were below the Fermi energy it would give complete-
ly different values of tilt angle which could not be much altered

TABLE III-1

Electron Fermi Surface

	Theory	Experiment
Area normal to the trigonal	0.018	0.020
Minimum area for H in the trigonal-bisectrix plane	0.0055*	0.0055
Tilt angle for minimum area	~ $+ 80°$	$+ 86° \pm 1°$
Fermi energy	58.7×10^{-14} ergs	31.0×10^{-14} ergs
Principal Effective Masses (1) binary (2) trigonal-bisectrix plane	0.11 0.038 0.94	0.135 0.127 1.52

Hole Fermi Surface

	Theory	Experiment
Cross-sectional area of the cylinders	6.9×10^{-5}*	6.9×10^{-5}
Tilt angle of the cylinders	$- 11°$	$- 10° \pm 1°$
Area of pockets normal to the binary	~ 9.6×10^{-3}	(13×10^{-3})
Tilt angle of minimum area	~ $+ 44°$	$+ 38° \pm 1°$
Fermi energy	58×10^{-14} ergs	28×10^{-14} ergs

All areas and masses are in atomic units (m, $\hbar$, e = 1).

* indicates that these values were chosen to fit experimental data

Fermi energies were derived from a parabolic band approximation.

by slight pseudopotential changes. The Fermi surface for holes
is shown pictorially in Figure III-8. It consists of six hole
pockets about the points H, each of approximately half the
volume of the electron ellipsoids, linked by long slender cylin-
ders with two-fold symmetry, each centred at a B point, which
lies on the top hexagonal face of the Brillouin zone. Because
there is only a single hole surface, it has the full crystal
symmetry $\bar{3}m$. The details of the surface are also listed in
Table III-1. The hole pockets are quite non-ellipsoidal, as
seen from Figure III-8, where the band maximum is labelled at
one of the H points. The Lin and Falicov model of the Fermi
surface will be compared to our experimental results in Chapter
V.
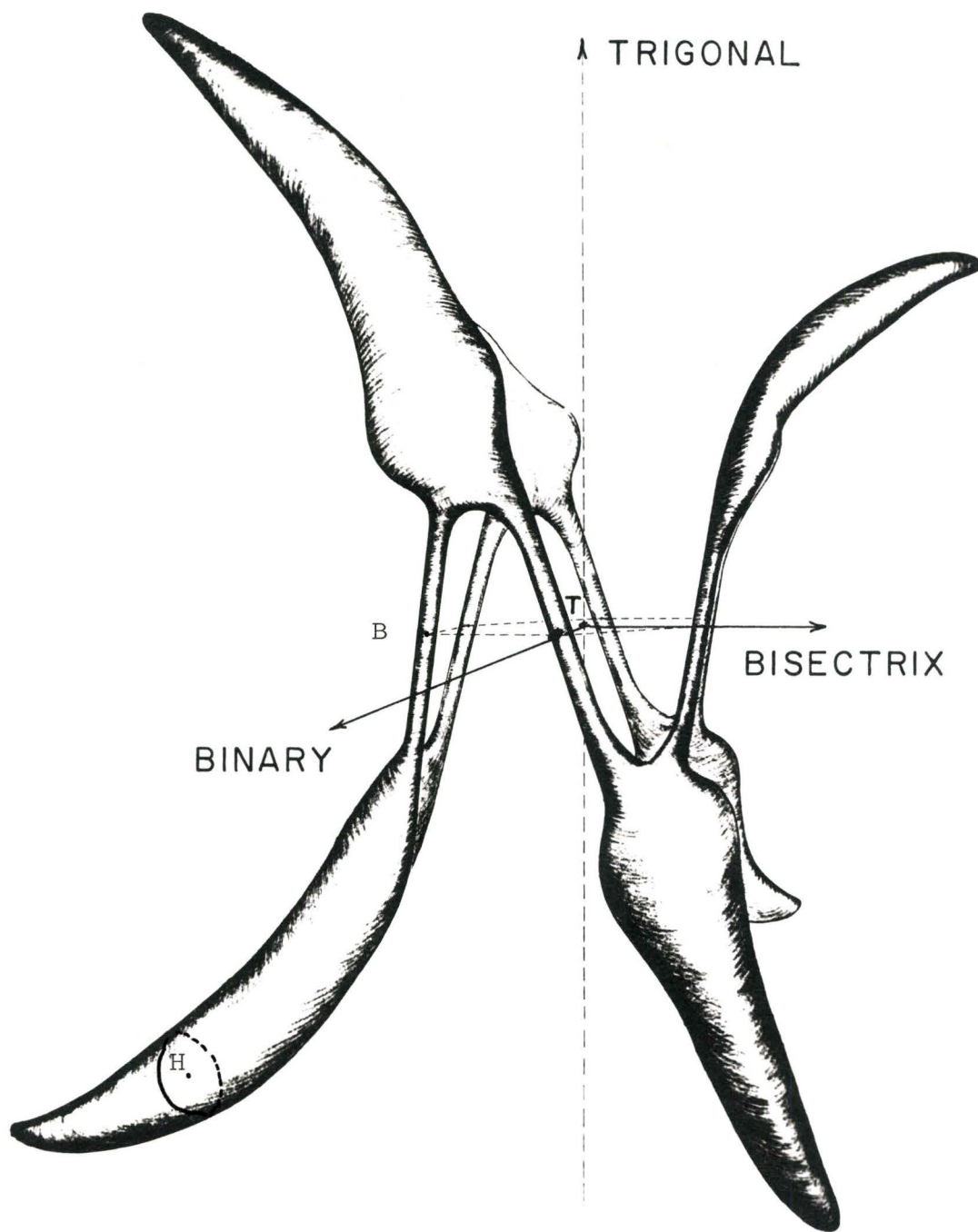
FIGURE III-8

THE HOLE FERMI SURFACE OF ARSENIC

CHAPTER IV

THE DE HAAS-VAN ALPHEN EFFECT IN ARSENIC

THEORY OF THE TORQUE METHOD

The torque on a magnetic dipole M in a magnetic field $\vec{H}$ is given by

$$\vec{T} = \mu(\vec{M} \times \vec{H}) = \vec{M} \times \vec{B} \qquad (IV-1)$$

We shall adopt units such that $\mu = 1$ in our further discussion. If the free energy F of a system is known, then the torque about an axis is

$$T_\Psi = - \left(\frac{\partial F}{\partial \Psi}\right)_H \qquad (IV-2)$$

where Ψ is the angle specifying rotation about the axis in question. Thermodynamically, the magnetic dipole moment of a system whose free energy F is known is

$$\vec{M} = - \left(\frac{\partial F}{\partial \vec{H}}\right)_{T,V} = - \vec{\nabla}_H F. \qquad (IV-3)$$

The torque along the ψ direction can also be written as

$$T_\psi = \hat{n}_\psi \cdot \vec{T} = - \hat{n}_\psi \cdot (\vec{\nabla}_H F \times \vec{H})$$

$$= \hat{n}_\psi \cdot (\vec{H} \times \vec{\nabla}_H F) \qquad (IV-4)$$

where $\hat{n}_\psi$ is a unit vector along the axis about which the torque is measured. These two definitions of torque can be shown to be equivalent.

Torque methods have been extensively used by Shoenberg,[45] who gives a summary of the dHvA effect. The torque will disappear for a certain segment of the Fermi surface if the cross-

44

sectional area is stationary with respect to the angle. These "blind spots" in general exist only for a few degrees around a symmetry axis where the sensitivity will be too low to observe a dHvA oscillation. Also the torque will not have the usual $\sin 2\theta$ angular amplitude dependence of a susceptibility because the magnetic field destroys the electronic symmetry and each piece of the Fermi surface contributes its own oscillations.

In the formula given for the dHvA effect (equation II-17), the only angularly dependent quantities are $\frac{\partial^2 S}{\partial p_H^2}$, the curvature of the Fermi surface, F, the frequency of the oscillations, and m^*, the effective mass. If we calculate the torque by finding $\frac{\partial F}{\partial \psi}$, then a number of terms will result, but the only one of importance will result from the differentiation of the frequency F, since the phase $\frac{2\pi F}{H}$ is usually quite large ($\sim 10^3$) at ordinary fields. If $\frac{\partial F}{\partial \psi} = 0$, then usually the first derivatives of the effective mass and curvature are also zero because of symmetry. Thus the torque is given by

$$T_\psi = 2VkT \left(\frac{eH}{hc}\right)^{3/2} \left|\frac{\partial^2 S}{\partial p_H^2}\right|_{\xi,pm}^{-1/2} \sum_{n=1}^{\infty} \frac{\exp(-2\pi^2 n\, k\, T_D/\beta H)}{n^{3/2}\sinh(2\pi^2 n\, K\, T/\beta H)} \times$$

$$\frac{2\pi n}{H}\left(\frac{\partial F}{\partial \psi}\right) \sin\left[\frac{2\pi nF}{H} - 2\pi n\gamma \mp \frac{\pi}{4}\right] \cos\left(\frac{n\pi g m^*}{2m}\right). \quad \text{(IV-5)}$$

Usually $2\pi^2 kT_D/\beta H \gg 1$ and $2\pi^2 KT/\beta H \gg 1$ and only the fundamental oscillation is of importance. Then the torque amplitude can be written as

$$T_\psi = (\frac{\partial F}{\partial \psi}) \ V \ T \ H^{1/2} \ \frac{e^{-\dfrac{2\pi^2 k(T_D + T)}{\beta H}}}{(1 - e^{-\frac{4\pi^2 kT}{\beta H}})} \ \sin \ (\frac{2\pi F}{H} + \Phi) \ \cos \ (\frac{\pi g m^*}{2m}). \quad (IV-6)$$

This formula will be useful if it is desired to find the effective mass from the temperature dependence of torque amplitude. A_ψ of the torque oscillations is used to plot $\ell n\{\frac{A_\psi}{T}(1 - e^{-\frac{4\pi^2 kT}{\beta H}})\}$ versus T at a specified magnetic field. The slope of this line will be $-\frac{2\pi^2 k}{\beta H}$ where $\beta = \frac{e\hbar}{m^* c}$. The Dingle temperature T_D can be determined once the value of β is determined. A plot of

$\ell n \ \{\frac{A_\psi}{H^{1/2}}(1 - e^{-\frac{4\pi^2 kT}{\beta H}})\}$ versus $\frac{1}{H}$ gives a line whose slope is

$-\frac{2\pi^2 k(T_D + T)}{\beta}$ from which T_D is readily extracted.

For several discussions later on the torque will be expressed as

$$T = \sum_i T_o^i \ (H, \Theta) \ \sin \ (\frac{2\pi F_i}{H}) \quad (IV-7)$$

where $\sum_i$ denotes a sum over all contributing parts of the Fermi surface and $T_o(H, \Theta)$ is a slowly varying function of the magnetic field and its angle with respect to an axis of the crystal. Any quantity derivable from the free energy such as the magnetization can be written similarly,

$$M = \sum_i M_o^i \ (H, \Theta) \ \sin \ (\frac{2\pi F_i}{H}) \ . \quad (IV-8)$$

The phase angle $\delta = - 2\pi\gamma \mp \frac{\pi}{4}$ is neglected in these formulas since usually $\frac{F}{H} \gg 1$ and we are interested only in phenomena which depend on F or H.

TORQUE MAGNETOMETER

The instrument used to measure the torque is a continuously operating electronic torque balance using a Weston model 1411 type 1 inductronic amplifier[46][47]. Condon and Marcus[46] were first to use such a device for dHvA torque measurements. In the present work the magnetometer has been modified and a complete description of the instrument is given. The heart of the system is the inductronic galvanometer movement which is similar to a panel meter except that provision is made for injecting a 200 kilocycle alternating field into the permanent magnetic meter yoke. Figure IV-1 shows a block diagram of the system used as a d.c. amplifier. A low level direct current causes a torque on its moving coil which turns the coil to pick up a 200 kilocycle alternating voltage. This voltage is used to frequency shift the oscillator driving the galvanometer's alternating field. A frequency discriminator gives a signal which, when applied to the galvanometer movable coil, will rebalance the system. If it is desired to measure a torque, the torque can be applied directly to the moving coil, since this torque can be considered to be equivalent to an electrical current flowing through the coil. Terminal A of the galvanometer is the excitation coil. Terminals B and C are actually identical, but the terminal B taps off the high frequency from the moving coil and terminal C is for the direct current from the frequency discriminator. A circuit diagram for the system is shown in Figure IV-2. The feedback loop is drawn in as external wiring and it consists of a range standard (see Figure

Gal. Field Excitation (200KC.)
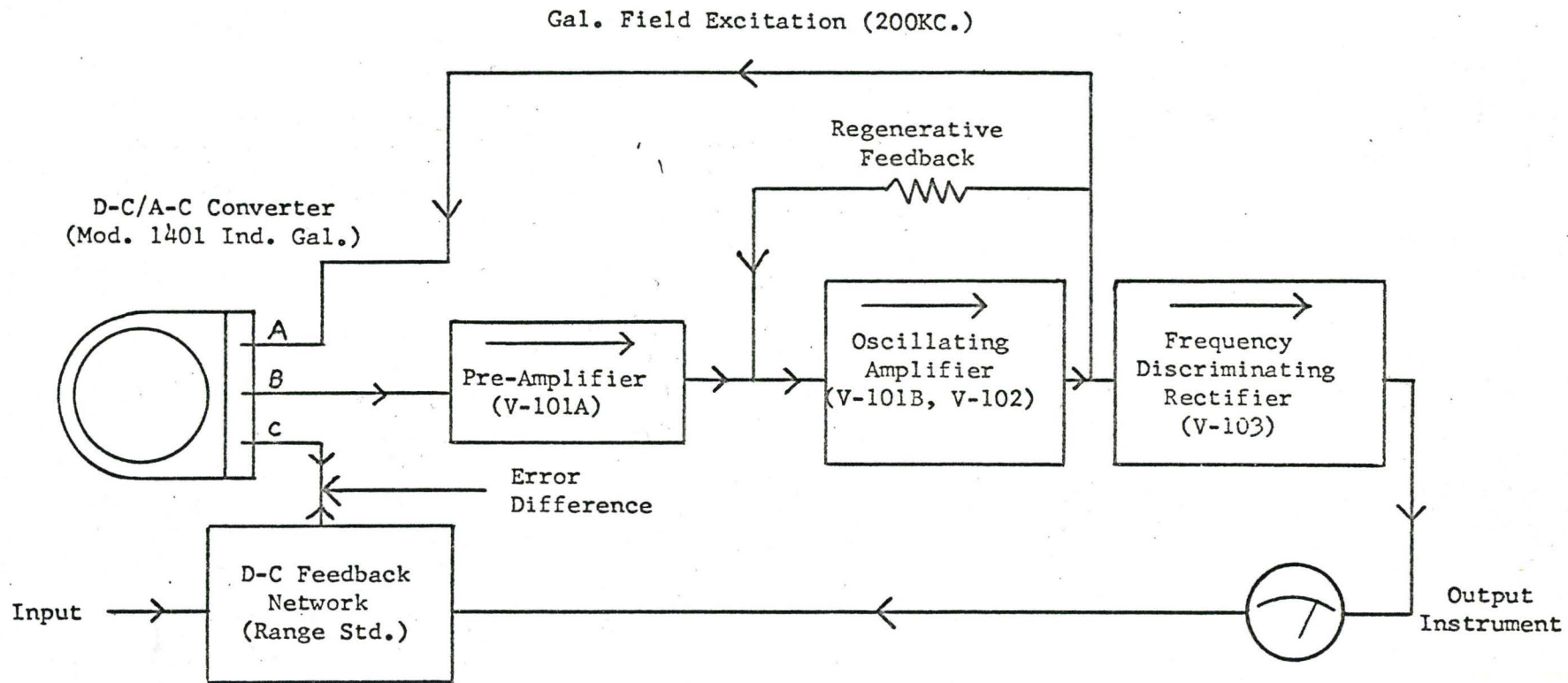
Block Diagram of Inductronic System

FIGURE IV-1
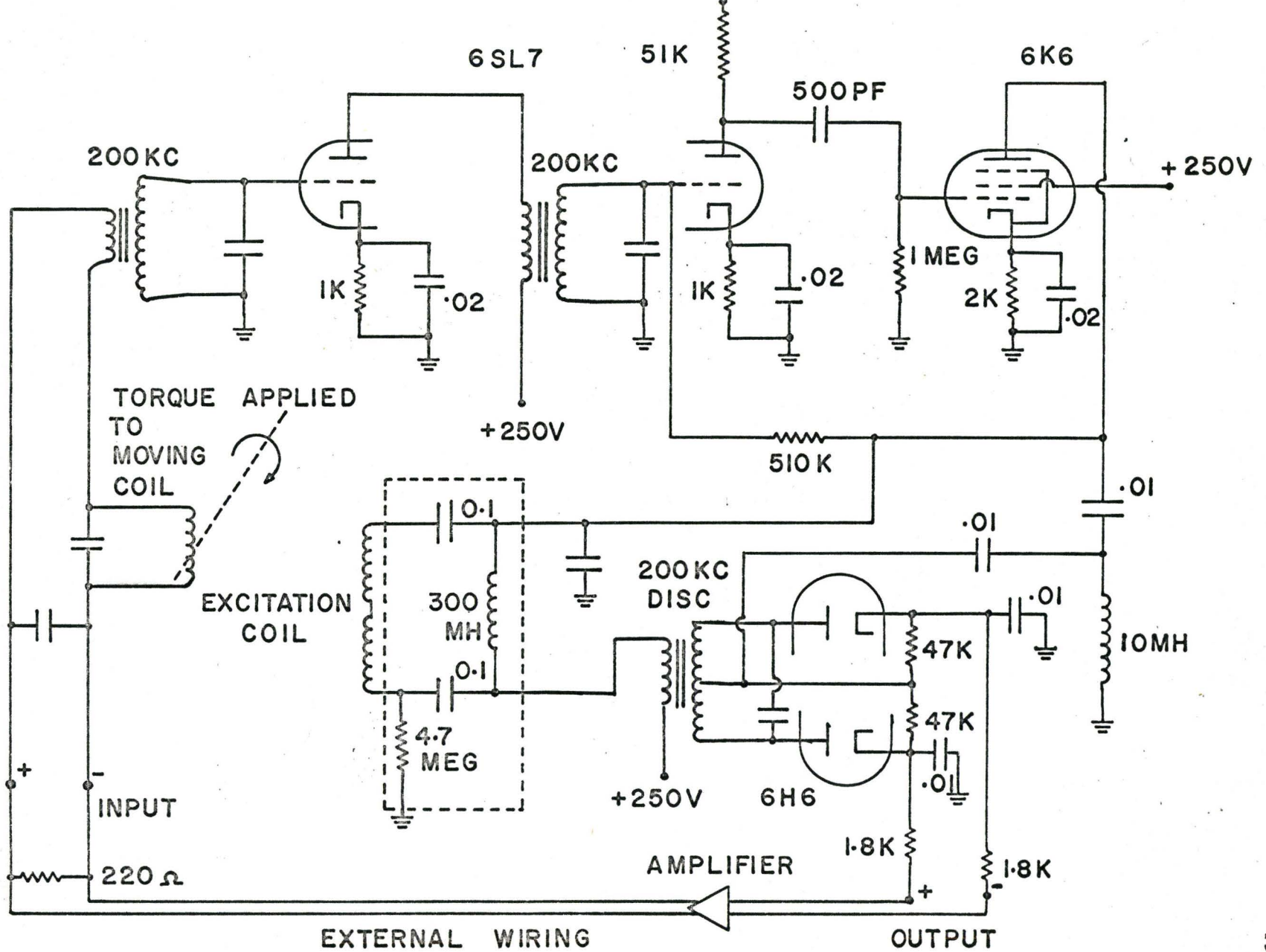
TORQUE MAGNETOMETER SCHEMATIC

FIGURE IV-2

IV-1)which allows the connection of an external feedback loop.
Polarity of the input and output connections is labelled. A
current flowing into the positive input lead causes the moving
coil to shift the frequency of the oscillator such that the
frequency discriminator will deliver a current output at the
positive output terminal. It was found that the original electro-
nics did not have enough gain to make the moving coil very
rigid against the application of dHvA torques. An amplifier
was added as shown in Figure IV-2 and it is shown schematically
in Figure IV-3. This amplifier acts as a buffer so that the
high output impedance frequency discriminator will have its
current amplified before the output is delivered to the 50 ohm
moving galvanometer coil. The two 1N2071 diodes limit the
maximum voltage across the coil to about $\pm$ 0.4 volts. Because
the frequency discriminator has a high output impedance of about
4000 ohms, the gain of the amplifier can be easily adjusted with
the 5000 ohm potentiometer across the two transistor bases.

The following is a detailed account of the circuit action
of the inductronic amplifier. The amplifier section in Figure
IV-2 consisting of the $\frac{1}{2}$ 6SL7 and 6K6 vacuum tubes operates as
a frequency-shift oscillator in which the feedback is provided
by the 510 K resistor. The main frequency determining component
is the second interstage transformer secondary. The oscillator
output is applied to the induction galvanometer to excite the
field. A.-C. developed by the deflection of the movable coil
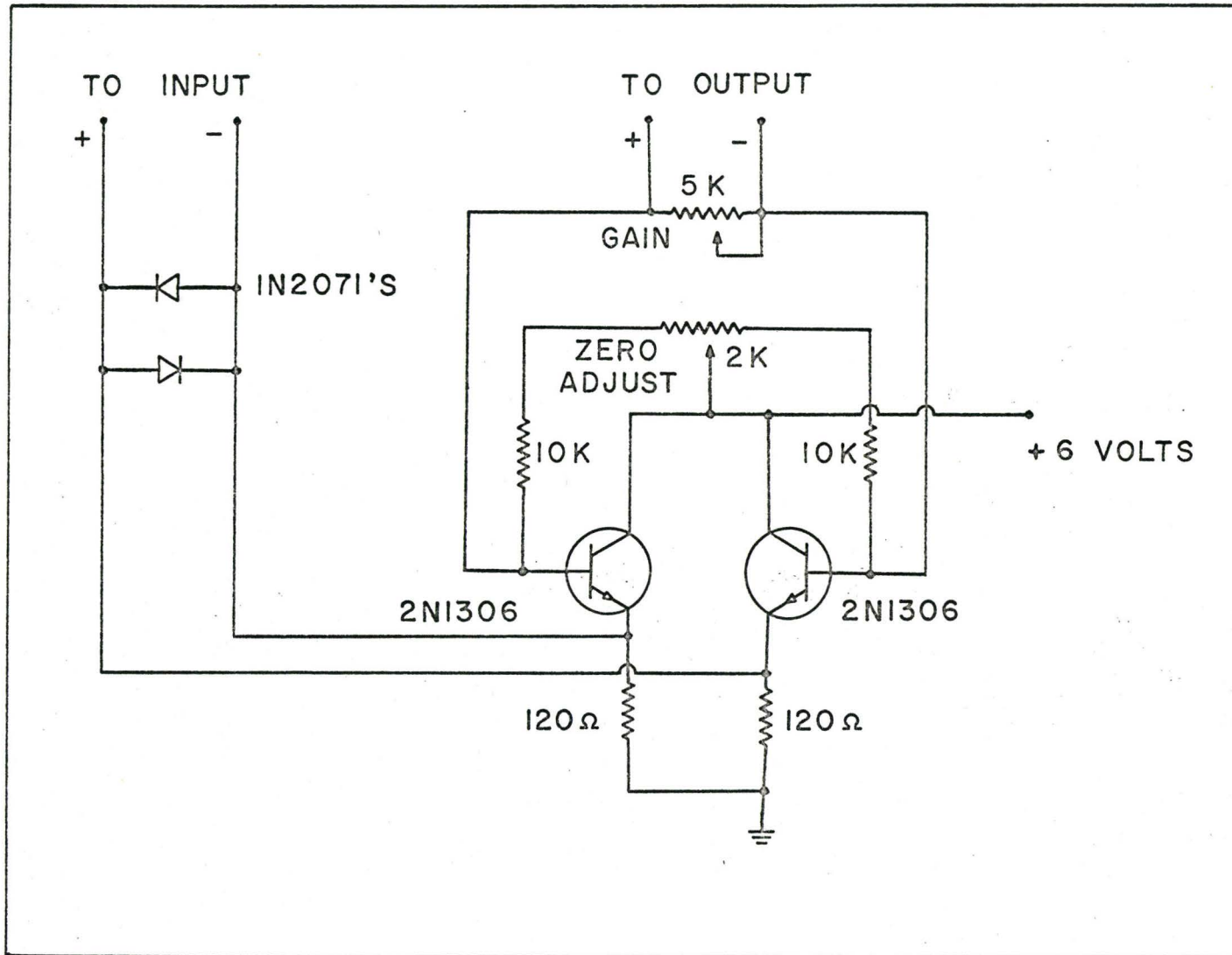
TRANSISTOR CURRENT AMPLIFIER

FIGURE IV-3

is applied via the first interstage transformer to the $\frac{1}{2}$ 6SL7 vacuum tube amplifier, and then fed to the oscillating amplifier as an additional feedback component. Because of the very loose coupling through the galvanometer with small movable coil deflections this feedback component is essentially in quadrature with the feedback through the 510 K resistor; the phase depends on the direction of deflection. This causes the frequency of oscillation to deviate from the centre frequency of 200 kilocycles in a direction and degree proportional to galvanometer deflection. The 6H6 double diode frequency discriminating detector develops an output direct current in response to the frequency shift. This current, after amplification by the transistorized amplifier, is introduced to the movable coil in such a phase as to reduce the deflection of the movable coil.

As a torque magnetometer, the galvanometer movement is employed as a self-balancing torque transducer. A copper (non-magnetic) stirrup is glued to the movable coil and the quartz rod is rigidly attached to the copper. The galvanometer is mounted on top of a dewar so that the quartz rod supporting the sample specimen hangs freely directly below the jewelled bearing of the movable coil. In initial experiments the galvanometer excitation coil had 250 volts D.C. applied to it and arcing would occur to metal vacuum parts as the system was pumped out. This was remedied by the components shown in the dotted rectangle of Figure IV-2. The two capacitors pass all the high frequency alter-

nating currents and block direct current while the inductor
(which should be ferrite because the Q must be high at 200 kilo-
hertz) allows the 6K6 tube to obtain plate current. The resist-
or prevents electrostatic charges from building up. With a
sample mounted, the 5000 ohm potentiometer is increased to just
below the point at which oscillations occur as monitored by an
oscilloscope at the galvanometer movable coil terminals. This
setting provided the magnetometer with the lowest angular com-
pliance, or equivalently, maximum angular stiffness.

The magnetometer was calibrated by applying a specified
torque and measuring the output voltage across the galvanometer
current coil. The torque was applied by a double beam assembly.
One light balsa wood beam was glued to the bottom of the quartz
rod in place of a sample and a second beam of equal length was
suspended from it by two equal lengths of silk thread attached
to the end of the beams. The lower beam was of known mass and
was twisted relative to the upper beam by forces in the horizon-
tal plane. These forces were applied by two silk threads at
right angles to the ends of the lower beam. A diagram of the
assembly is shown below.
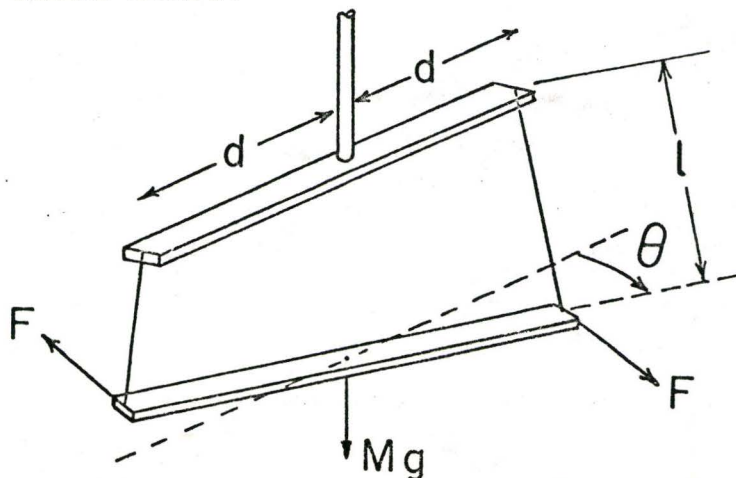
From a force analysis, the torque on the upper beam was determined to be given by

$$T = Mg \frac{d^2 \sin \theta}{\ell \sqrt{1 - \frac{4d^2}{\ell^2} \sin^2 (\frac{\theta}{2})}} \qquad \text{(IV-9)}$$

where M is the mass of the lower beam, g is the acceleration due to gravity, d is the half length of the balsa wood beams, ℓ is the length of the silk thread in the suspension, and θ is the angular displacement of the lower beam relative to the upper beam. The sensitivity at the input to the galvanometer coil was determined to be 0.33 mV/dyne-cm.

The angular compliance of the magnetometer is defined by

$$\eta = \frac{\partial \theta}{\partial T} \qquad \text{(IV-10)}$$

where θ is the angular rotation of the sample and T is the applied torque. It was measured by determining the angular displacement with torque of a small pencil beam spotlight reflected from a mirror that was attached to the end of the quartz rod. This measurement, made at room temperature, was taken to be the compliance of the magnetometer during an experiment. The compliance was 11.4 x 10^{-5} rad/dyne-cm with the original design of Condon and Marcus[46] and this was reduced to 1.42 x 10^{-5} rad/dyne-cm using a 2 mm. quartz rod for sample suspension and the additional amplifier (Figure IV-3) to provide current gain in the feedback loop. The latter was used in the final experiments.

SAMPLE PREPARATION AND QUALITY

The arsenic samples were kindly supplied by Dr. J. B. Taylor of the National Research Council of Canada. Single crystals were grown from high-purity arsenic by a modified Bridgman technique. Analysis showed that Si was one of the chief impurities of the crystal (up to 200 ppm). The residual resistivity ratio of each crystal was approximately 1000. Rectangular samples were cut from a single crystal by cleaving it and then cutting it with a Servomet spark cutter. Orientation was possible by observation of the cleavage face (which is perpendicular to the trigonal axis) and striations on the surface of this face which are parallel to binary axes. In certain cases the striations were not visible enough and back-reflection x-ray Laue methods were used. Samples were mounted on the quartz rod in a simple holder and attached with G.E. Glyptal cement or 7031 varnish.

Samples in general exhibited a great deal of asterism in the Laue photographs, indicating that the surfaces were not very good. The surfaces used for x-ray study usually were cleavage planes, and it may be that cleaving leaves the surface damaged. Also, the crystals were grown in thick-walled quartz tubes which, on cooling, could strain crystals due to differential thermal expansion. Several samples were subjected to metallurgical compression tests along the trigonal axis and it was found that plastic flow occurred for almost no applied

load. The effect had some of the characteristics of a Bausch-
inger strain[48], but a better explanation was felt to be that
microcracks or voids were introduced into the crystals by the
method of growth in quartz tubes. In any event, the crystals,
though pure, seemed to be highly strained. Unstrained crystals
grown by Ketterson and Eckstein[39] in a large quartz bomb were
used in the dHvA experiments of Priestley et al[40]. The fact
that they observe more of the electron Fermi surface than the
experiments of Williamson[38] and ourselves may well be due to
a greater amount of imperfections in the crystals of the latter
two experiments.

EXPERIMENTAL APPARATUS AND TECHNIQUES

Torque experiments employed the tor que magnetometer
described earlier, using a quartz rod to transmit the torque
from the sample to the torque transducer. The rod hung in a
helium cryostat which had a vacuum housing at the top for the
transducer. Electrical leads were brought out through vacuum
kovar seals and a helium transfer entrance and pumping line were
provided. The tail of the cryostat dewar was placed between
the pole faces of a large electromagnet so that the arsenic
sample hung on the quartz rod precisely in the region where the
magnetic field was quite homogeneous. Liquid helium was trans-
ferred into the cryostat and the temperature of the bath was
reduced to 1.2°K by lowering the vapour pressure above the liquid.

The electromagnet was provided with tapered pole tips having an air gap of two inches. This gave a maximum field of 24 kilogauss. Pole tips of an alloy of 35% Co and 65% Fe were used to give a field of 33 kilogauss in a one-inch gap. The magnet power supply was current controlled and possessed extremely poor linearity at high fields. This was remedied by winding a pickup coil of 2500 turns around one of the pole tips and utilizing an operational amplifier connected to the power supply regulator circuitry such that the rate of change of total flux through the coil could be maintained constant. As added benefit the sweep speed was instantly adjustable to any value by purely electronic means. Most data were taken with the field increasing uniformly with time while the signal was recorded on a strip chart recorder. The magnetic field intensity was measured to an accuracy of about 0.5% with a Rawson-Lush rotating coil gaussmeter that was calibrated by NMR and by ESR of diphenyl picryl hydrazl (DPPH) at a frequency of 35 GHz. An electronic attachment was designed and built for the gaussmeter which emitted a signal pulse each time that the field increased by one kilogauss. This signal pulse was added in series with the dHvA signal and the resulting "pips" served as accurate field markers. In many cases there were large steady torques which varied with the square of the applied field. These were bucked out by deriving a voltage proportional to the square of the field from two Hall probes placed in the field. One was driven from a bat-

tery. Its output varied as H and was used as the current source for the second probe. The output of the second varied as H^2 and was put in series opposition to the signal from the torque magnetometer.

Experiments were also done by varying the magnetic field orientation while keeping its magnitude fixed. A motor and chain drive were used to rotate the magnet uniformly. This method of obtaining data is discussed more fully in the section on angular rotation. After the magnetometer was made more rigid, the mechanical mass of the system did not limit the response to very low frequencies, and it became possible to do experiments in which the magnetic field was modulated at low audio frequencies. A Princeton Applied Research HR-8 lock-in amplifier was used to synchronously detect the torque signal which was modulated with a vector modulation in the plane of rotation of the electromagnet. Two perpendicular sets of coils and a two channel power amplifier supplied the modulation, using the internal oscillator of the lock-in amplifier. A detailed discussion is given in the section on modulation theory.

Magnetothermal or magnetocaloric experiments were done using a two inch magnet air gap. The sample was cooled to $1.3^{\circ}K$ in a vacuum sealed can. These experiments are described in detail in Chapter V. Magnetoresistance experiments were also done in a 55 kilogauss Westinghouse superconducting magnet, employing D.C. methods to measure the effect. The sample turning

mechanism fitted inside an inner helium dewar with inside
diameter of 0.82 inch. This dewar fitted into the solenoidal
magnet which had its own liquid helium dewar. More details
are presented in Chapter V.

ANALYSIS OF THE DATA

Since most of the data for bismuth, antimony[49] and
arsenic[32][38] is in terms of periods rather than frequen-
cies, this convention will be maintained to facilitate compari-
son of the data. dHvA frequency can be obtained from the
reciprocal of the period, $F = 1/P$. From the data, the number
of oscillations n is counted between two magnetic fields H_1
and H_2. The period is then defined as

$$p = \left(\frac{\frac{1}{H_1} - \frac{1}{H_2}}{n} \right),$$

$\qquad$ (IV-11)

in units of gauss^{-1}. This procedure yields accurate results if
many oscillations can be counted over a considerable field
interval. In the case of the long periods this is not true
and the procedure there adopted is to plot maxima and minima of
an oscillation as odd and even integers against the values of
reciprocal fields for the maxima or minima. The slope of the
line drawn through the experimental points gives P, or, equiv-
alently, F.

If there are two oscillations which occur together, beats
are formed. The beat can be characterized by a period P_B such

that each maximum of the envelope marks another beat oscillation. The two periods present are then related by

$$P_2 = \frac{P_1 \, P_B}{P_1 \pm P_B} \, , \qquad \qquad (IV-12)$$

where the ambiguity caused by the sign is a result of our inability to tell which period is larger. A detailed analysis can be done on one beat envelope to determine the sign, but for consistency of the data it is usually easy to determine which sign is required. A good first guess is that higher periods are more dominant since they occur from small extremal areas and generally have smaller effective masses. This results in a larger amplitude. Near a symmetry axis of a Fermi surface segment the torque generally disappears and lower periods not having the same symmetries may become dominant.

A typical recorder trace of the torque on an arsenic sample as a function of magnetic field is shown in Figure IV-4. It displays five important features of the dHvA effect in arsenic. The most notable features are the short period oscillations and the beat pattern that they produce. They have a period of about 5×10^{-7} gauss^{-1} or a frequency of 2×10^{6} gauss. There are also long period oscillations with a period of about 2.5×10^{-5} gauss^{-1} or a frequency of 4×10^{4} gauss. These beat, producing a beat pattern which extends over many kilogauss per beat. Finally, the torque has a component that is steady and varies precisely with the square of the applied field. This steady diamagnetic term is the result of a slightly temperature dependent

ARSENIC
DE HAAS VAN ALPHEN EFFECT

A typical curve showing
the de Haas-van Alphen effect in
Arsenic for a magnetic field
direction in the bisectrix-trigonal
plane.

MAGNETIC FIELD- KILOGAUSSES

TORQUE - ARBITRARY UNITS
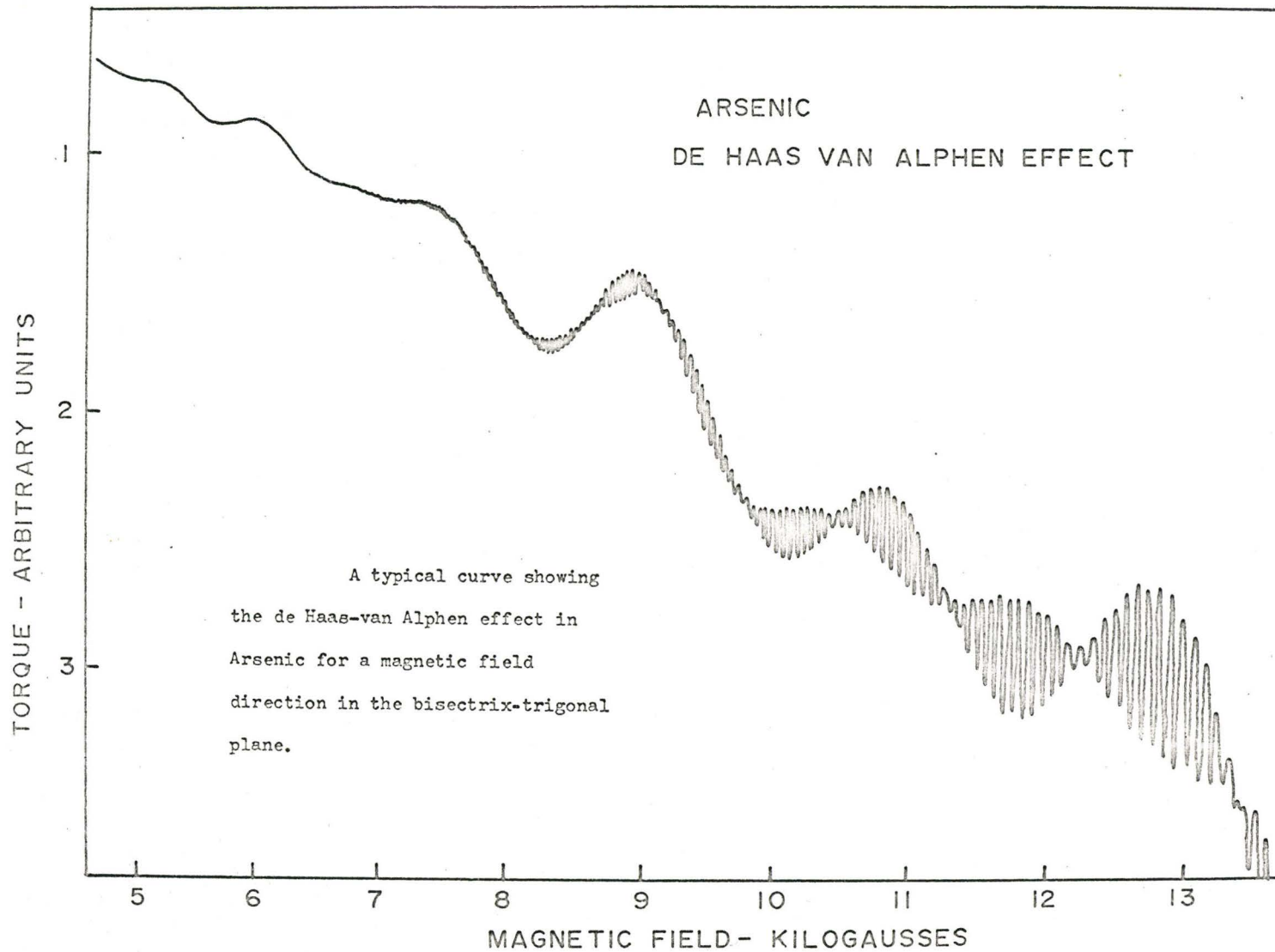
FIGURE IV-4

magnetic anisotropy in arsenic. It is contributed by the lowest Landau levels in the Fermi surface from contributions when S = 0 (Chapter II). Berlincourt[32] measured a temperature dependence which is identical to the values noted by us. His values for $\chi_{\parallel} - \chi_{\perp}$, the susceptibilities parallel and perpendicular to the trigonal axis, are given for three temperatures. These values have the wrong sign, as has been pointed out[50]. Correcting the sign, the values for $(\chi_{\parallel} - \chi_{\perp})$ and the thermal energies kT are:

$^\circ$K	$\chi_{\parallel} - \chi_{\perp}$		kT	
300	0.54		0.41	
77	0.80	x 10^{-6} emu/g	0.106	x 10^{-13} ergs
4.2	0.91		0.0058	

Although arsenic is paramagnetic at low temperatures and becomes diamagnetic at ~ 90°K[50], the paramagnetic susceptibility will not have as much angular dependence as does the diamagnetic contribution. Thus the values of $(\chi_{\parallel} - \chi_{\perp})$ are a good indication of the temperature dependence of the diamagnetism. According to Lifshitz and Kosevich[10], this depends on the peak points of the Fermi surface S = 0. Thus we expect the diamagnetic effects from the sharp peak points of the hole surface as predicted by Lin and Falicov (Figure III-8). The electron surfaces are ellipsoids with much less curvature, and will have far greater values of $(\frac{\partial S}{\partial p_0})$ at the peak points. This derivative occurs in the denominator of the integral expression for the

non-oscillatory part of the free energy. (See reference 10, equation P.1). A glance at the values of the thermal energies shows that the Fermi energy which characterizes the peak points must be of the order of 10^{-13} ergs.

A more accurate analysis is not warranted as yet because the theoretical formulas are not certain. It is of interest to note that the Fermi energy characterizing the cylinders in the Fermi surface is about 1.6×10^{-14} ergs, and these carriers may also contribute to diamagnetic effects.

Several other important details of data analysis are discussed in this chapter in sections for which they are more relevant.

TILT ANGLE DETERMINATION

In the experiments of Berlincourt[32] and later of Shapira and Williamson[38], there is an ambiguity in the sign of the tilt angles of the assigned pieces of the Fermi surface. In the trigonal-bisectrix (y-z) plane the directions labelled ΓX and ΓL distinguish the two bisectrix axes from each other. (Figure III-1). In arsenic the angle between ΓT and ΓX is $58°17'$ and the angle between ΓT and ΓL is $72°50'$. The convention of Shoenberg[51] and Berlincourt[32] will be unified with the definition of the theoretical papers[30][42]; all angles will be positive in the sense of a rotation from ΓT $(0°)$ to X $(58°17')$.

This present work was checked for the proper tilt angle determination by taking back reflection x-ray Laué pictures on either side of the trigonal axis to obtain the proper symmetry at the ΓX and ΓL directions. A Laué picture in the ΓX direction shows two rows of spots at precise right angles. In the ΓL direction there is pseudo-trigonal (sometimes called pseudo-hexagonal) symmetry, with angles of approximately 63.5°, 54°, and 62.5° between rows of spots. The directions are labelled on all the ΓX and ΓL data for the trigonal-bisectrix planes. The tilt angle of a Fermi surface pocket will be defined as the angle from the trigonal axis of the long direction of the pocket. This will correspond to the direction of maximum period, which is the direction of minimum extremal area of the Fermi surface.

TORQUE MODULATION

The dHvA data usually consist of one dominant oscillatory term and several lesser terms. In order to observe the small amplitude oscillations, a method of discrimination must be used to reduce or null the amplitude of the large unwanted signal. Higher frequency oscillations (larger segments of the Fermi surface) usually have larger effective masses (smaller β) which reduces the dHvA amplitude. Time differentiation of the signal as the field is swept can be employed to increase the amplitude of these higher frequency oscillations with respect

to the dominant one at lower frequency in the ratio of frequencies. Multiple differentiation has been used by some experimenters[52]. This method was used in the present experiments but noise components at higher frequencies caused the differentiated signal to have no advantage over the original signal.

The method used for discrimination is similar to a method described by Windmiller[49] using vector modulation techniques. Let us modulate the magnetic field at an angle α with respect to the D.C. magnetic field. If the torque magnetometer response time τ is considerably less than $1/f_{mod}$, then the torque can be represented by the simple relation

$$T = T_o(H) \sin \left(\frac{2\pi F(\Theta)}{H}\right) . \qquad (IV-13)$$

The angle which the resultant magnetic field $\vec{H}$ makes with the crystal axis is (to first order in h_m/H_o)

$$\Theta \cong \Theta_o + \frac{h_m \sin \omega t}{H_o} \sin \alpha \qquad (IV-14)$$

where h_m is the amplitude of the modulating field, and ω is its frequency. The magnitude of the resultant field is

$$H = |\vec{H}| \cong H_o + h_m \sin \omega t \cos \alpha , \qquad (IV-15)$$

again to first order. Assuming that both $\frac{\partial T_o}{\partial \Theta}$ and $\frac{\partial T_o}{\partial H}$ are very
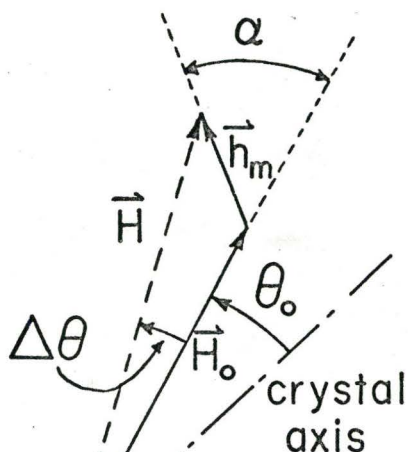
small compared with differentiation of the rapidly oscillating sinusoid, the torque is

$$T \cong T_o(H_o) \sin \frac{2\pi(F_o + \frac{\partial F}{\partial \Theta} \frac{h_m \sin \omega t}{H_o} \sin \alpha)}{H_o + h_m \sin \omega t \cos \alpha}$$

which becomes, upon using the binomial expansion,

$$T \cong T_o(H_o) \sin \frac{2\pi F_o}{H_o} (1 + \frac{1}{F_o} \frac{\partial F}{\partial \Theta} \frac{h_m \sin \omega t}{H_o} \sin \alpha - \frac{h_m}{H_o} \sin \omega t \cos \alpha) \quad \text{(IV-16)}$$

If we let $\quad \xi = \frac{2\pi F_o}{H_o} \left(\frac{1}{F_o} (\frac{\partial F}{\partial \Theta}) \sin \alpha - \cos \alpha \right) \frac{h_m}{H_o} \quad \text{(IV-17)}$

$$T \cong T_o(H_o) \sin \left(\frac{2\pi F_o}{H_o} + \xi \sin \omega t \right)$$

$$= T_o(H_o) [\sin \frac{2\pi F_o}{H_o} \cos (\xi \sin \omega t) + \cos \frac{2\pi F_o}{H_o} \sin(\xi \sin \omega t)]$$

$$T = T_o(H_o) \left[\sin(\frac{2\pi F_o}{H_o}) \left(J_o(\xi) + 2 \sum_{n=1}^{\infty} J_{2n} (\xi) \cos 2n\omega t \right) \right.$$

$$\left. + \cos (\frac{2\pi F_o}{H_o}) \quad 2 \sum_{n=0}^{\infty} J_{2n+1}(\xi) \sin(2n+1)\omega t \right] \quad \text{(IV-18)}$$

Physically, ξ is the amplitude of the phase modulation and it appears as argument in the Bessel functions.[53] These functions give the amplitude of the harmonics generated by the non-linear torque versus field curve. The harmonic of interest to us is the fundamental, since higher frequencies are usually attenuated by the magnetometer or occur near mechanical resonances of the system. The D.C. component detected by a phase sensitive detector

will be equal to $2\,T_O(H_O)\,\cos\dfrac{2\pi F_O}{H_O}\,J_1(\xi)$. If it is desired to discriminate against this dHvA oscillation two methods are available. The zeroes of $J_1(x)$ occur for $x = 0, 3.832, 7.016,$ --- so that if the amplitude of modulation is chosen to make $\xi = 3.832$, for example, the signal at frequency ω will be zero for the particular single dHvA oscillation we are considering. Other frequencies are not likely to have their factor ξ such that $J_1(\xi) = 0$. If the modulation angle is zero as in ordinary modulation ($\alpha = 0$), then for $\xi = 3.832$, $F_O = 2 \times 10^6$ Gauss and $H_O = 20$ kilogauss, we find $h_m \simeq 100$ gauss and this value of modulation is rather large. It becomes a useful method if a high frequency component is dominant, but this does not normally happen. In order to keep ξ constant as the field is varied, the modulation amplitude must be proportional to H_O^2.

An important deduction is the following. If $\xi \ll 1$, as is usually the case, $J_p(\xi) \simeq K\xi^p$ where $K = \dfrac{2^{-p}}{p!}$, so that

$$\xi = \frac{2\pi F_O}{H_O}\left\{\ \frac{1}{F_O}(\tfrac{\partial F}{\partial\theta})\ \sin\alpha\ -\ \cos\alpha\right\}\frac{h_m}{H_O}\ =\ 0 \qquad\text{(IV-19)}$$

gives the condition for this oscillation to vanish. A trivial solution is to set $h_m = 0$, but this means that there is no modulation. The modulation angle α can be varied to a value α_O such that the curly bracket vanishes.

$$\frac{1}{F_O}\ (\tfrac{\partial F}{\partial\theta})\ \sin\alpha_O\ -\ \cos\alpha_O\ =\ 0\ .$$

This gives the condition to discriminate completely against any dHvA frequency F;

$$\frac{1}{F} \left(\frac{\partial F}{\partial \theta}\right) = \cot \alpha_0 \quad . \tag{IV-20}$$

It is easy to see that at this modulation angle, the phase of $\frac{2\pi F}{H}$ is stationary for changes in the modulation field.

If it is desired to maximize the output of a certain oscillation for ξ small, we must maximize ξ . Thus

$$\frac{d\xi}{d\alpha}\bigg|_{\alpha_{\pm}} = 0 = \frac{1}{F_0} \left(\frac{\partial F}{\partial \theta}\right) \cos \alpha_{\pm} + \sin \alpha_{\pm} = 0$$

giving

$$\frac{1}{F_0} \left(\frac{\partial F}{\partial \theta}\right) = \cot \left(\alpha_{\pm} \pm \frac{\pi}{2}\right) \tag{IV-21}$$

as the condition on the modulation angle $\alpha_{\pm}$ to maximize the signal. It is obvious that for any single oscillation the modulation angles for maximum signal and no signal are at right angles. ($\alpha_0 = \alpha_{\pm} \pm \frac{\pi}{2}$). In order that a certain oscillation not be over-modulated, ξ for it must be kept less than 2, which approximately causes a maximum for $J_1(\xi)$. Thus we have the inequality

$$\left| \frac{2\pi F}{H} \left\{ \frac{1}{F} \left(\frac{\partial F}{\partial \theta}\right) \sin \alpha - \cos \alpha \right\} \frac{h_m}{H_0} \right| < 2 \quad . \tag{IV-22}$$

Since the modulation angle is not set to any specific angle for this oscillation, the maximum of the curly bracket gives the maximum value of h_m such that the inequality is always satisfied. This means that $\alpha = \alpha_{\pm}$. The maximum absolute value of the bracket is $\left[\frac{1}{F^2}\left(\frac{\partial F}{\partial \theta}\right)^2 + 1\right]^{1/2}$ so the condition that an oscillation not be overmodulated reduces to

$$\frac{h_m}{H_0} < \frac{H_0}{\pi} \left[\left(\frac{\partial F}{\partial \theta}\right)^2 + F_0^2\right]^{-1/2} \quad . \tag{IV-23}$$

The major disadvantage of modulation methods applied to torque magnetometers is that even small applied modulation fields cause appreciable eddy currents. These eddy currents cause oscillatory torques since the shape of the sample and its tensorial conductivity cause the magnetization to be turned away from the magnetic field direction. Large torques occurring at the fundamental modulation frequency can be largely eliminated by using a cylindrically shaped sample and by adjusting properly the phase of the synchronous detector. Eddy current effects are generally 90° out of phase compared to the true oscillatory dHvA torques.

Modulation frequencies were chosen so that mechanical resonances of high Q-factor did not occur near frequencies of the fundamental and first few harmonics. 35 Hertz was commonly chosen as the best operating frequency. The coils used in modulation were perpendicular to each other, driven by a two channel amplifier with independent gain controls and a polarity reversing switch to one channel so that all modulation angles were possible. It was possible to null dominant oscillations with the technique and observe weaker oscillations, especially in the trigonal-bisectrix plane. Long period oscillations could not be adequately observed because the modulation depth could not be increased above approximately 10 gauss without severe distortion of the preamplifier in the lock-in amplifier. Another difficulty with the method is that for some orientations

the desired signal has very nearly the same value of $\frac{1}{F}$ $(\frac{\partial F}{\partial \theta})$
as the dominant signal, and it is hence impossible to reduce
one with respect to the other.

ANGULAR ROTATION

A valuable way to obtain dHvA data is to observe oscil-
lations at a fixed magnetic field as a function of the orientat-
ion of the magnetic field with respect to the crystal axes. In
this way the variations in extremal area are mapped out directly.
The electromagnet was rotated slowly by a motor and chain drive.
One dHvA frequency, which is then a reference frequency, must
be determined at a specific angle θ_o by sweeping the magnetic
field at constant field orientation. Each oscillation recorded
means that the phase of cos $(\frac{2\pi F}{H})$ has changed by 2π . If n
oscillations occur, the dHvA frequency F at the new orientation
is related to the reference dHvA frequency F_o by the equation

$$F(\theta) - F_o(\theta_o) = \pm n H_o \qquad (IV-24)$$

where H_o is the constant value of the magnetic field. The cor-
rect sign is chosen on the basis of preliminary experiments
which determine whether the extremal areas increase or decrease
for a specific rotation of the field direction. Several oscil-
lations can usually be followed simultaneously if they are dis-
tinctly different in oscillation rate as the field direction
rotates.

An important situation arises when the field rotates through an angle β at which the dHvA frequency is stationary, that is,

$$\left(\frac{\partial F}{\partial \Theta}\right)_{\Theta=\beta} = 0 \qquad \text{(IV-25)}$$

If the torque is being measured, it will reverse phase by π on passing the angle β . Suppose, for example, that the dHvA frequency F is given by

$$F \simeq F_O [1 + k (\Theta - \beta)^2] \qquad \text{(IV-26)}$$

at a maximum $(k<0)$ or minimum $(k>0)$ extremal area. The free energy is then proportional to

$$F \quad \alpha \quad \cos \left(\frac{2\pi F_O [1 + k(\Theta-\beta)^2]}{H}\right) .$$

The torque $T = - \left(\frac{\partial F}{\partial \Theta}\right)$ will be proportional to

$$T \quad \alpha \quad k(\Theta-\beta) \quad \sin \frac{2\pi F_O [1 + k(\Theta-\beta)^2]}{H} \qquad \text{(IV-27)}$$

which will reverse phase as Θ passes through the angle β . When this is taken into account, such situations are easily analyzed. Experiments which do not depend on the angular derivative, such as the magnetothermal effect or a measure of the magnetization, will not suffer a phase change as a stationary point is passed.

In general the constant magnetic field, at which the rotation experiments are performed, should be as low as possible, but such that the desired oscillation can be easily followed. This gives a higher density of points on the plots of $F(\Theta)$, which are usually the end product of dHvA data.

DIFFERENTIAL SUSCEPTIBILITY EXPERIMENTS

An experiment will be briefly described which was performed on arsenic to see if the experiments of Williamson[38] could be improved. This measurement consisted of a modulation method employing a pick-up coil containing the sample, essentially as described by Goldstein et al[21]. The acquisition of a 55 kG Westinghouse superconducting magnet allowed these experiments to be carried out to relatively high fields.

The sample turning mechanism and modulation pick-up coil assembly were made by Mr. John Moss of this laboratory for his own studies. A power supply was built for the magnet which allowed reasonably linear field sweeps versus time[54]. The principle of operation is that the magnet, when superconducting, has characteristics at low sweep rates that approximate an ideal inductor. This means that if the voltage across such a magnet is maintained constant, then the current i will change relatively linearly with time as predicted by

$$v = L \frac{di}{dt} , \qquad (IV-28)$$

where L is the inductance of the solenoid. For restricted field sweeps the linearity of current with time is within 1% of a straight line and the field is probably linear to within 2%. Since the power supply has remote voltage sensing leads to the superconducting wires themselves, a field sensing pickup coil at the centre of the solenoid could have been constructed to allow truly linear field sweeps. This was not deemed necessary in the present experiments.

A schematic diagram of the circuit is shown in Figure IV-5, designed for a 55 kG, 15 ampere solenoid with an inductance of 50 Henrys and a minimum energization time of 3 minutes.

Experiments were performed on arsenic in the trigonal-bisectrix plane, using modulation frequencies between 10 Hertz and 5000 Hertz. The amplitude of modulation was restricted to < 10 gauss since the modulation coil was placed inside the inner dewar. Higher modulation fields led to excess liquid helium boil-off rates. The best modulation frequencies tended to be in the region of a few hundred Hertz. At very high frequencies the two halves of the pick-up coil could not be adequately balanced. Low frequencies tended to lower the sensitivity of the apparatus. In a survey experiment the results were not improved over the dHvA studies of Williamson[38] using similar methods and the experiments were discontinued.

One point worth noting in the experiments was that the amplitude of oscillations was often maximum at a field near 30 to 40 kilogauss, using a constant modulation depth. This is interpreted as evidence that the measured quantity $\frac{dM}{dH} = \frac{-d}{dH} \left(\frac{\partial F}{\partial H} \right)$ varies as given by

$$\frac{dM}{dH} \alpha \; H^{-3/2} \; \frac{e^{-\frac{2\pi^2 k T_D}{\beta H}}}{\sinh \left(\frac{2\pi^2 KT}{H} \right)} \; \cos \frac{2\pi F}{H} \qquad \text{(IV-29)}$$

if only the first dHvA harmonic is considered. There will be a maximum for this quantity as the field is increased. If it
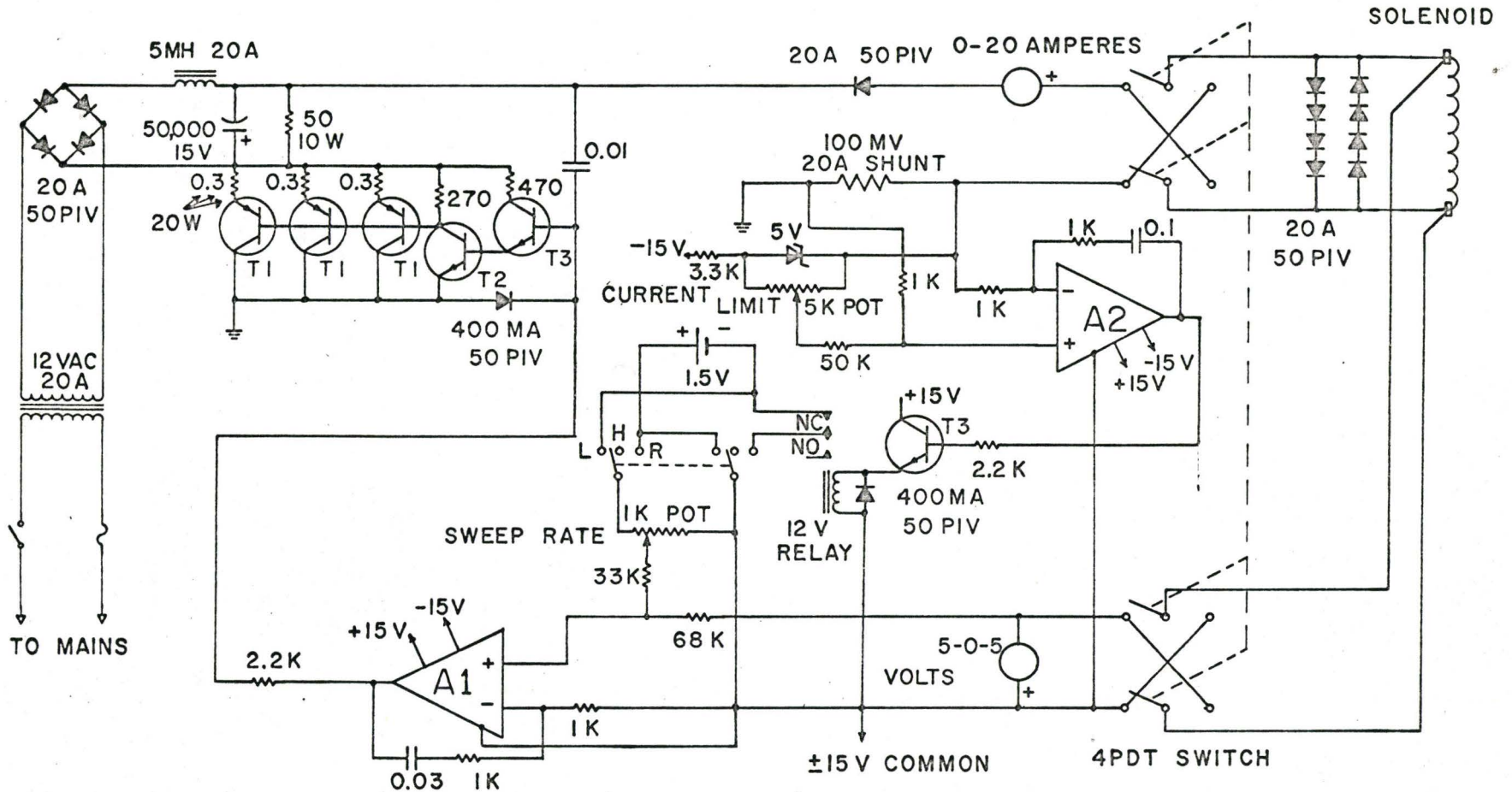
ALL CAPACITORS IN MICROFARADS , ALL RESISTORS IN OHMS AT ONE WATT UNLESS MARKED
T1 = 2N278 , T2 = RCA 40250 , T3 = 2N3405 , A1-A2 = PHILBRICK P65AU OPERATIONAL AMPLIFIER

FIGURE IV-5

74

is assumed that

$$\frac{2\pi^2 k(T_D + T)}{\beta H} < 1,$$
(IV-30)

then it is easy to show that the maximum amplitude of oscillations will occur for a field such that (approximately)

$$H_{max} \simeq \frac{2\pi^2 k(T_D + T)}{\beta}.$$
(IV-31)

Substituting values of β and T_D common to arsenic gives values for H_{max} of 50 kilogauss, which is in reasonable accord with observations. The physical reason for the maximum is that although the amplitude of the free energy and magnetization oscillations increase with field, the frequency in the variable H changes as $\frac{1}{H^2}$ due to the cos $\frac{2\pi F}{H}$ factor. Oscillations become spread out as H increases and the small constant modulation depth causes less change in the phase $\frac{2\pi F}{H}$.

NON-LINEAR EFFECTS

This section contains detailed study and observations on an effect found in torque measurements of the dHvA oscillations in arsenic. It will be advantageous to recall the non-linear effects which have been summarized in the first two chapters. In semi-metals there may be shifts of the Fermi energy at high magnetic fields as observed in bismuth by Smith et al[28]. The shift occurs when only a few Landau levels are below the Fermi energy. The Fermi energy itself oscillates to preserve charge neutrality since the hole and electron surfaces have

different shapes. This causes a frequency modulation of the subdominant oscillations by those which are responsible for the energy shifts.

A second equally fundamental effect was proposed by Shoenberg[12] and discussed by Pippard[14]. The actual field which the conduction electrons experience is $\vec{B}$, not $\vec{H}$, and thus $\vec{H}$ must be replaced by $\vec{H} + 4\pi\vec{M}$ in the formula for the magnetization. Using the magnetization formula in the simple form for a single oscillation we have

$$M = M_o(H,T) \sin \frac{2\pi F}{B}$$

$$= M_o(H,T) \sin \left(\frac{2\pi F}{H + 4\pi M}\right) \qquad \text{(IV-32)}$$

where $M_o(H,T)$ is a slowly varying function of the field (disregarding the distinction between B and H) and the temperature. Since $\frac{M}{H} \ll 1$, the above equation can be written as

$$y = a \sin(x - y) \qquad \text{(IV-33)}$$

where

$$y = \frac{8\pi^2 FM}{H^2}$$

$$x = \frac{2\pi F}{H} \qquad \text{and} \qquad a = \frac{8\pi^2 FM_o}{H^2} .$$

This equation has non-sinusoidal solutions for $y = y(x)$. If $|a| > 1$, the solution is multivalued. Step discontinuities will occur which are smoothed by eddy currents that flow in the sample due to the rapid change in M[14]. If some segment of the Fermi

surface produces a dominant magnetization, it will sinusoidal-
ly alter the $\vec{B}$ seen by the subdominant carriers, whose dHvA os-
cillations will have a frequency modulation by the dominant
oscillation in a manner quite analagous to that caused by an
oscillatory Fermi energy. The resulting extraneous frequencies
have been observed in antimony by Windmiller[49].

The theory of the dHvA effect by Lifshitz and Kosevich[10]
predicts harmonic frequencies, but these are of low amplitude
except at extremely low temperatures or high magnetic fields.
They occur in arsenic because effective masses and cross-
sectional areas of the Fermi surface are both low. Character-
istic of the non-linearity caused by an oscillatory Fermi energy
is that it occurs under much the same conditions as the theor-
etical dHvA harmonics, while the B-H effect is only appreciable
for those carriers which have a large free energy contribution
and a large frequency F. Non-linearities may also be intro-
duced into the dHvA effect when observed by the torque method[55].
A literature survey revealed that Brandt et al[56] may have
observed the effect also. The effect will be analyzed in con-
siderable detail and experimental justification will be given
for various predictions.

dHvA oscillations have usually a high phase (F/H >> 1)
and at any field the dominant behaviour is oscillatory. Thus
we write for the torque of the ith carrier

$$T^i = T_o^i \ (H,T) \ \sin \ (\frac{2\pi F_i}{H}) \qquad\qquad \text{(IV-34)}$$

where $T_o^i(H,T)$ represents a slowly varying function of field
and temperature. Assuming that the compliance of the torque
magnetometer ($\eta = \frac{\partial \Theta}{\partial T}$) is non-zero only for rotations about the
quartz rod axis, a torque T will cause a rotation of the crystal
axis of $- \frac{\Delta\Theta}{\eta}$. The negative sign appears because the crystal
is turning, but the angle which is important is that between
a crystal axis and the magnetic field direction. Let us con-
sider first a single dHvA oscillation, and thus

$$T = T_o \sin \left[\frac{2\pi \ F(\Theta_o + \Delta\Theta)}{H}\right] \qquad \text{(IV-35)}$$

which can be expanded to first order since $\Delta\Theta$ is typically very
small. We obtain

$$T = T_o \sin\left[\frac{2\pi(F_o + \frac{\partial F}{\partial \Theta}\Delta\Theta)}{H}\right]$$

and reinserting $\Delta\Theta = - \eta T$ there results

$$T = T_o \sin \left[\frac{2\pi \ F_o}{H} - \frac{2\pi}{H}(\frac{\partial F}{\partial \Theta})\eta \ T\right] \qquad \text{(IV-36)}$$

which can be written in the form

$$y = a \sin (x - y)$$

where

$$y = \frac{2\pi}{H}(\frac{\partial F}{\partial \Theta})\eta T \ , \quad x = \frac{2\pi F_o}{H} \qquad \text{(IV-37)}$$

and

$$a = \frac{2\pi}{H}(\frac{\partial F}{\partial \Theta})\eta \ T_o \ .$$

The equation is formally identical to the one involving the mag-
netic interaction proposed by Shoenberg. The shape of the oscil-

lations can be determined by a graphical plot of the equation

$$x = [\sin^{-1}(y/a)] + y .$$ (IV-38)

If $|a| << 1$, then an expansion of the equation gives (to second order in a)

$$y/a \simeq (1 - \frac{3a^2}{8}) \sin x - \frac{a}{2} \sin 2x + \frac{a^2}{8} \sin 3x .$$ (IV-39)

Examples of oscillations for $a = 0.7$ and $a = 1.5$ are shown below.
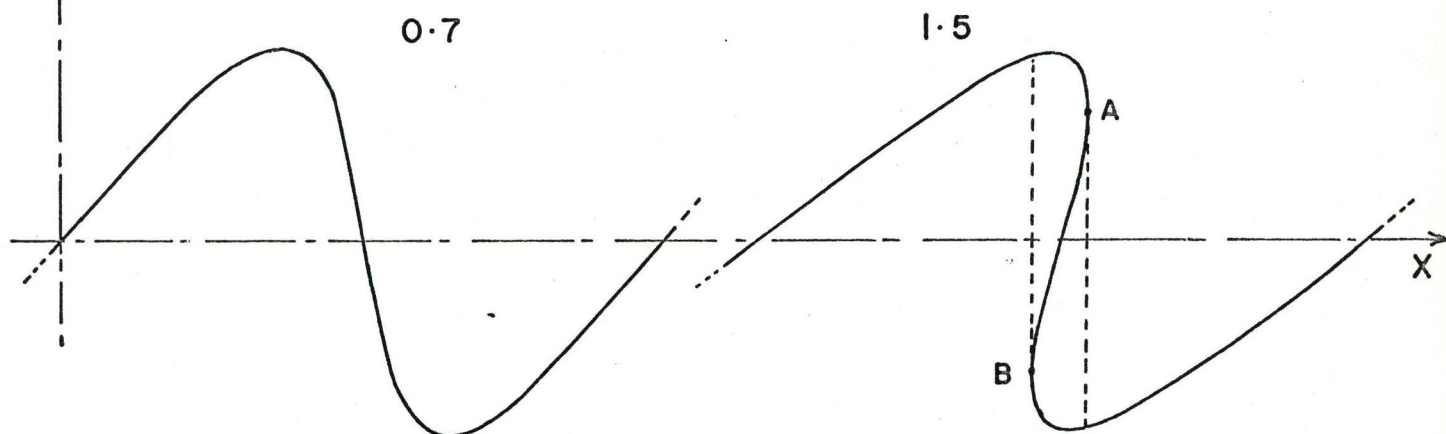
They are skewed in nature and have a large harmonic content. The skewing increases as $|a|$ increases and the largest slope of the curve will become infinite when $|a| \rightarrow 1$. If $|a| > 1$, there will be a discontinuous change in the torque at point A as the field is increased. We see physically that when $|a| > 1$, a small angular displacement is unstable since the resulting change of dHvA phase causes a greater change in torque than the restoring force couple of the magnetometer. When the field is reversed, the discontinuous jumps will occur at a different field point B.

If $|a| \gg 1$, then the solution of the equation will have approx-
imately n stable solutions, where n is the largest integer so
that

$$|a| > (n - \frac{3}{2}) \pi \quad . \tag{IV-40}$$

Shown below are a few oscillations for $a = 6$, $\therefore$ $n = 3$. Three
stable solutions are labelled by crosses at a certain field
value. If the variable x is increased, the torque (y) will
follow the dashed line.
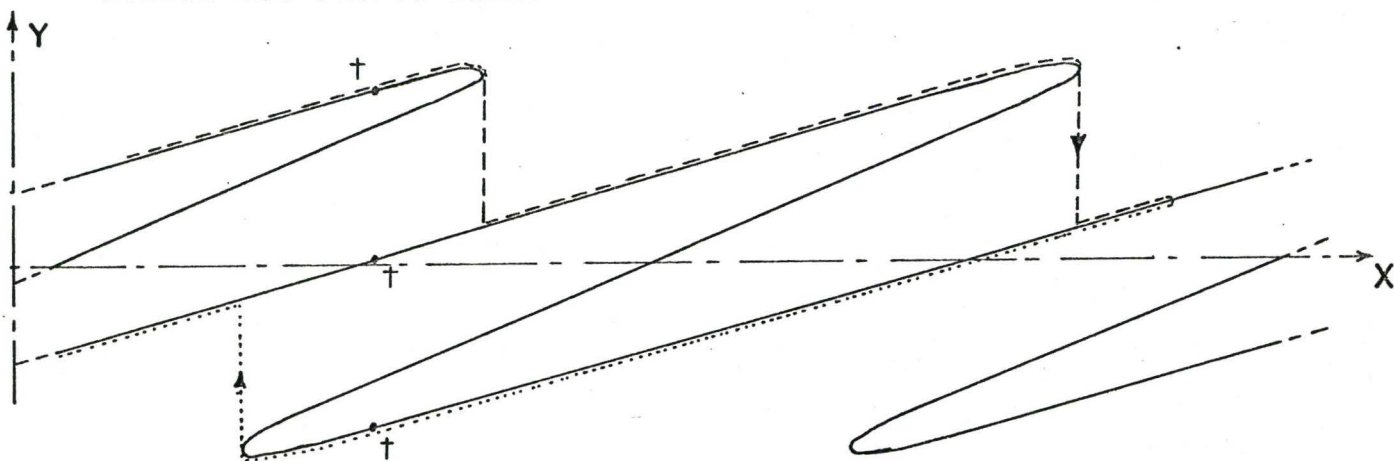
If the field is reversed, a hysteresis of about $(2n-1)\pi$ will
result for the x variable before oscillations resume, following
an inverted saw-tooth pattern on the lower half of the curve.

Usually $|a| < 1$ and the violently non-linear effects dis-
cussed above do not occur. However, if there are several dHvA
oscillations, then mixing can occur due to the compliance of the
suspension. Let us consider that two frequencies are present and
the torque can be written as

$$T = T_1 \sin \frac{2\pi F_1(\Theta + \Delta\Theta)}{H} + T_2 \sin \frac{2\pi F_2(\Theta + \Delta\Theta)}{H} \qquad (IV-41)$$

Working to first order in $\Delta\Theta$ and assuming $\frac{2\pi}{H}(\frac{\partial F_1}{\partial\Theta})\,\Delta\Theta \ll 1$ and $\frac{2\pi}{H}(\frac{\partial F_2}{\partial\Theta})\,\Delta\Theta \ll 1$, we obtain for the torque $T = -\Delta\Theta/\eta$

$$T = T_1 \sin \frac{2\pi F_1}{H} + T_2 \sin \frac{2\pi F_2}{H} + \frac{\pi\eta}{H} T_1 T_2 (\frac{\partial F_2}{\partial\Theta} - \frac{\partial F_1}{\partial\Theta}) \sin \frac{2\pi(F_2 - F_1)}{H}$$

$$- \frac{\pi\eta}{H} T_1 T_2 (\frac{\partial F_1}{\partial\Theta} + \frac{\partial F_2}{\partial\Theta}) \sin \frac{2\pi(F_1 + F_2)}{H}$$

$$- T_1^2 (\frac{\partial F_1}{\partial\Theta}) \frac{\pi\eta}{H} \sin \frac{4\pi F_1}{H} - T_2^2 (\frac{\partial F_2}{\partial\Theta}) \frac{\pi\eta}{H} \sin \frac{4\pi F_1}{H} \qquad (IV-42)$$

Thus the non linear action has introduced sum and difference frequencies, as well as harmonics, to first order. The harmonics and sum frequencies generally change the shape of the two beating oscillations and are not as easily observable as the difference frequency, which occurs at the same frequency as the beats. This low frequency will cause an effective change in the position of a node. The node for positive torque is moved opposite to that for negative torque, each being displaced in magnetic field by

$$\Delta H = H_0 \eta \, |T_1 - T_2| \, \frac{\partial}{\partial\Theta} \, \ell n(F_2 - F_1) \qquad (IV-43)$$

where H_0 is the field at the centre of the two displaced nodes and $|T_1 - T_2|$ is the amplitude of the envelope at the node.

If there are three frequencies present, of fundamentals F_1, F_2, and F_3, the main mixing products to first order will be $F_1 - F_2$, $F_2 - F_3$, $F_1 - F_3$, $2F_1$, $2F_2$, $2F_3$, $F_1 + F_2$, $F_2 + F_3$ and $F_1 + F_3$. The above equations have been given for small values of η and $\Delta\Theta$

since the equations are not soluble in closed form. Some other factors which have hitherto been neglected will now be discussed.

The description of a single dHvA oscillation as given by equation (IV-34) must be modified so that $T_o(H,T)$ contains an angular dependence. Referring back to the expression for the free energy, we see that T_o must contain the curvature of the Fermi surface $\frac{\partial^2 S}{\partial p_z^2}$ and the effective mass m^*, both of which have angular dependences. For non-cubic crystals there is often a torque which varies as H^2 and has a $\sin 2\theta$ angular variation. It arises from diamagnetic and paramagnetic effects. For one oscillation then, we can write

$$T = T_o(H,T,\ \theta + \Delta\theta)\sin\frac{2\pi F(\theta + \Delta\theta)}{H} + k(\theta + \Delta\theta)\ H^2\ .$$

Since the phase $\frac{2\pi F}{H} \gg 1$, terms in $\frac{\partial T_o}{\partial \theta}$, $\frac{\partial F}{\partial \theta}$, $\frac{\partial^2 F}{\partial \theta^2}$ and $\frac{\partial k}{\partial \theta}$ should be retained in the calculation. Let us consider the various terms in turn. The term in $\frac{\partial F}{\partial \theta}$ results in the equations described earlier and, if terms in $\frac{\partial^2 F}{\partial \theta^2}$ are included equation (IV-37) would become

$$y = a \sin (x - y + by^2) \qquad\qquad \text{(IV-44)}$$

where $b = \frac{H}{4\pi} = (\frac{\partial^2 F}{\partial \theta^2}) / (\frac{\partial F}{\partial \theta})^2$. The term by^2 causes the shape of oscillations to be different for positive and negative y. Normally $\frac{F}{H} \gg 1$, and the parameter b will be small, but near stationary values of F, when $\frac{\partial F}{\partial \theta}$ becomes small, b may become large. Near these points, however, the torque amplitude T_o will

be low since it depends on $\frac{\partial F}{\partial \theta}$. Hence $|a| << 1$ and the non-linear effects are suppressed. The effect of b is that as a increases, the slope of $y = y(x)$ does not become infinite at $y = 0$, but at a value of $y \cong -\frac{2b}{1 + 12b^2}$. The condition for multivalued solutions becomes $|a| \geqslant 1 - 2b^2$, to second order in b. b is normally small and this condition differs insignificantly from the earlier one, $|a| \geqslant 1$.

The term containing $\frac{\partial T_o}{\partial \theta}$ basically results in an oscillatory change in T_o. This can be interpreted as causing a to be replaced by $(a + \gamma y)$, where $\gamma = -\eta(\frac{\partial T_o}{\partial \theta})$. This term again causes an effect very similar to the above, in that the slope of $y = y(x)$ first becomes infinite at $y \sim 2\gamma$, for a value of a such that $|a| \geqslant 1 - 2\gamma^2$. This effect then is also insignificant if γ is relatively small. The parabolic term $k(\theta + \Delta\theta) H^2$ in the torque has a quite different effect on the measured dHvA oscillations. The term in $\frac{\partial k}{\partial \theta}$ can be neglected, but the steady torque kH^2 twists the crystal always in one direction as the field is increased. If F_o is the dHvA frequency when $H = 0$, then due to the small rotation the frequency F at a field H will be closely represented by

$$F = F_o - \eta T(\frac{\partial F}{\partial \theta}) = F_o - \eta k(\frac{\partial F}{\partial \theta}) H^2 . \qquad \text{(IV-45)}$$

The torque T in the middle expression is taken as the H^2 term. (Allowing T to be oscillatory would merely recreate the theory presented earlier.) Thus the dHvA frequency changes continuously with field, and strict periodicity of oscillations in reciprocal

magnetic field is no longer valid. If two frequencies are present as well as a kH^2 torque, the beat structure may be quite strange if $F_1 \sim F_2$ and $\frac{\partial F_1}{\partial \theta} \neq \frac{\partial F_2}{\partial \theta}$.

Experimental justification of the foregoing ideas came from a torque dHvA measurement on several large crystals of arsenic. The compliance of the magnetometer was originally high, and thus the parameter $a = \frac{2\pi}{H} (\frac{\partial F}{\partial \theta}) \eta T_o$ was appreciable for magnetic fields of about 20 kilogauss. At certain orientations of the field, it was observed that as the magnetic field was increased, a pronounced skewing of the oscillations resulted, and, at still higher fields, the signal displayed a step discontinuity limited in speed by the torque magnetometer response. Upon reversal of the magnetic field sweep, the field retraced most of the oscillations monotonically but the step discontinuity or torque "snap" occurred at a displaced magnetic field. An oscillation exhibiting this striking effect is shown in Figure IV-6 for increasing and decreasing magnetic field. The dashed lines indicate the discontinuity of the torque. This oscillation was the first to display hysteresis and the value of $|a|$ was calculated from the maximum torque excursion and the slope $\frac{\partial F}{\partial \theta}$ of the dHvA frequency versus angle. It was found that $|a| = 0.9$. This is rather good agreement with the simple theory of equation (IV-37) (which predicts that for "snap" $|a| \geqslant 1$) in view of the fact that several other effects could influence the effective value of $|a|$ for "snap" to occur. Additional oscillations tend to increase dy/dx and reduce the value of $|a|$ for
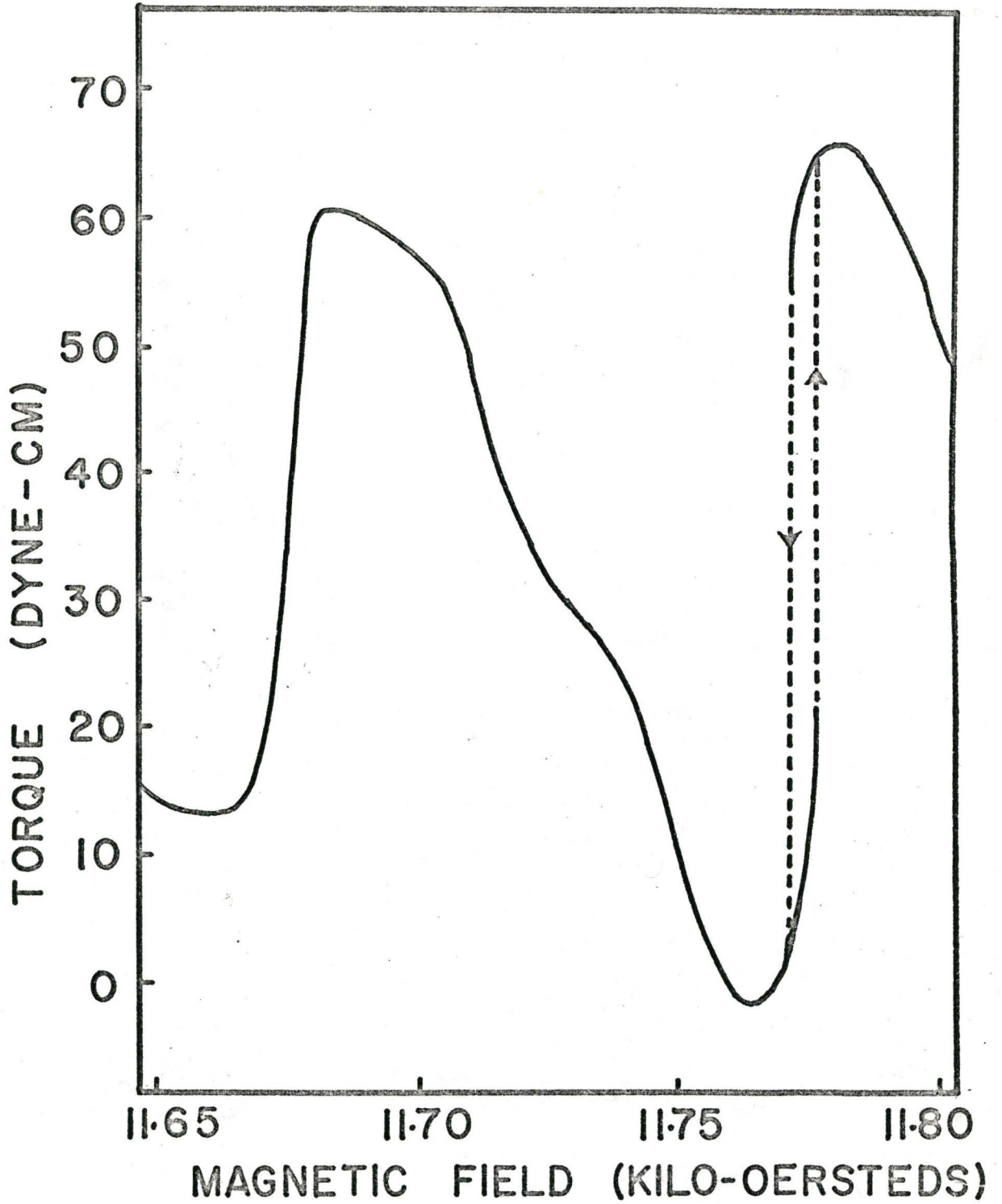
FIGURE IV-6

snap to occur. Some other oscillations are visible in Figure IV-6. Also, angular displacements about a second axis would also cause snap for lower values of $|a|$. The vector torque has a component of torque perpendicular to the quartz rod, causing it to bend. In this present discussion it is assumed that the largest compliance exists for rotations about the quartz rod axis and this seems to be borne out in the experiments.

The shape of each oscillation based on equation (IV-37) was checked for several runs where only one dominant dHvA oscillation occurred. Figure IV-7 shows several oscillations which have a parameter $|a|$ of approximately 0.7, as calculated by normalizing the first oscillation which has "snap" to $|a| = 1$. There is good similarity between Figure IV-7 and the theoretical plots of the equation

$$y = 0.7 \sin (x - y) ,$$

given earlier, and this attests to the basic accuracy of the analysis. The shape of the oscillations have somewhat straighter sides than the theoretical predictions and this is attributed to the nature of the torque magnetometer. It may have a restoring torque $\eta \Delta T = - \Delta \theta + k(\Delta \theta)^3$ which can cause this. Most skewed oscillations having a lower torque excursion obey theory much more closely. The easiest method to estimate the value of a if the condition of "snap" is not satisfied at the highest magnetic field, is to measure the ratio of the slopes of two adjacent zero crossing points. This ratio has

MAGNETIC FIELD (KILO-OERSTEDS)

24·5

24·0

TORQUE (ARBITRARY UNITS)
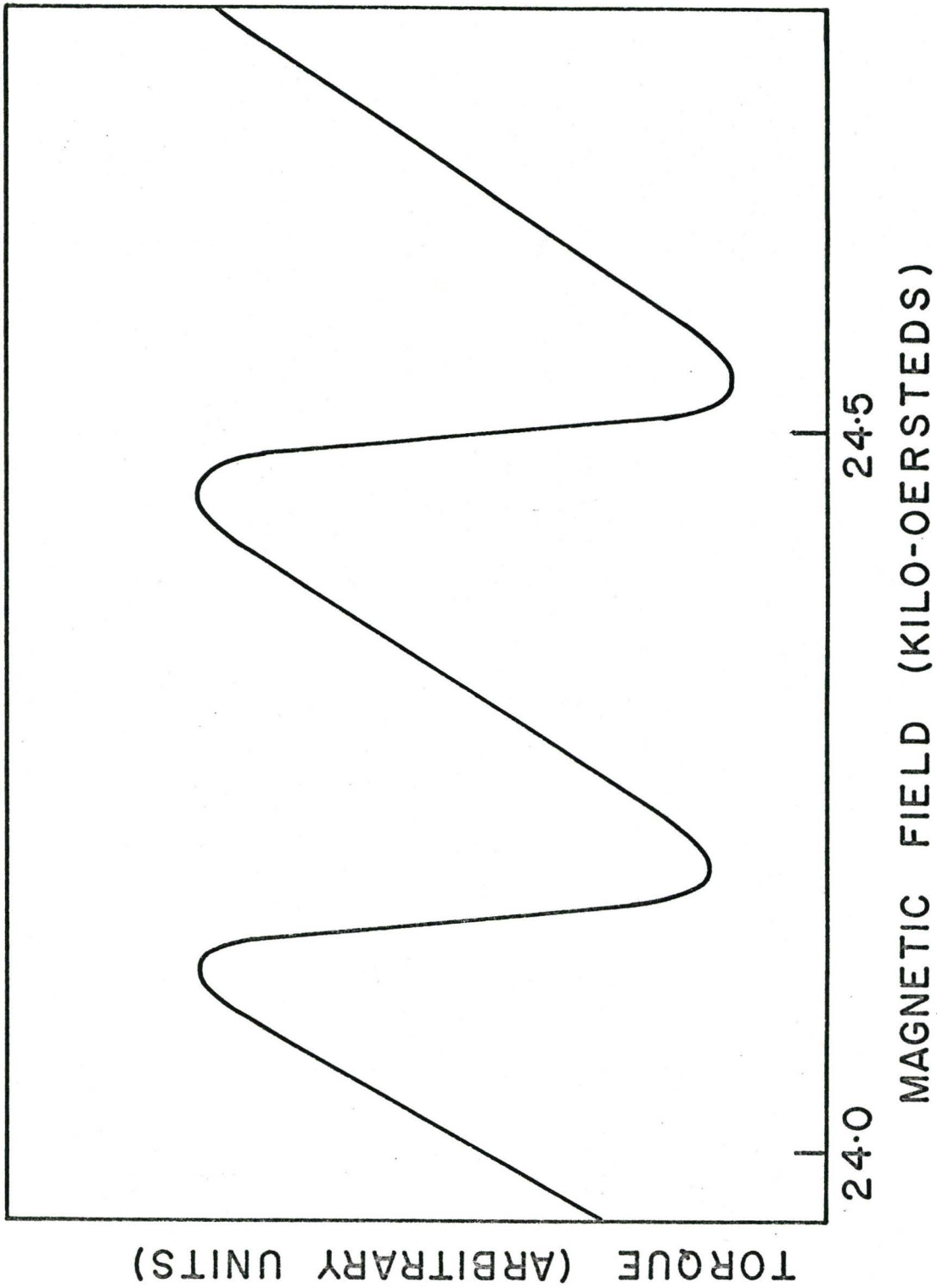
FIGURE IV-7

the value - $(1 + a)/(1 - a)$.

Figure IV-8 shows the effect of magnetometer compliance if there are two dominant dHvA frequencies present. The difference frequency is quite easily visible by following the midpoint between the upper and lower envelopes of the oscillations. Phase of the difference frequency as predicted by equation (IV-42) is correct also. Nodes will occur when

$$\frac{2\pi F_2}{H} = \frac{2\pi F_1}{H} + (2n + 1)\pi$$

or

$$\frac{2\pi (F_2 - F_1)}{H} = (2n + 1)\pi \qquad (IV-46)$$

This shows that at the nodes the difference frequency crosses zero since it has a $\sin \frac{2\pi (F_2 - F_1)}{H}$ oscillatory behaviour. The shift of the nodes at the top to the left and those at the bottom to the right is clearly visible. It is caused by the low difference frequency.

A drastic reduction of the magnetometer compliance (as described in the section 'Torque Magnetometer') resulted in dHvA oscillations of low harmonic content and no more spurious effects were encountered. Therefore, the above observations must have been due to the torque effects and not to magnetic interaction of the carriers. Because the two effects do have similar equations governing the observables, it is of interest to give a relative comparison of the two effects. This can be done by calculating the parameter "a" for each effect. A
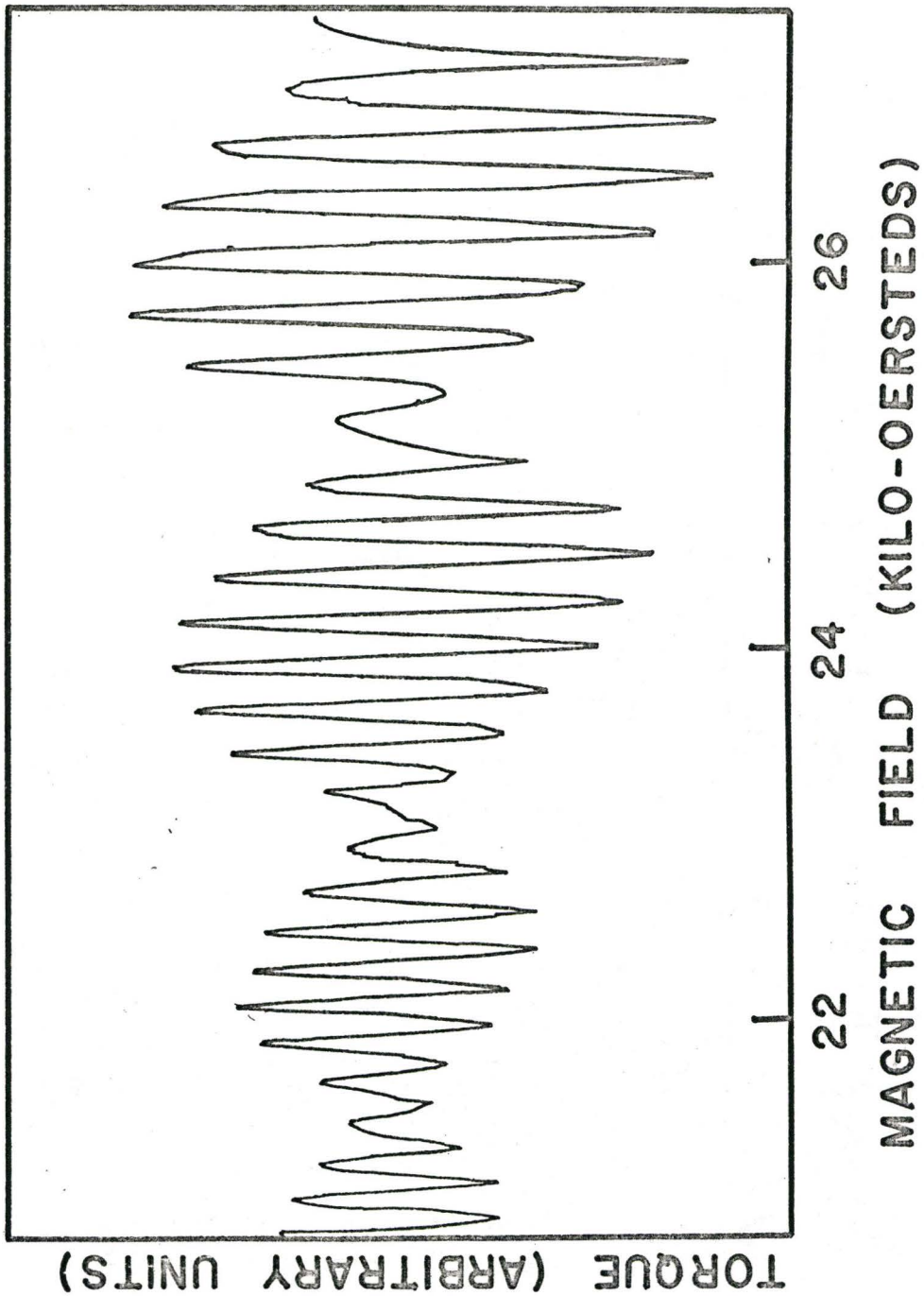
FIGURE IV-8

generalization of the magnetic interaction must be made before this is possible.

The oscillatory dHvA free energy will be written (from equation (II-17) as

$$F_{osc} = A(H,T) \cos \frac{2\pi F}{H} \quad . \qquad \text{(IV-47)}$$

The total magnetization will be written explicitly as the dipole moment $\vec{M}$ per unit volume, multiplied by the volume V of the crystal.

$$\vec{VM} = -\vec{\nabla}_H \ F_{osc}$$

$$= -\vec{\nabla}_H \ (\frac{2\pi F}{H}) \quad A(H,T) \ \sin \frac{2\pi F}{H} \qquad \text{(IV-48)}$$

Neglecting demagnetization factors, we replace $\vec{H}$ by $\vec{H} + 4\pi\vec{M}$. This changes the phase $\frac{2\pi F}{H}$ by an amount given by

$$\vec{\nabla}_H(\frac{2\pi F}{H}) \ . \ 4\pi\vec{M} \qquad . \qquad \text{(IV-49)}$$

Fortunately, the vector gradient $\vec{\nabla}_H \ (\frac{2\pi F}{H})$ is anti-parallel to $\vec{M}$, so that the equation becomes

$$\vec{VM} = - \ \vec{\nabla}_H(\frac{2\pi F}{H}) \quad A(H,T) \quad \sin \ [\frac{2\pi F_o}{H_o} -|\vec{\nabla}_H \ (\frac{2\pi F}{H})| \ 4\pi|\vec{M}|]$$

Rewriting this into the required form for the lengths of the vector $|\vec{M}| = M$ gives

$$4\pi \quad |\vec{\nabla}_H(\frac{2\pi F}{H})| \quad M = - \ \frac{4\pi}{V} \ |\vec{\nabla}_H(\frac{2\pi F}{H})|^2 \quad A(H,T) \quad x$$

$$\sin \ [\frac{2\pi F_o}{H_o} - 4\pi|\vec{\nabla}_H(\frac{2\pi F}{H})|M] \quad . \qquad \text{(IV-50)}$$

Thus for the magnetic interaction

$$a_{B-H} = \frac{4\pi}{V} \ \left| \vec{\nabla}_H \left(\frac{2\pi F}{H}\right) \right|^2 A(H,T) . \qquad (IV-51)$$

The total torque is given by

$$T = - \frac{\partial F_{osc}}{\partial \Theta}$$

$$= - \frac{2\pi}{H} \left(\frac{\partial F}{\partial \Theta}\right) A(H,T) \ \sin \frac{2\pi F(\Theta + \Delta\Theta)}{H} \qquad (IV-52)$$

where $\Delta\Theta = - \eta T$ as discussed earlier.

Then we have

$$-\frac{2\pi}{H} \left(\frac{\partial F}{\partial \Theta}\right) \eta T = - \frac{4\pi^2}{H^2} \left(\frac{\partial F}{\partial \Theta}\right)^2 \eta A(H,T) \ \sin \left[\frac{2\pi F_0}{H} - \frac{2\pi}{H}\left(\frac{\partial F}{\partial \Theta}\right)\eta T\right] \quad (IV-53)$$

which gives a for the torque nonlinearity.

$$a_{Torque} = - \frac{4\pi^2}{H^2} \left(\frac{\partial F}{\partial \Theta}\right)^2 \eta \ A(H,T) \qquad (IV-54)$$

The relative effects of the two phenomena can be gauged by the ratio

$$\Gamma = \frac{a_{Torque}}{a_{B-H}} = \frac{\frac{\eta \pi V}{H^2} \left(\frac{\partial F}{\partial \Theta}\right)^2}{\left| \vec{\nabla}_H \left(\frac{2\pi F}{H}\right)\right|^2} \qquad (IV-55)$$

The crystal volume V occurs in this ratio since M causes non-linearities as an intensive parameter, while the total torque affects the angle through which the crystal is turned. As a rough approximation, the denominator $\left| \vec{\nabla}_H \left(\frac{2\pi F}{H}\right) \right|^2$ can be set equal to $\frac{4\pi^2}{H^4} \left(\frac{\partial F}{\partial \Theta}\right)^2$ to give an estimate for Γ . Then we have

$$\Gamma \simeq \frac{\eta \ V \ H^2}{4\pi} \qquad (IV-56)$$

In our case $\eta = 11.4 \times 10^{-5}$ rad/dyne-cm,

$$V = 10^{-1} \ cm^3,$$

and $H = 2 \times 10^4$ gauss, and we have $\Gamma \sim 350$.

Thus for arsenic the effects of torque nonlinearity certainly dominate. To make $\Gamma = 1$ would require $\eta \simeq 3 \times 10^{-7}$ radian/dyne-cm. This value of the compliance would result in roughly equivalent effects due to torque compliance and magnetic interaction, for the values of field and crystal size stated. It is interesting to notice that the relative strengths of the two effects do not depend strongly on the dHvA frequency F, but the magnitude of either effect depends closely on the value of F^2.

It must be pointed out that great care must be exercised in interpreting harmonic effects, because the twisting of the crystal will cause non-linearity to be observed in all oscillatory dHvA properties.

EXPERIMENTAL RESULTS

This section is concerned with presenting the bulk of the data obtained from the dHvA effect of arsenic. These data consist of the plots of periods P of the dHvA oscillations as a function of the orientation of the magnetic field with respect to the crystal axes. They are divisible into sets of short period oscillations and long period oscillations. Short periods that were measured for magnetic field directions in the trigonal-bisectrix, trigonal-binary and binary-bisectrix planes are shown in Figures IV-9, IV-10 and IV-11, respectively. Each point on these graphs represents the analysis of the oscillations as a function of magnetic field for that particular
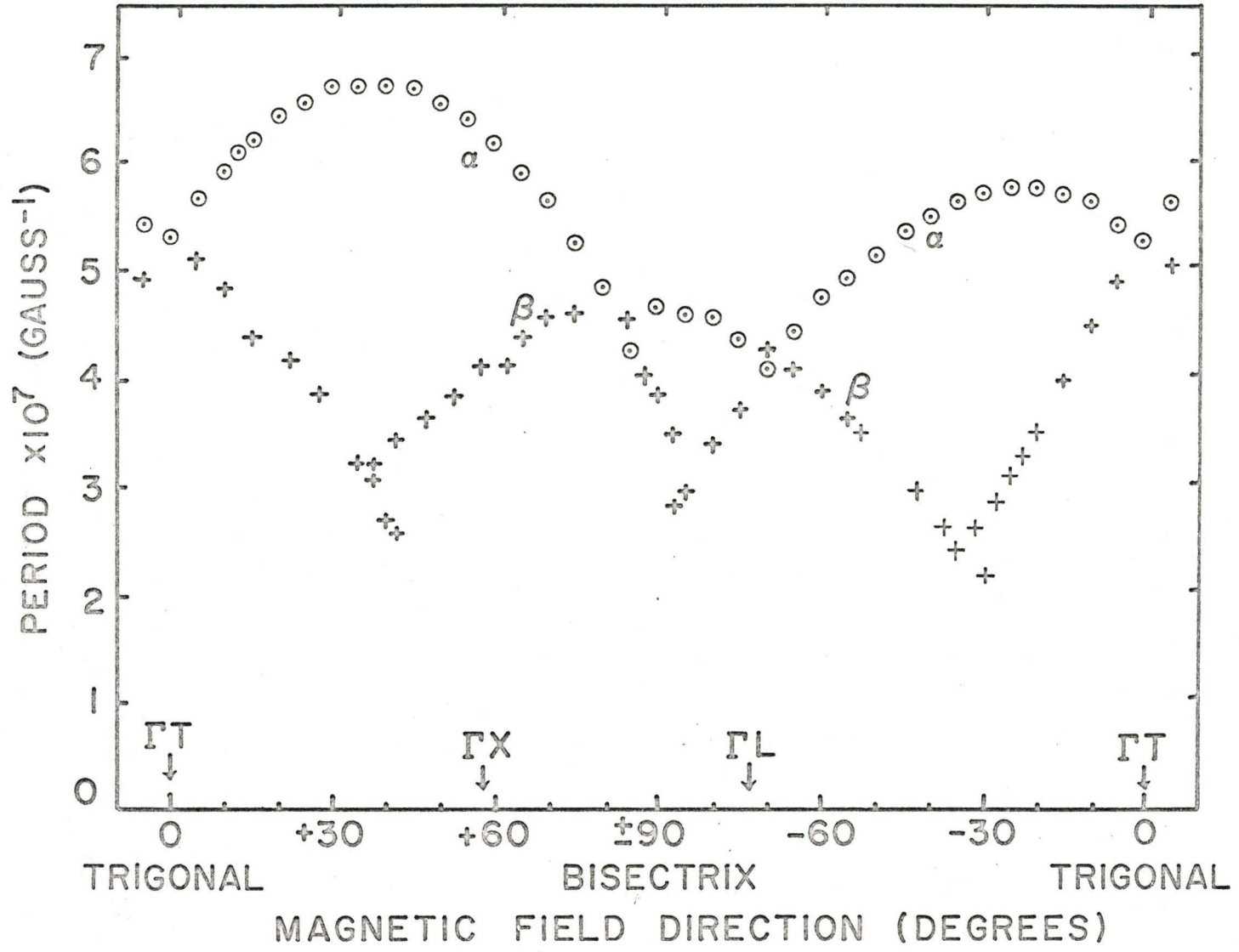
FIGURE IV-9

FIGURE IV-10

94
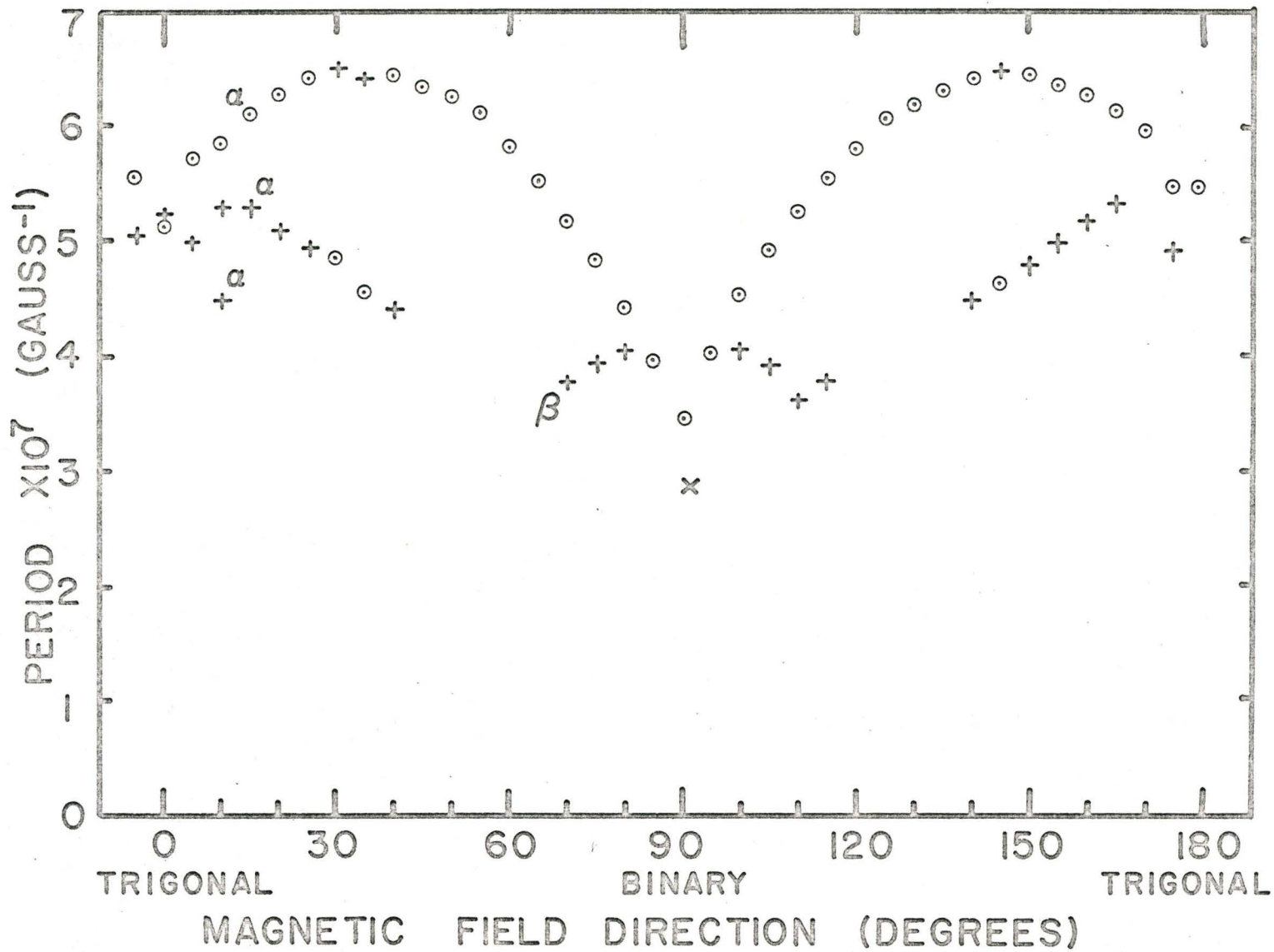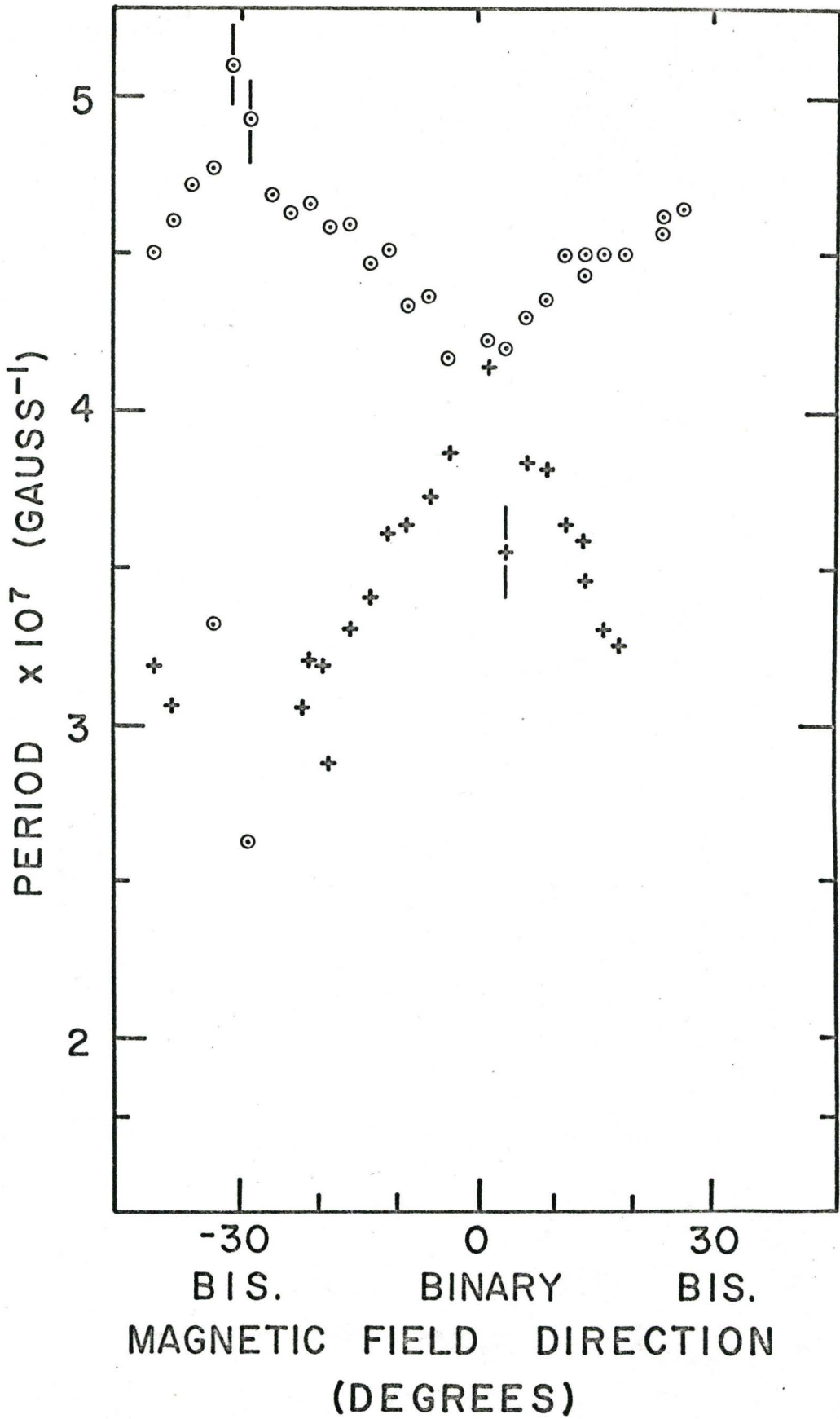
FIGURE IV-11

orientation. The circles are determined as dominant oscillat-
ions, and the crosses are obtained from an analysis of the beats.
There are two distinct sets of oscillations labelled the α and
β branches. The α carriers were observed by Berlincourt in
1955[32], and the β- carriers represent a new segment of the
Fermi surface. Band structure determinations of Lin and Fali-
cov[42] for arsenic provide a basis for the interpretation of
the experimental results. Their model of the Fermi surface
consists of three electron pockets and a single, multiply-
connected hole surface. Each electron pocket resembles a
distorted ellipsoid. The hole surface consists of six pockets
which are connected by six thin cylindrical sections. For each
band of carriers in the trigonal-bisectrix plane, there is a
principal branch of periods and two degenerate non-principal
branches that are related to the principal one by $\pm$ 120° rotat-
ions.

In Figure IV-9, the angles are defined according to
the convention given in Chapter III. The maximum period of the
principal branch of the α carrier is 6.75 $\pm$ 0.05 x 10^{-7} G^{-1}
at an angle + 38° $\pm$ 1°. This branch is degenerate with the
non-principal branches at the trigonal axis. Hence the maximum
period of the non-principal branches is 5.80 $\pm$ 0.05 x 10^{-7} G^{-1}
at an angle - 22° $\pm$ 1°. Only one period branch of the β carrier
was observed. This was the principal branch with maximum period
of 4.70 $\pm$ 0.04 x 10^{-7} G^{-1} at an angle + 86° $\pm$ 1°. The lower

periods in Figure IV-9 were obtained from beats, magnetic field modulation and derivative techniques.

Three period branches of the α carriers and one branch of the β-carrier are evident in Figure IV-10. This assignment of period branches is made from the tilt angles of the pockets seen in Figure IV-9, as well as the degeneracy of the three α carrier branches at the trigonal axis. At first glance, the period of 2.9 x $10^{-7}G^{-1}$ at the binary belongs to the β carrier branch that is symmetrical about the binary axis, but an ellipsoidal fit indicates that this branch should have a lower period. It is assigned to the hole orbit which is not in the mirror plane but arises from a skew orbit associated with the junction of the necks and the α pockets[40]. There are indications that the β carrier branch observed is not a single branch. 20° from the binary axis it can hardly be analyzed and there are indications that three periods of about 3 x 10^{-7} G^{-1} are beating in this area.

The data of the binary-bisectrix plane repeats every 60°, and each binary or bisectrix axis is also a mirror plane for the periods in Figure IV-11, so that all information is available in a 30° interval. Analysis of these data were difficult because of competition between the α and β carriers. In this plane the dominant oscillations were due to only the β carriers since these have a period 4.70 x 10^{-7} G^{-1} at the bisectrix axis. The α carriers were faintly visible but could not be analyzed except near

the binary axis (~3.15 x 10^{-7} G^{-1}) and possibly near the bisectrix axis (3.3 x 10^{-7} G^{-1}).

The long periods for the trigonal-bisectrix plane are shown in Figure IV-12. There are two branches having periods that are quite low near the bisectrix axis. The solid curves are plots of $P = P_{max} \cos \theta$. This is the plot for an infinite cylinder. The fit to the data is good except near the bisectrix directions where the period is smaller than for a cylinder. This indicates that this section of the Fermi surface may have the general shape of a hyperboloid of revolution because the area is larger than for a cylinder. The tilt angle θ from the trigonal direction of the period maximum of the non-principal branch is related to the tilt angle δ of the section by the relation

$$\tan \delta = - \tan \theta \cos 60^{\circ}. \qquad (IV-57)$$

Since $\theta = + 5^{\circ} \pm \frac{1^{\circ}}{2}$, the tilt angle δ is $-10^{\circ} \pm 1^{\circ}$. Then, for a hyperboloid of revolution

$$(x^2 + y^2)/a^2 - z^2/b^2 = 1 , \qquad (IV-58)$$

$$P(\theta) = P_{max} \cos \theta [1 - (a/b)^2 (\sec^2 \delta \sec^2 \theta - 1)]^{1/2} \qquad (IV-59)$$

for the non-principal branch, where θ is the direction of H in the trigonal-bisectrix plane, measured from the period maximum at $+ 5^{\circ}$. A fit of equation (IV -59) to the data of Figure IV-12 yields a value for a/b of 0.12 ± 0.04. This means that the small sections have a gentle flare at each end. The principal branch
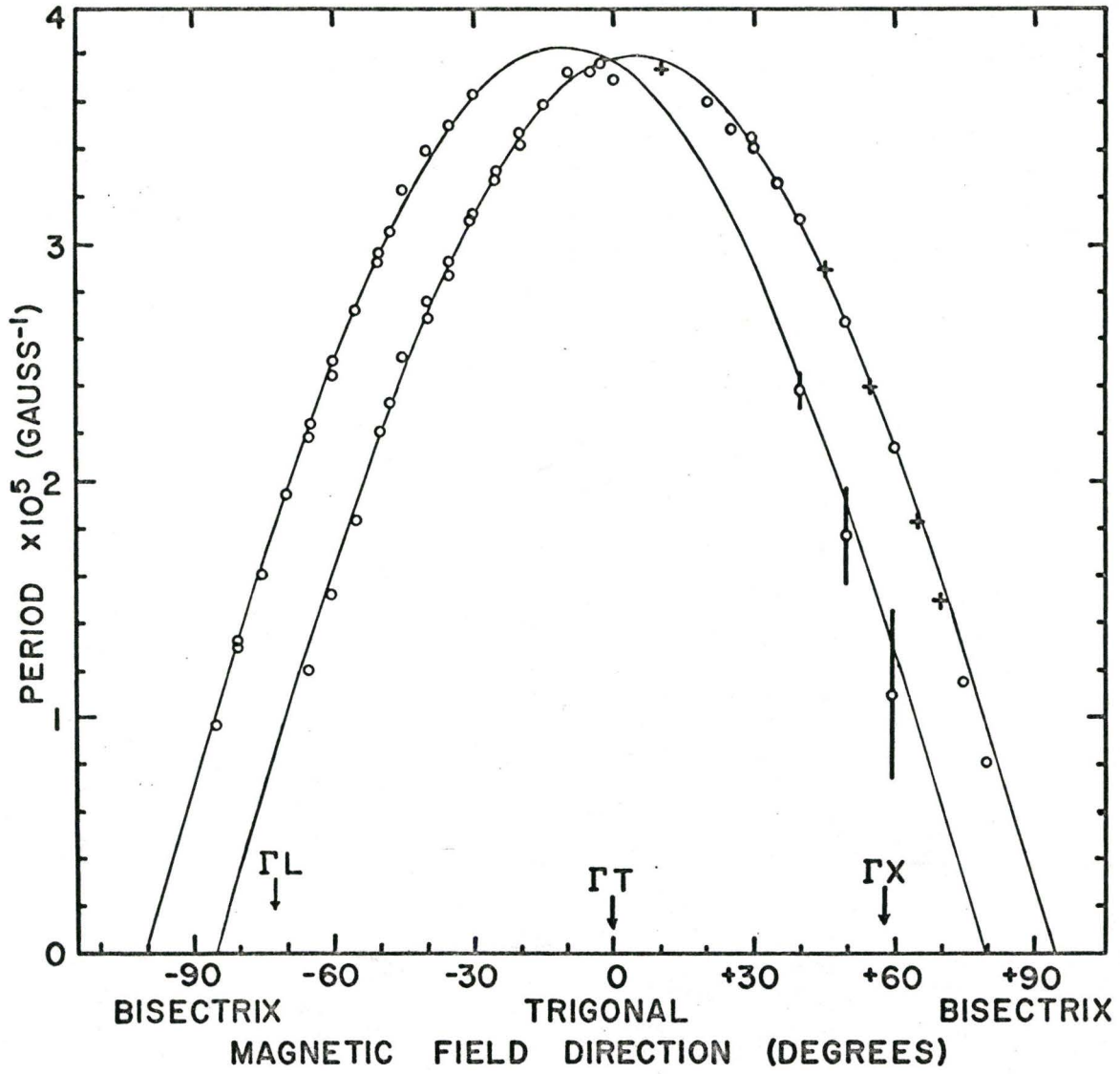
FIGURE IV-12

is not as clearly defined as the non-principal branch, but shows
directly that the tilt angle of the hyperboloidal sections is
$- 10^o \stackrel{+}{_-} 2^o$ from the trigonal axis. The branches had maxima of
3.82 and 3.80 x 10^{-5} G^{-1} for principal and non-principal branches
respectively.

Figure IV-13 shows the results of data in the trigonal-
binary plane which were in general difficult to analyze. The kink
in one branch at 55° from the trigonal axis may be partially due
to these difficulties. However, the shape of the branches in this
region is consistent with the idea that the hyperboloidal sections
join on to other sections of the Fermi surface. The three branch-
es show directly that there are three or six hyperboloidal sect-
ions. The curves are drawn through the experimental points.

Several experiments with large crystals were carried
out with H in the binary-bisectrix plane. Little or no long-
period oscillations were observed. This is consistent with a
tilt angle of $- 10^o$ for which the orbits are nearly cut off with
the magnetic field in this plane.

Most of the data of Figure IV-12 and IV-13 were obtain-
ed by plotting maxima and minima of the oscillations as integers,
versus the corresponding value of 1/H. The slopes of these lines
yield the period, and the intercept with the integer axis yields
the phase constant of the dHvA formula. This was a very tedious
procedure. Beats are evident in these plots as kinks or nonlinear-
ities. The maxima and minima of torque are determined by the
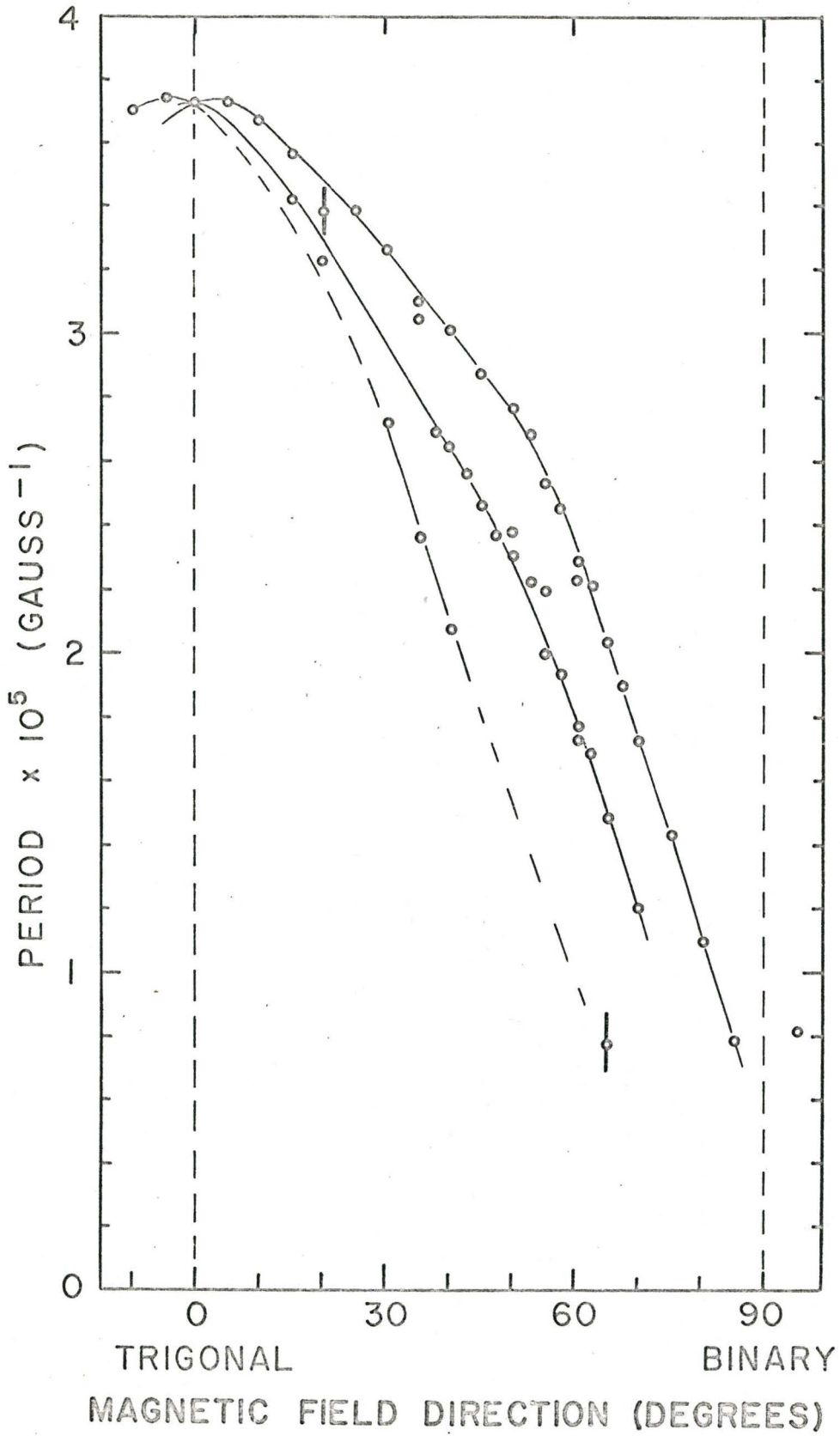
FIGURE IV-13

relationship of the oscillations to the parabolic H^2 torque term, as will be more fully explained in the discussion. Figure IV-14 shows a plot of the maxima and minima of torque against integers and half integers for several directions in the trigonal-binary plane. The plot gave reasonably straight lines. Phase shifts will be discussed in Chapter VI.

When a motor and chain drive were added to allow the magnet to be slowly rotated, several crystal planes were studied in this manner. Figure IV-15 shows the data obtained for the short periods in the trigonal-bisectrix plane using angular rotation methods. The smoothness of the data is apparent but little extra information is provided since there is no way of discriminating against dominant oscillations so that less dominant ones emerge. The α carriers are better defined and this will allow us to make a good estimate of the carrier density. Figure IV-16 shows the angular rotation data in the binary-bisectrix plane. There was a large oscillation from only one carrier which we see must be the β-carrier from the comparison of periods at the binary and bisectrix axes in the three crystal planes. The period of ~ 3×10^{-7} G^{-1} near the binary axis is attributed to the skew orbit seen by Priestley et al[40]. Near the binary axis there was also a period 0.97×10^{-7} G^{-1} which was determined at a beat of two longer period oscillations. This period is 25% lower than the lowest period of the β-carrier[40]. It is close to the fourth harmonic of the longer period oscillations, but the
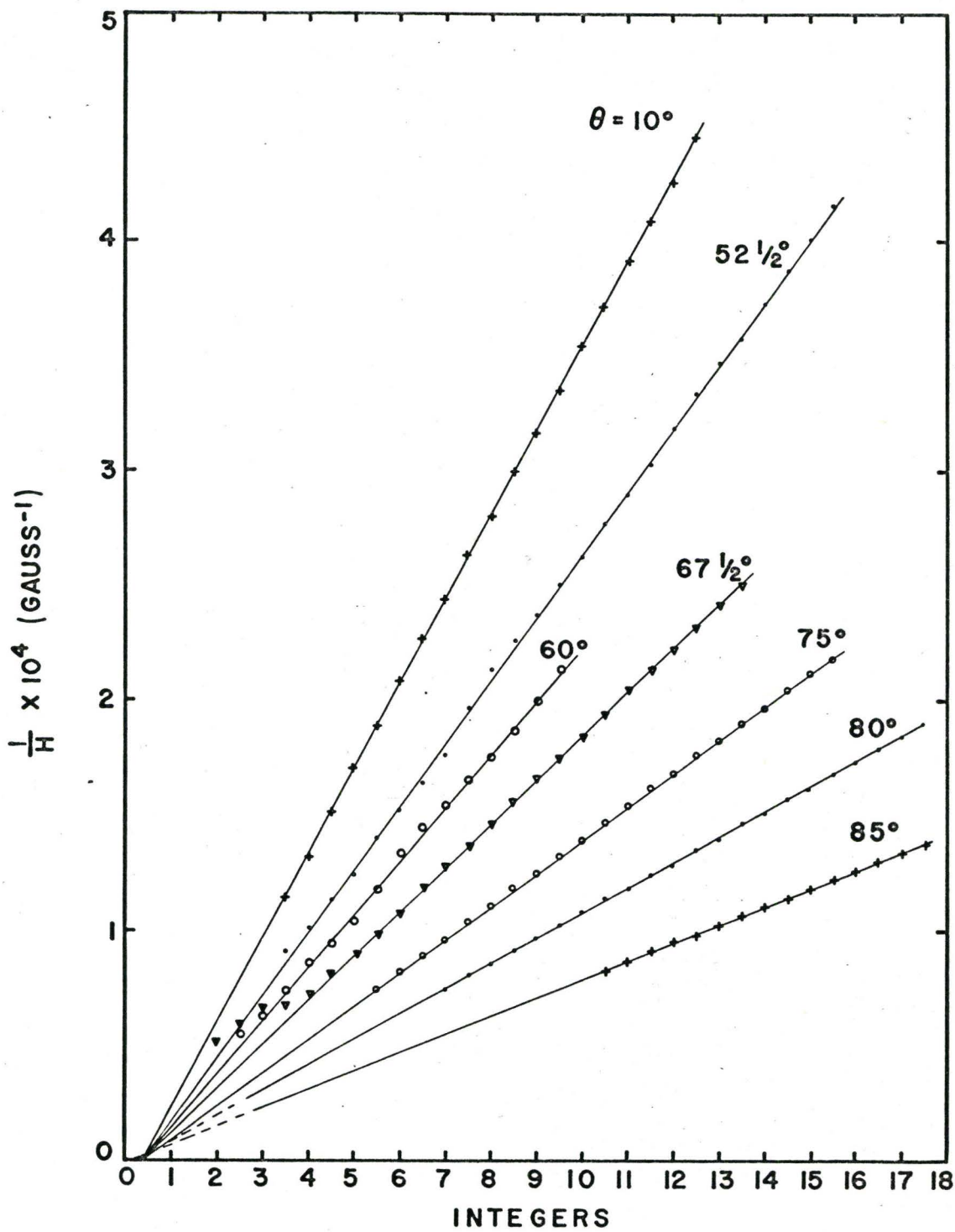
FIGURE IV-14
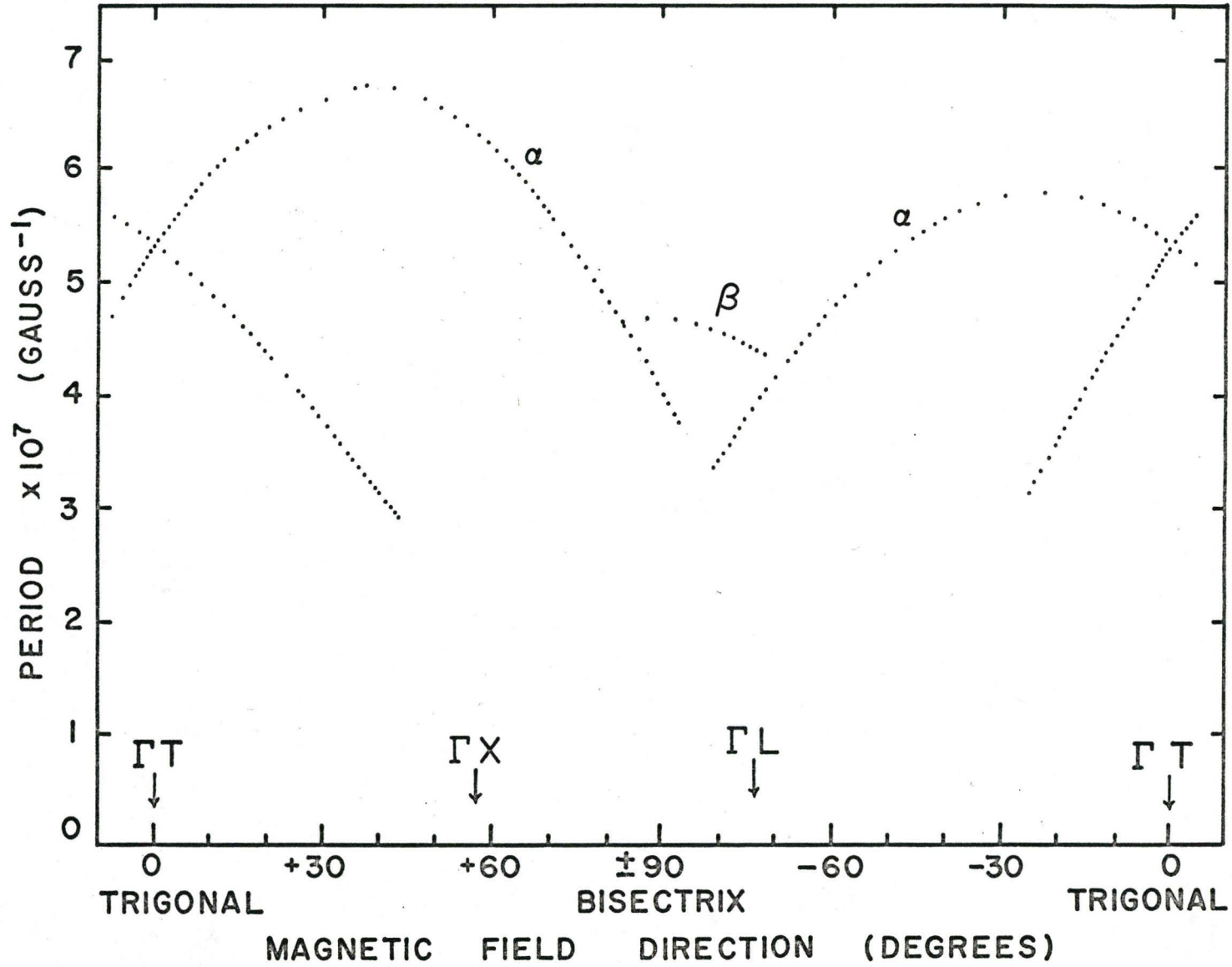
FIGURE IV-15
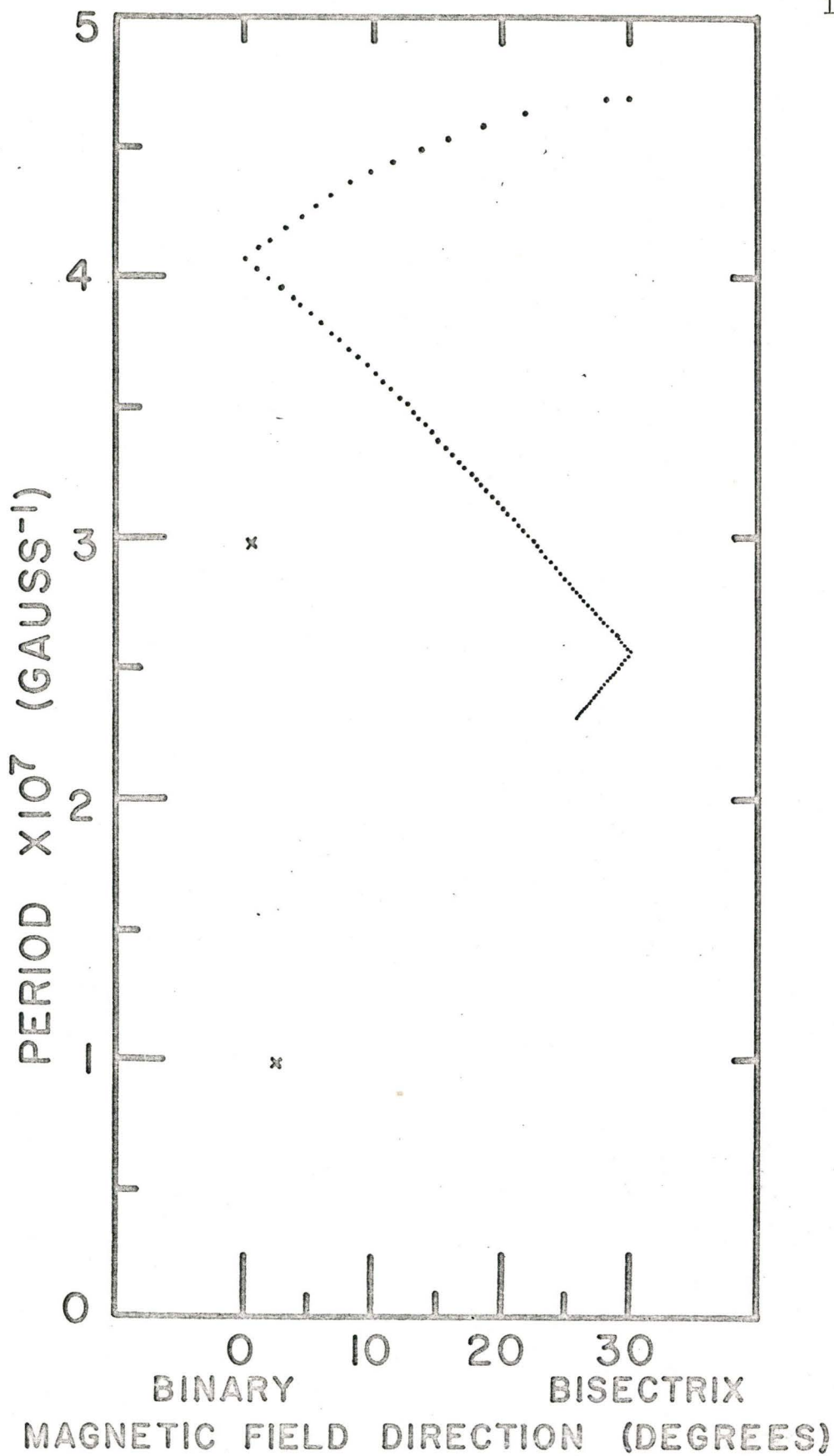
FIGURE IV-16

fourth harmonic is expected to be of very low amplitude. Thus, the period 0.97×10^{-7} G^{-1} could be from the hole orbit which is in the mirror plane and in the central section of the α pocket for H parallel to the binary axis. The period of this orbit is small since the orbit encloses a large area. This orbit was not measured by Priestley et al but was detected in a cyclotron re-sonance experiment[57].

Figure IV-17 shows a plot of the long periods in the trigonal-bisectrix plane as measured by angular rotation methods. There are only a few plotted points near the top of both branches because the rotation was done at fairly large values of magnetic field. This could have been improved by lower fields, but from the earlier plots it is known that a cos θ fit at the top is very accurate. These fits are drawn in as dotted lines. The circled data points represent the two reference periods from which the others were obtained.

A plot of the short periods in the trigonal-binary plane as measured by angular rotation methods is shown in Figure IV-18. Again the smoothness of the data is apparent, but no extra infor-mation is available. The dashed rectangle indicates an area where there is some confusion as to whether we are observing an α or a β carrier. The earlier graphs seem to indicate that the α carrier and two β carrier branches are found in this region.
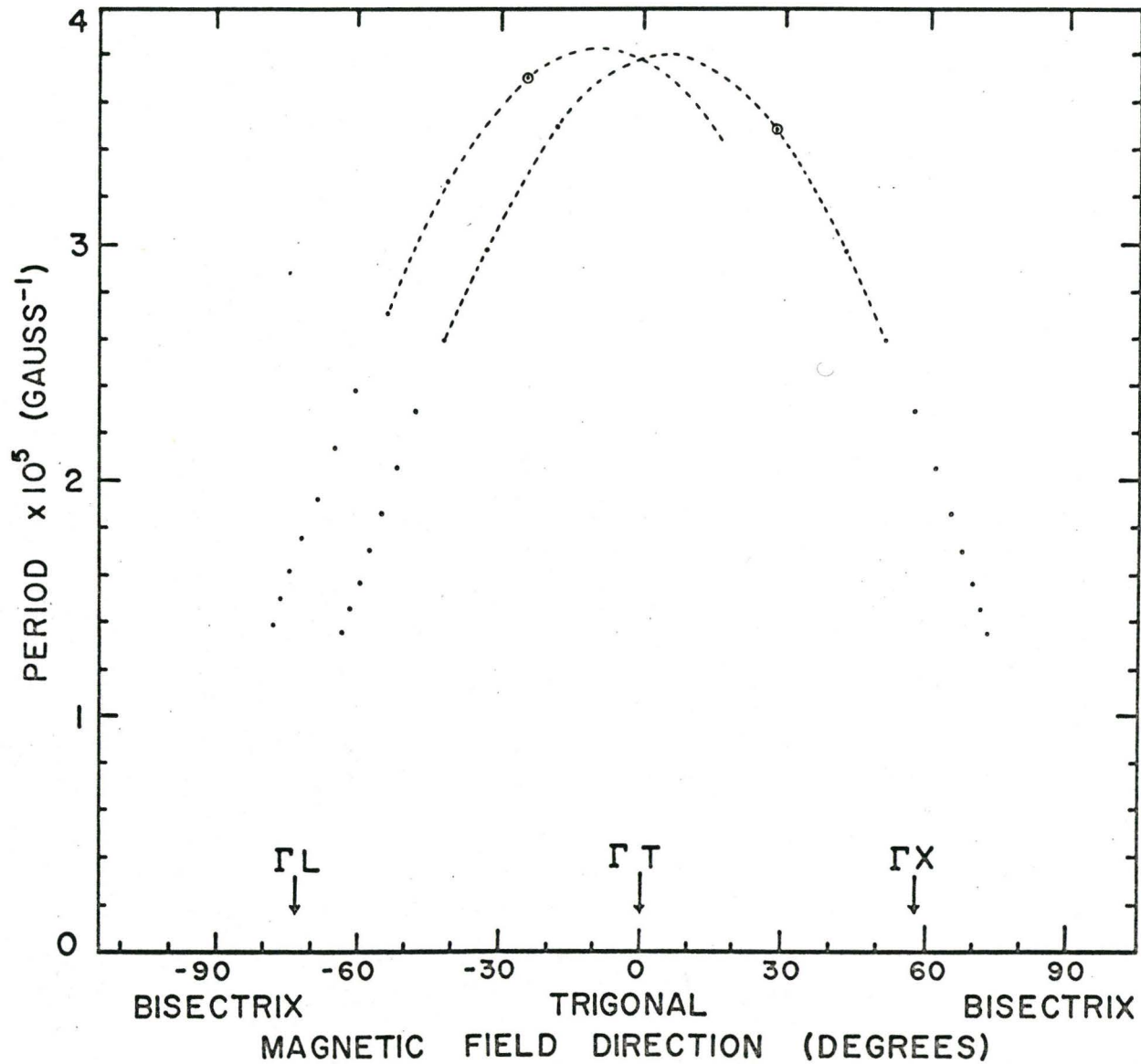
FIGURE IV-17
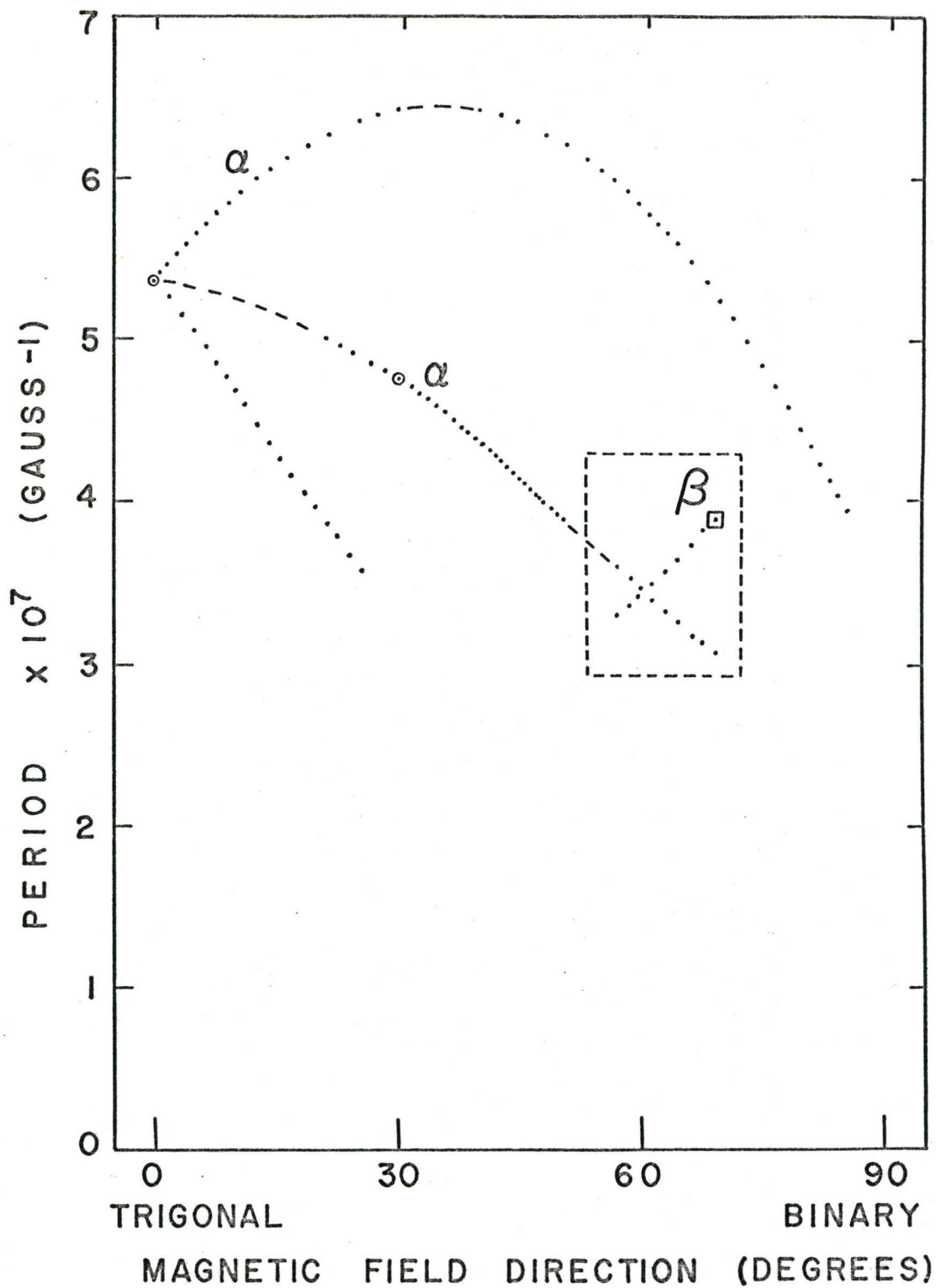
FIGURE IV-18

TEMPERATURE DEPENDENCE AND EFFECTIVE MASSES

The cyclotron effective mass $m^* = \frac{1}{2\pi}(\frac{\partial A}{\partial E})$ can be obtained from the dHvA effect since it is the phenomenological constant which describes the energy between two adjacent Landau levels at the extremum of the Fermi surface. Referring back to equation (IV-5), we shall see that the amplitude A of the dHvA oscillations is proportional to

$$A \propto T \, [\sinh(2\pi^2 kT/\beta H)]^{-1} \, . \qquad \text{(IV-60)}$$

Expanding the hyperbolic sine function into its two exponentiala it is easy to show that the above proportionality can be written

$$\ln[\frac{A}{T}\{1 - e^{-\frac{4\pi^2 kT}{\beta H}}\}] = -\frac{2\pi^2 kT}{\beta H} - K \qquad \text{(IV-61)}$$

where K is a constant. Thus a plot of $\ln[\frac{A}{T}\{1-e^{-\frac{4\pi^2 kT}{\beta H}}\}] + K$ versus T will yield a line of slope $-\frac{2\pi^2 k}{\beta H}$, where $\beta = \frac{eh}{m^* c}$. Because β is not initially known, a first approximation to β can be derived from a plot of $\ln \frac{A}{T}$ versus T. This value of β can be used to plot $\ln[\frac{A}{T}\{1 - e^{-\frac{4\pi^2 kT}{\beta H}}\}] + K$ versus T, giving a second approximation to β. This iterative process can be repeated until a satisfactorily accurate value of β is obtained. In arsenic more than one iteration is seldom necessary, and often the initial approximation is excellent, especially when T is large and H is small.

The Fermi degeneracy energy from the band minimum can

be approximated by the assumption that the difference in energy between each Landau level is a constant and if n of them occur inside the Fermi surface then the degeneracy energy will be

$$E_F = n \hbar \omega_c \ . \tag{IV-62}$$

This can easily be shown to give

$$E_F = \beta/P = \beta F, \tag{IV-63}$$

where $P = 1/F$ is the dHvA period. For a segment of the Fermi surface in which the dispersion law is quadratic, the degeneracy energy E_F will be constant at all orientations, but not otherwise.

An accurate measurement of temperature is obtained by comparison of the He^4 vapour pressure with the well known temperature-vapour pressure curves[58]. The pressure was determined with mercury manometers and a calibrated thermal conductivity automatic vacuum gauge. The amplitude of the oscillations is obtained from the envelope of the oscillations, preferably at orientations where beats do not exist. If two oscillations are beating, the envelope will have maxima T_{max} and minima T_{min}, and the amplitudes of the two components are found from

$$A_1 = (T_{max} + T_{min})/2, A_2 = (T_{max} - T_{min})/2. \tag{IV-64}$$

Figure IV-19 shows two plots of $\ell n [\frac{A}{T}(1 - e^{-\frac{4\pi^2 kT}{\beta H}})] + K$ versus T at the direction $\theta = -80°$ for the β carrier. The crosses in the trigonal bisectrix plane, represent values of $\ell n \frac{A}{T}$ and the circles are the corrected values after one iteration, as des-
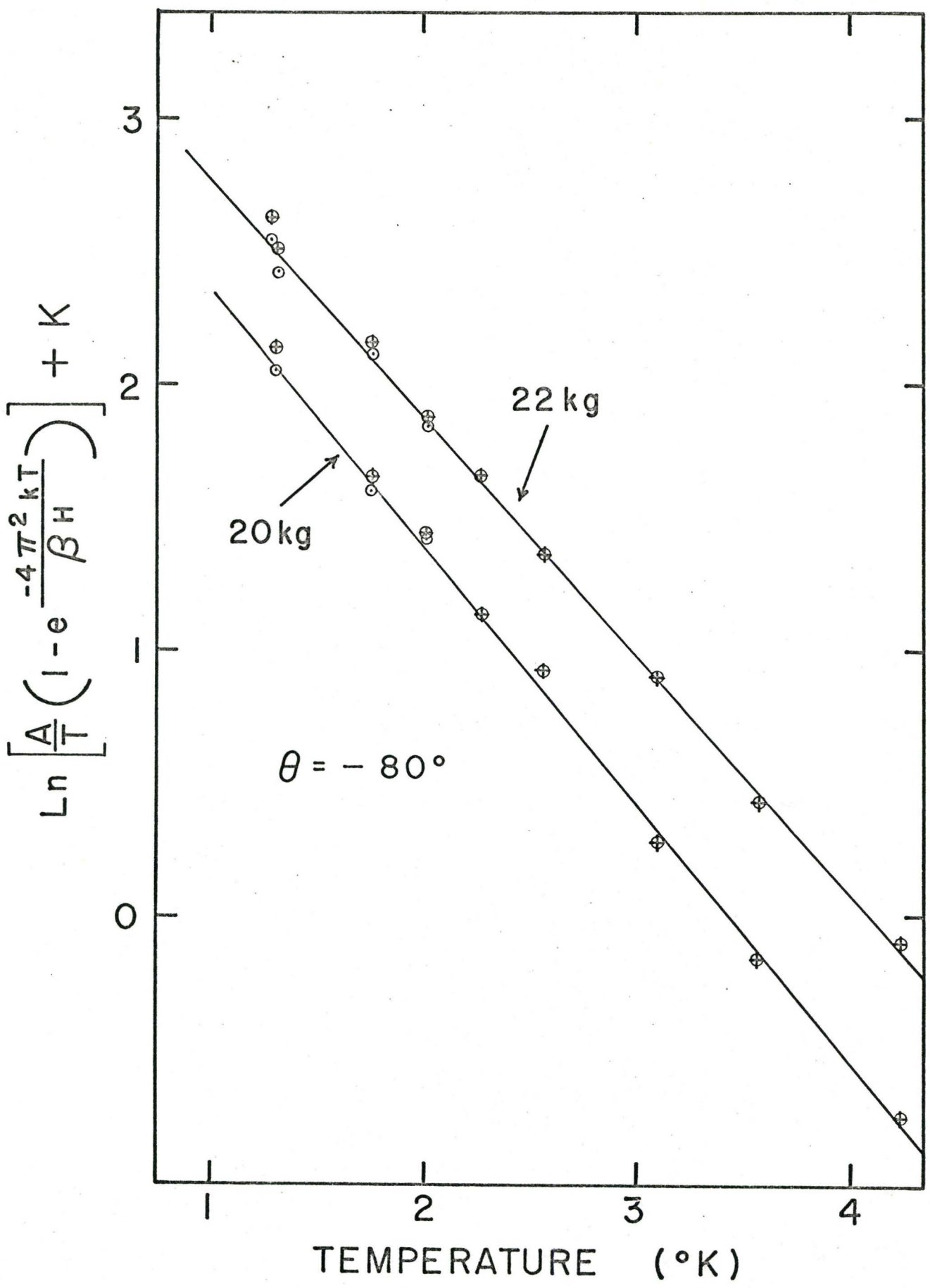
FIGURE IV-19

cribed above. The slope of the curves gives the Fermi energy for these carriers as 31.0 ($\pm$ 0.3) x 10^{-14} ergs. The effective mass $m^* = 0.132\ m_o$.

A good estimate of the Dingle temperature is also available for this orientation, by comparing the amplitudes at various temperatures for the two field values. From equation (IV-6), the variation of amplitude with magnetic field is given by

$$A \propto H^{1/2}\ \frac{e^{-\frac{2\pi^2 k(T + T_D)}{\beta H}}}{[1 - e^{-\frac{4\pi^2 kT}{\beta H}}]}\ . \qquad \text{(IV-65)}$$

It is found that $T_D \simeq 2.77\ ^oK$.

The temperature dependence of the α carriers was measured in the trigonal-bisectrix plane at an orientation $\theta = 28^o$. Figure IV-20 shows plots of the amplitude for several magnetic fields. An analysis yields a Fermi energy of about 28 x 10^{-14} ergs, since the curves have a slight positive curvature and it is not precisely clear what slope should be taken. The cyclotron effective mass is $m^* = 0.100\ m_o$. The curvature may or may not be real. It has been observed in single-crystal mercury[59] and the effect is also not understood. An estimate of the Dingle temperature gives $T_D = 2.65\ ^oK$.

Temperature dependence of the carriers seen in the binary-bisectrix plane gives a Fermi energy of 30.3 x 10^{-14} ergs, indicating that these carriers are the β carriers. At an angle

The y-axis is labeled $Ln\left[\frac{A}{T}\left(1-e^{\frac{-4\pi^2 kT}{\beta H}}\right)\right] + K$

The x-axis is labeled TEMPERATURE (°K)

Labels on the plot: 22 kg, 20 kg, $\theta = 28°$
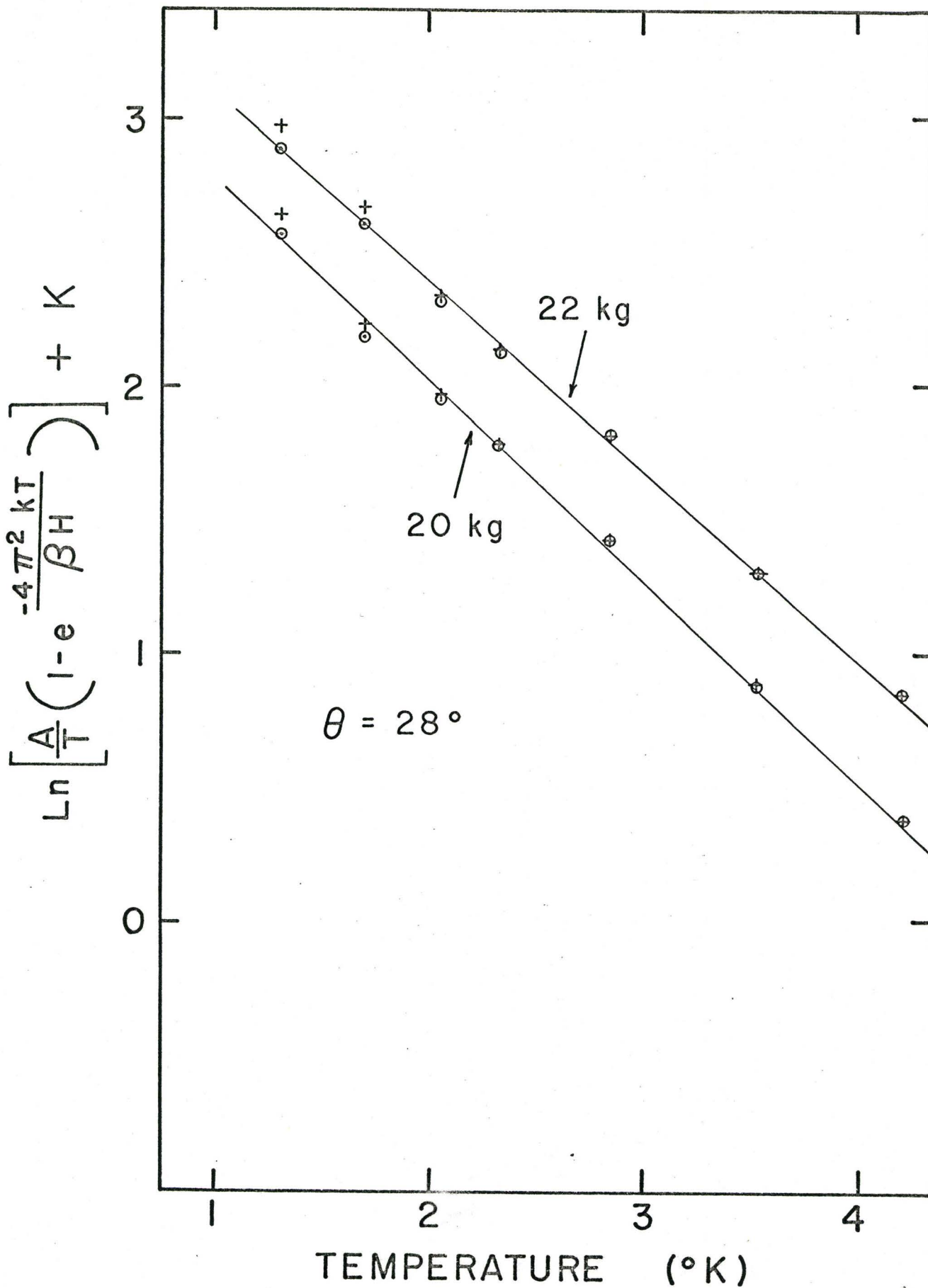
FIGURE IV-20

of 12° from the binary axis, the cyclotron mass $m^* = 0.138 \ m_o$. This value is in excellent agreement with that measured by cyclotron resonance[57] experiments, which give a value of $m^* = 0.14 \ m_o$.

CHAPTER V

MAGNETOTHERMAL AND MAGNETORESISTANCE EXPERIMENTS

MAGNETOTHERMAL EXPERIMENTS

As was stated earlier, there are many ways to observe the effect of a magnetic field on the condensation of conduction electrons on Landau levels. One that was realized only in the fairly recent experiments of Kunzler et al[22] is to measure temperature changes of a thermally isolated sample as the field is varied. The experiments must be done at low temperatures and since there is some eddy current heating due to the magnetic field sweep, the sample must have a controlled heat leak to the surroundings. This can be achieved with gaseous helium used as a thermal conductor or by various rigid mechanical heat leaks. The thermometer used to measure the temperature of the sample need not have high absolute accuracy but must have a high sensitivity because typical variations in temperature are found to be 10^{-4} ^{o}K. At low temperatures, it is found that ordinary Allen-Bradley (Ohmite) carbon resistors are excellent thermometers with predictable characteristics[60] because of their semi-conducting

115

properties.

In the experiments reported here on arsenic, the arsenic sample was supported in an evacuated can by a small graphite block which had very low thermal conductivity at low temperatures. Allen-Bradley resistors of the 1/4 watt composition variety with nominal resistances of 270 and 470 ohms were used. Identical resistors were used in a Wheatstone bridge circuit, with one resistor glued to the sample and another fastened to the evacuated container. One side of each resistor was carefully ground off and the flat side was bonded to the sample or can with G.E. 7031 varnish so that there would be an intimate thermal contact of the surface with the semi-conducting material itself. Copper wire of B. and S. gauge 44 was used to attach the sample resistor to kovar terminals leaving the can. The fine copper wires were thermally bonded to the sample with varnish so that no lagging of the carbon resistor to the bath would occur. The thermal time constant from the sample to the can was adjusted by the length of copper wire used from the sample to the kovar.

In operation the evacuated can is placed in a helium IV cryostat and the temperature of the helium bath and can is reduced to 1.2°K. It was found that, using a time constant of 30 seconds, the sample and its resistor were about 1/10 $^{\circ}$K warmer than the helium bath, and in-

dependent of the thermometer power, for powers less than 10^{-6} W. This was probably due to vibrations caused by the vacuum forepumps which were used to reduce cryostat pressure by pumping on the helium bath. As a result, the two matched resistors did not have the same resistance and magnetoresistance, and it was too difficult to extract meaningful information from any slowly varying background signal. Oscillations were not affected and the dHvA results of two important crystal planes are given in Figures V-1 and V-2. These are to be compared with the data from the torque method found in Figures IV-9, IV-10 and IV-15.

The choices of components for a magnetothermal experiment are based on several decisions. Thermometer power must be kept less than about 10^{-7} watts to avoid heating. Experiments here described used a Hewlett-Packard model 425A microvoltammeter with an imput impedance of 1 megohm on sensitive ranges. Thus the resistors in the Wheatstone bridge should have lower resistances at their operating temperatures to prevent loading of the bridge and subsequent error in the measured temperature excursions. If the bridge impedance is matched to the voltmeter, corrections must be applied for the loading effects. The next criterion is that a large resistance is desirable since this permits a higher bridge voltage commensurate with a thermometer power less than 10^{-7} watts. In the experiments
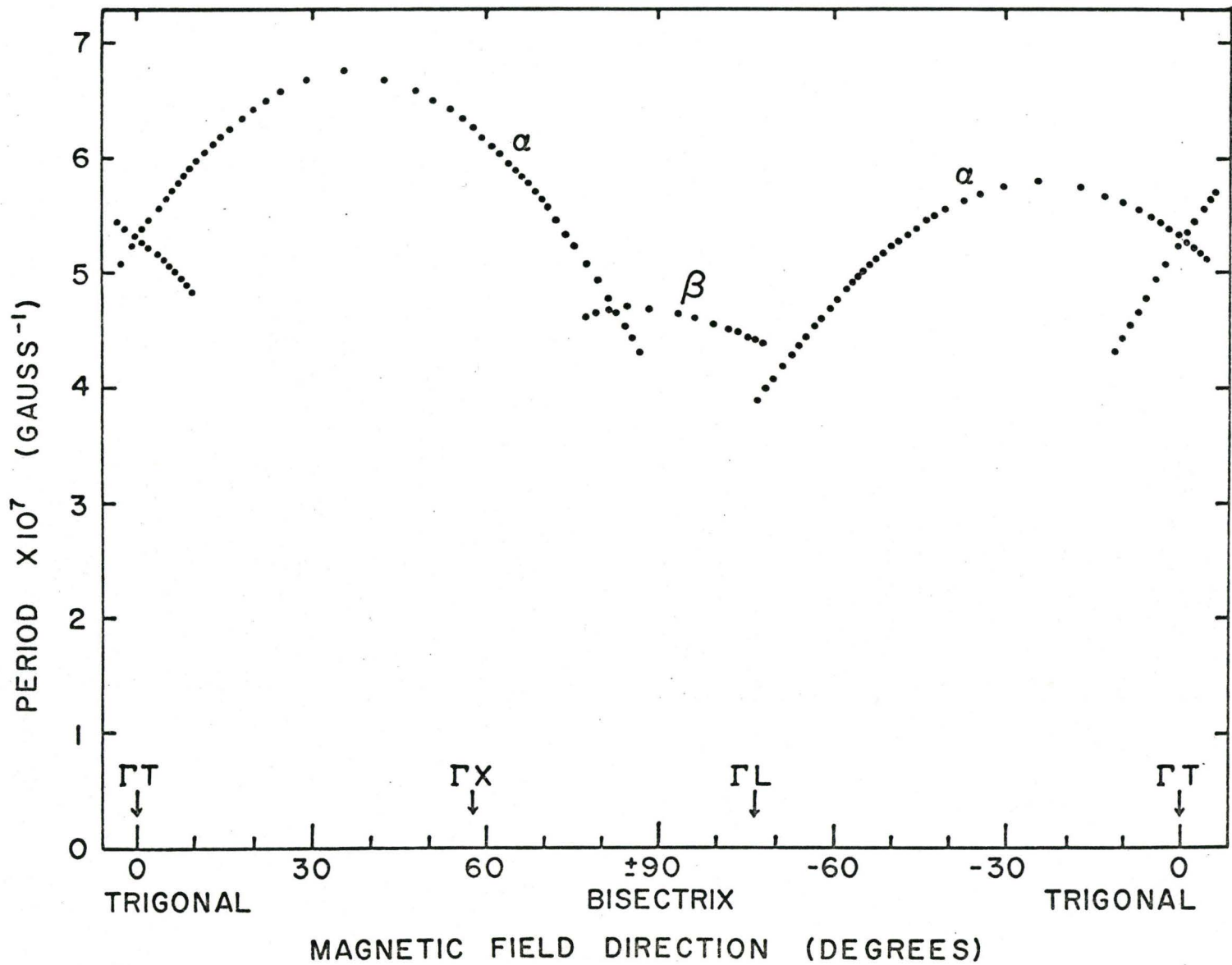
FIGURE V-1
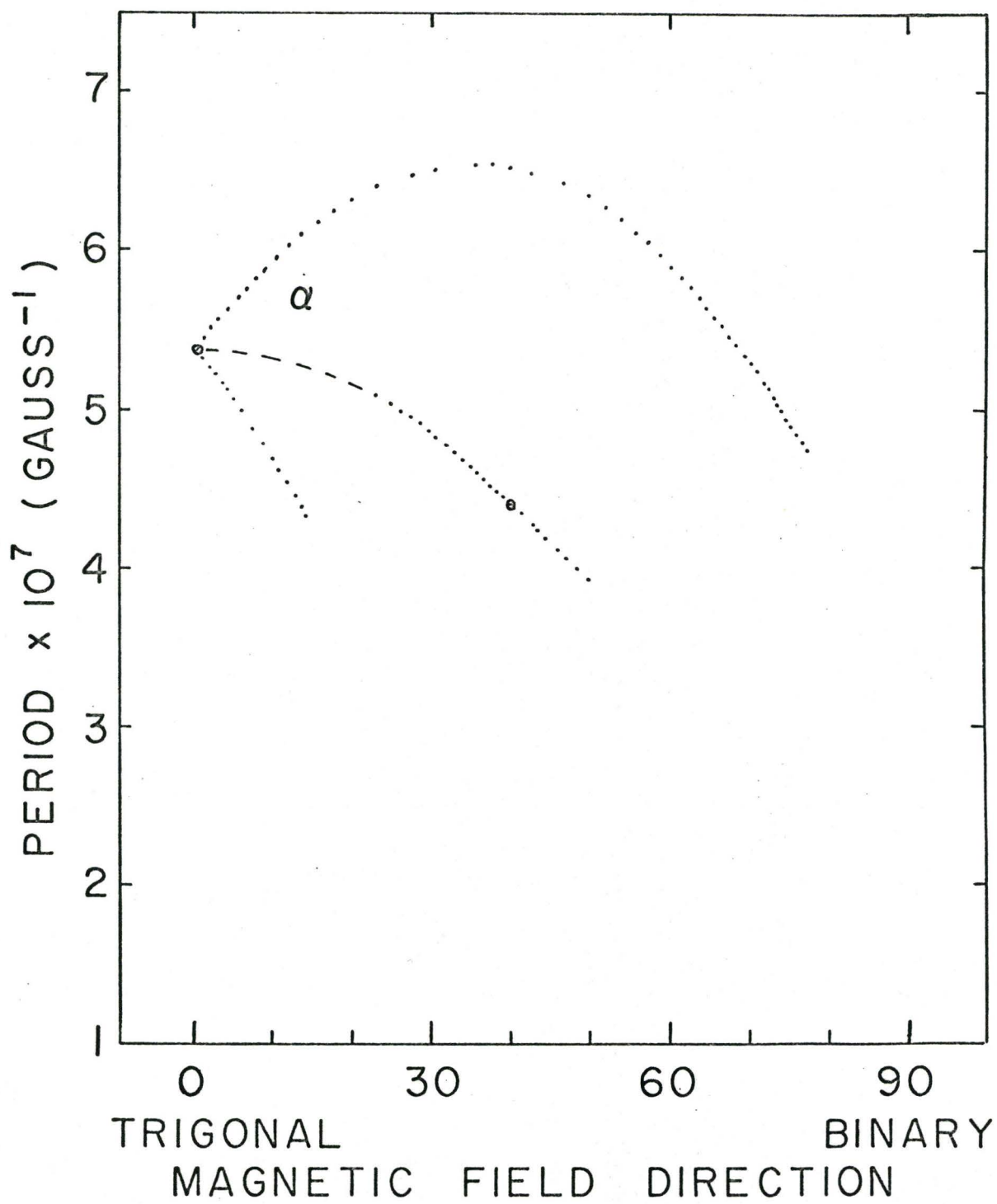
FIGURE V-2

nominal 470 ohm resistors were used and applied voltages were about 0.1 volt. This gave reasonable sensitivity for the voltmeter mentioned above. Noise, which was presumably due to temperature fluctuations in the cryostat or vibrations of the lead-in wires in the magnetic field, limited the smallest observable oscillatory temperature excursion to about 10^{-5} °K. To determine the thermal time constants of the sample to the bath and of the resistor to the sample, a pulse of electrical energy was sent through the sample resistor and the unbalance voltage was measured as a function of time. Figure V-3 shows a graph of the voltage unbalance, which is accurately proportional to the temperature difference ΔT of the two thermometer resistors. The initial negative segment marks the end of the application of the electrical heat pulse. It is seen that immediately thereafter the voltage difference is negative, indicating a warm sample resistor. The temperature initially decays to its equilibrium value with a time constant of approximately 3 seconds and this is interpreted as the thermal time constant between the resistor and the arsenic sample. The final difference voltage decays with a 25 second time constant and it represents the relaxation of the sample temperature to that of the can at bath temperature. This was in accord with a study of the amplitude of dHvA oscillations as a function of the field sweep rate.
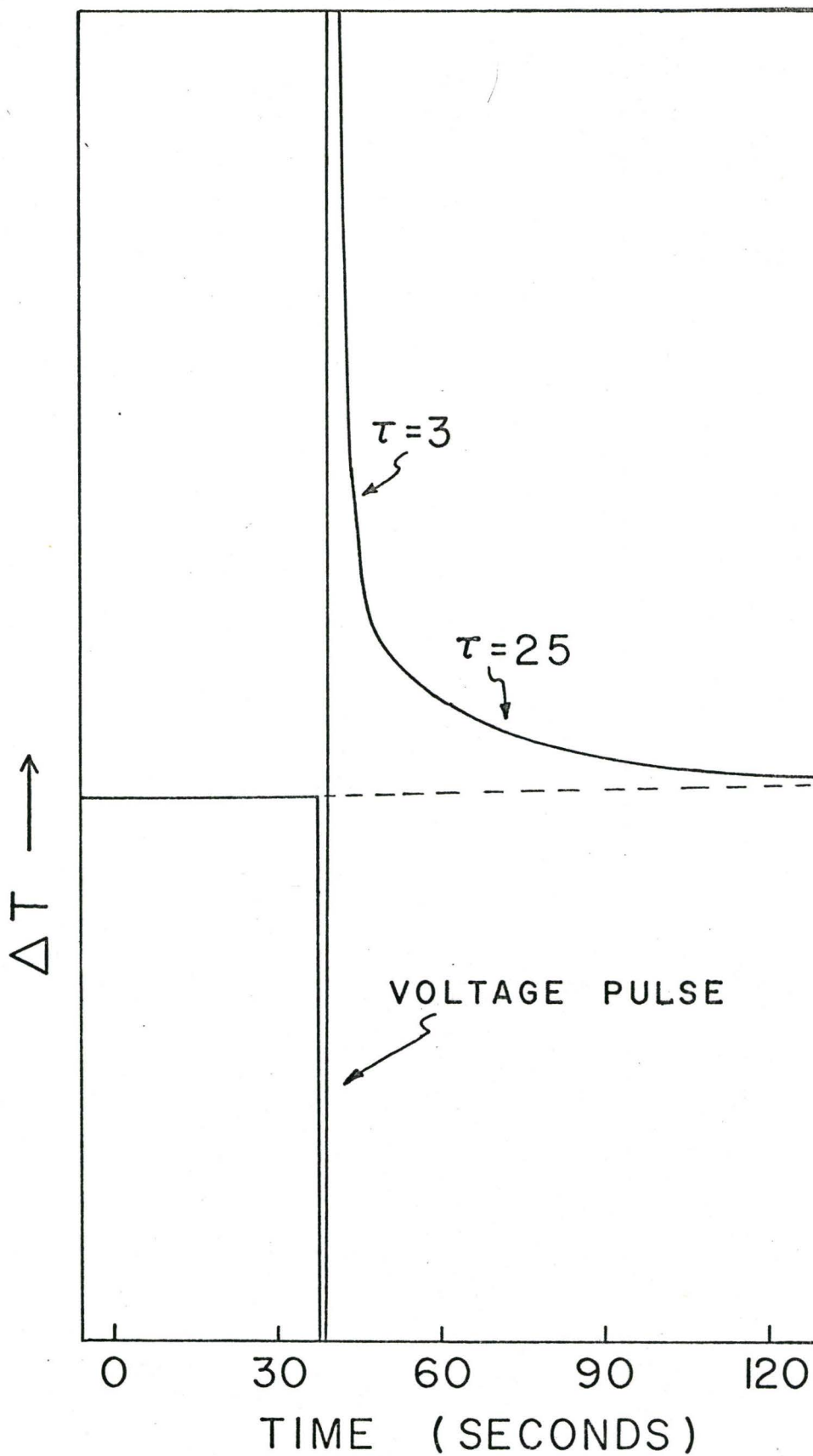
FIGURE V-3

At low fields there was heating of the sample during the time that the magnetic field was swept. Figure V-4 shows traces in which the field was swept up and down. When sweeping up from H = 0 there is a peak in the heating at about 500 gauss; on sweeping down the peak is somewhat higher and occurs at the end of the field sweep. These observations indicate that the effect was due to eddy currents which disappear at higher fields because the magnetoresistance goes up approximately as the square of the applied field. As the field is swept upwards from the minimum remanent field of the magnet, heat is produced by the eddy currents which flow perpendicular to the direction of the increasing field. This heat will build up the sample temperature but the increasing transverse magnetoresistance will rapidly decrease eddy currents. Thus as the field increases a point will soon be reached at which the amount of heat created by the eddy currents is less than the heat necessary to maintain the higher sample temperature because of the controlled heat leak. The sample temperature decreases rapidly to its equilibrium value. When the field reaches 2 kilogauss very little more change occurs. The linear behaviour of the baselines in Figure V-4 is due to linear signal bucking and the parabolic behaviour is due to magnetoresistance of the resistance thermometer. It does not decay if the field is held constant.

$$\frac{\partial H}{\partial t} = 0$$

← Time

Time →

ΔT →

MAGNETIC FIELD (KILOGAUSS)
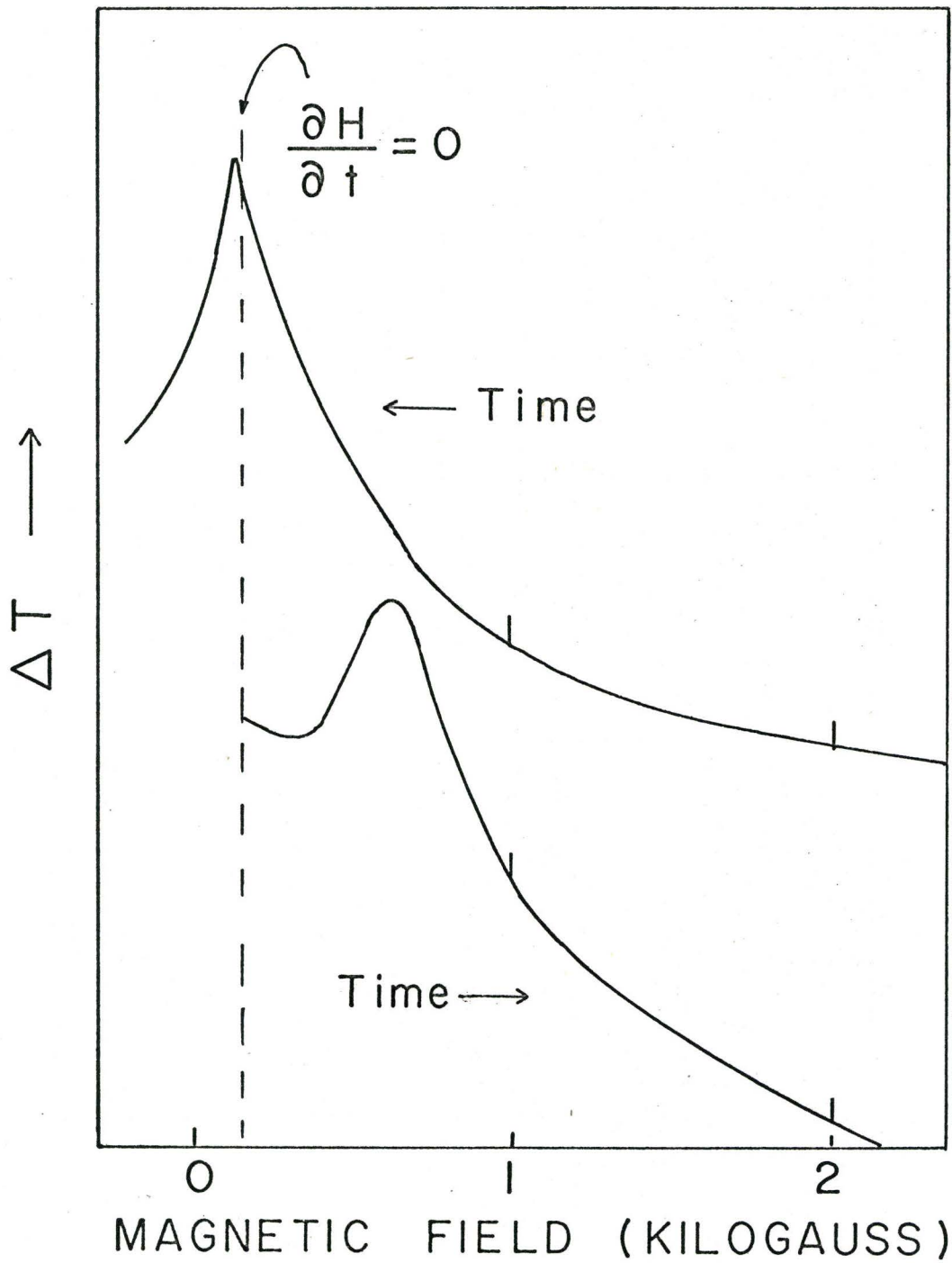
FIGURE V-4

When the field is swept downwards, heating effects will occur as the magnetoresistance of the sample decreases. The maximum temperature of the sample (somewhat higher for the same sweep rate) will occur when the sweep stops because the eddy current heating is largest at the lowest field. The temperature is lower in the case of upward swept field since more heat is produced in the start of the field sweep and this allows more heat to be conducted away by the heat leak before the maximum temperature is reached. This effect has little bearing on the dHvA studies but it provides a positive indication that at high fields heating effects will be very small for almost any sweep rate.

DISCUSSION OF MAGNETOTHERMAL EXPERIMENTS

The sweep rate that is best to measure a temperature oscillation is determined by the time constants in the experiment. Heat from the sample flows to the external helium bath with a time constant of 25 seconds. This is equivalent to saying that a differentiating time constant τ_D of 25 seconds reduces the amplitude of the oscillations. If the oscillations have a frequency in time of ω, then they are reduced in amplitude by a factor

$$\beta = \frac{\omega \tau_D}{\sqrt{1 + \omega^2 \tau_D^2}} \quad . \tag{V-1}$$

The sample resistor follows the temperature oscillations of the sample with a 3 second integrating time constant τ_I, and the actual oscillation amplitude that is measured will be reduced by another factor

$$\gamma = \frac{1}{\sqrt{1 + \omega^2 \tau_I^2}} \ . \tag{V-2}$$

The measured oscillations are thus reduced from the theoretical maximum amplitude by the factor

$$\beta\gamma = \frac{\omega \ \tau_D}{\sqrt{1 + \omega^2 \tau_D^2} \ \sqrt{1 + \omega^2 \tau_I^2}} \tag{V-3}$$

and this function will have a maximum of

$$(\beta\gamma)_{max} = \frac{\tau_D}{\tau_D + \tau_I}$$

for

$$(V-4)$$

$$\omega_{max} = \frac{1}{\sqrt{\tau_I \ \tau_D}} \ .$$

The value of $\omega_{max} = 0.115$ sec^{-1} for $\tau_D = 25$ seconds and $\tau_I = 3$ seconds, which means that each oscillation is best covered in about 50 seconds. Actually each oscillation could occur in about 5 seconds with little change in output amplitude, hence we must conclude that the time constant τ_I is considerably less than 3 seconds. Perhaps our pulse measurement technique measures the lag caused by the outer coating of the measuring resistor. It must also be remembered that the equations above

describe simple equivalent circuits of resistors and capacitors but heat flow actually requires the solution of more complex heat flow equations with distributed parameters.

The oscillations were observed both as a function of magnetic field and magnet orientation. It was hoped that β oscillations would be more pronounced and that symmetry directions could be more easily observed by magnetothermal methods. Considerable experimental difficulties occurred in the experiments and neither of the above goals were achieved. The observed oscillation periods are shown in Figures V-1 and V-2 and are in good agreement with the results presented in Chapter IV. The long periods are observed but because they have such a low frequency as the field is swept, phase shifts occur. These oscillations are quite sinusoidal as opposed to the oscillations in bismuth[22] which show spin splitting. One reason for this is that the effective masses for the long period carriers in arsenic are higher ($m^* \simeq 0.033\ m_o$) than those in bismuth ($m^* \simeq 0.01\ m_o$). Hence the Landau levels in arsenic are closer together and more thermal smearing is expected to occur, causing averaging and more sinusoidal oscillations. Another difficulty in arsenic was that at higher fields the short period oscillations would mask any fine structure of the long period oscillations. Finally, it must be remembered that in arsenic these carriers form long cylinders, whereas in bismuth the Fermi surface is described by a 4 ellipsoid model. It is also very likely that the bismuth single crystals were less strained

than our arsenic crystals and hence that the Dingle factor for bismuth was near unity for the higher harmonics, allowing more structure to be observed on the dHvA magnetothermal oscillations.

THEORY OF THE MAGNETOTHERMAL EFFECT

Let us idealize the problem of calculating the magneto-thermal effect by allowing no heat transfer from the sample to the helium bath and eddy current heating effects will also be neglected. Then a small change in external magnetic field will cause a small change in temperature of

$$dT = (\frac{\partial T}{\partial H})_{S,P} \; dH \qquad (V-5)$$

and this can be written as

$$dT = - \frac{T}{\gamma_{P,H}} \; (\frac{\partial M}{\partial T})_{H,P} \; dH \qquad (V-6)$$

by Maxwell's relations[61]. Here M is the magnetization per unit volume and $\gamma_{P,H}$ is the specific heat per unit volume at constant pressure and magnetic field. At the very low temperatures at which the experiments are performed, the electronic specific heat will usually be the most important contribution, since the lattice specific heat has a T^3 dependence. Since the total temperature excursion is known to be less than $10^{-2} \; {}^{\circ}K$, the parameter $\frac{T}{\gamma_{P,H}}$ can be considered to be constant in our approximation. $\gamma_{P,H}$ will have some oscillatory dependence on magnetic field, but this will be small because the electronic

specific heat results from an integration over the whole Fermi surface. The derivative $(\frac{\partial M}{\partial T})_{H,P}$ can be evaluated if the free energy is known, because $M = -(\frac{\partial F}{\partial H})_{T,V}$. Thus eqn. V-6 gives the measured magnetothermal effect in a field modulation experiment. This has been done by McCombe et al[62] using thermometers with extremely short (10^{-2} sec.) relaxation times to the sample.

In the present experiments the temperature is recorded as the field is swept, and equation V-6 must be integrated to give the $T = T(H)$ relationship. This is virtually impossible since the theoretical forms of $(\frac{\partial M}{\partial T})_{H,P}$ and $\gamma_{P,H}$ are very complicated and the variables T and H cannot be separated. However, a good insight into the effect can be had by a somewhat simplified analysis.

We are only interested in the oscillatory phenomena and it will be assumed that at all times the temperature is close to the temperature T_o at zero magnetic field. Any steady diamagnetic or paramagnetic effects will vary slowly with field and their heat will be conducted away by a small heat leak. Thus equation V-6 can be approximately integrated in the form

$$\int_{T_o}^{T_o+\Delta T} dT = -\frac{T_o}{\gamma_{P,H}} \int_0^H (\frac{\partial M_{osc}}{\partial T})_{H,P} dH \qquad (V-7)$$

where only the oscillatory magnetization is considered. All temperatures on the right hand side of this expression will be

set equal to T_o after the calculation. M_{osc} is given by $-(\frac{\partial F_{osc}}{\partial H})_T$, where F_{osc} is the oscillatory free energy as given in equation II-17, and equation V-7 can be written

$$(\Delta T)_{osc} = + \frac{T_o}{\gamma_{P,H}} \frac{\partial}{\partial T} \left[\int_0^H (\frac{\partial F_{osc}}{\partial H})_T \, dH \right]_H \quad \text{(V-8)}$$

which is easily seen by reversing the order of the integration and differentiation. Then we have finally

$$(\Delta T)_{osc} = \frac{T}{\gamma_{P,H}} (\frac{\partial F_{osc}}{\partial T})_H \quad \text{(V-9)}$$

which we expect will be a good approximation to the magneto-thermal effect if temperature excursions are small and the specific heat $\gamma_{P,H}$ is not greatly dependent on the magnetic field.

To gain physical insight into the measurement of the magnetothermal effect, we shall give expressions for equation V-9 using only the dHvA fundamental oscillations in equation II-17. It is easy to show that $(\Delta T)_{osc}$ is given by

$$(\Delta T)_{osc} \cong - \frac{1}{\gamma_{P,H}} (\frac{2\pi^2 kT}{\beta H} \coth[\frac{2\pi^2 kT}{\beta H}] - 1) \, F'_{osc} \quad \text{(V-10)}$$

where F'_{osc} denotes only the fundamental oscillation for $p = 1$. For positive values of $\frac{2\pi^2 kT}{\beta H}$ the bracket is positive, although in arsenic $\frac{2\pi^2 kT}{\beta H}$ is usually greater than unity, and the hyper-

bolic cotangent is very nearly unity also. In any event, the oscillations of the temperature have a phase opposite to those of the free energy. This was to be expected since an increase in the magnetic energy will require that thermal energy be taken from the crystal lattice, which subsequently cools.

Another way of looking at the problem is to consider the entropy of the magnetic system exchanging with the entropy of the crystal lattice, as is done by Kunzler et al[22]. They discuss bismuth results for low Landau level numbers and show that the crystal will have a cooling peak as the bottom of a Landau level passes through the Fermi surface. The ideas presented above are for much higher Landau level numbers so that the temperature variations as a function of field or orientation are quite sinusoidal and total temperature excursions are small ($\approx 10^{-3}$ $^\circ$K).

The variations of temperature were compared to calculated values on the basis of equation V-10. Amplitudes of oscillation of the free energy were determined from the dHvA torque oscillations. Knowing the value of $\frac{\partial F}{\partial \Theta}$ in equation IV-52 allows calculation of A(H,T), the amplitude of the oscillatory free energy. The electronic and lattice specific heats are found from published data on arsenic[74] and the predicted magneto-thermal effect is about 5 x 10^{-3} $^\circ$K or somewhat higher, which is a factor of five greater than actually observed. This is not good agreement but does indicate that the simple calculations indicate the correct order of magnitude.

MAGNETORESISTANCE

Both magnetoresistance and magnetothermal experiments were undertaken to ascertain if the electron Fermi surface could be more easily observed in these experiments than a torque dHvA experiment. The magnetoresistance measures the change in relaxation time of the conduction electrons near the Fermi surface and the total available phase space for scattered particles. Since the density of states at the Fermi surface oscillates in a manner similar to the free energy, there will be an oscillatory conductivity which is called the Shubnikov-de Haas effect. There will also be a normal transverse magnetoresistance term which varies as H^2. This is due to the fact that the current carriers are now not only under the influence of electric fields in the direction of the current, but a Lorentz force e $\vec{V} \times \vec{B}$ acts on the carriers and tends to make them move in circular arcs. A Hall electric field will be set up to counteract this, but such a field can never compensate for both holes and electrons. Since the relaxation time of the carriers will be substantially constant, the carriers will not have moved as far along the current direction with the magnetic field applied.

Several calculations exist for the oscillatory magnetoresistance. Adams and Holstein[24] were first to obtain correct formulas for the effect. Other references and several corrections and improvements in the theory are given in a paper

by Soule, McClure and Smith[64]. The ratio of the oscillatory to non-oscillatory conductivity is given by

$$\frac{\Delta\sigma_{xx}}{\sigma_{xx}} = \frac{5}{2\sqrt{2}} \left(\frac{H}{F}\right)^{1/2} \left(\frac{2\pi^2 kT}{\beta H}\right) \frac{e^{-\frac{2\pi^2 kT_D}{\beta H}}}{\sinh\frac{2\pi^2 kT}{\beta H}} \cos\left(\frac{2\pi F}{H} + \delta\right) \quad \text{(V-11)}$$

Here T_D is the Dingle temperature given by $T_D = \frac{h}{\pi k \, \tau_{col}}$, where τ_{col} is the collision relaxation time. The expression is valid only for the first harmonic and for large Landau level numbers, which is expected to be quite close to the truth for the short periods in arsenic. Any experiment in which the boundaries of the specimen determine the current direction measures not the conductivity, but the resistivity tensor. We must invert equation (V-11) to obtain resistivities. It turns out that the Hall coefficients in arsenic are quite small[65] so that

$$\frac{\Delta\rho_{11}}{\rho_{11}} = -\frac{\Delta\sigma_{11}}{\sigma_{11}} \quad \text{(V-12)}$$

and thus equation (V-11) can also be used for $-\frac{\Delta\rho_{11}}{\rho_{11}}$.

A piece of arsenic was cut with a Servomet spark cutter so that the long axis was along the bisectrix axis. Current contacts were applied to the ends and potential contacts were applied near the ends of the sample by using silver paste to attach fine copper wires to the sample. Experiments were done up to 57,000 gauss using a superconducting solenoid with a sample rotation device to turn the sample in the trigonal-bisectrix plane.

The turning mechanism used nylon stranded string and had a possible orientation error of $5°$, so the results of the period analysis were not done as completely as the torque and magneto-thermal experiments.

The residual resistivity ratio $\rho_{300°K}/\rho_{4.2°K}$ between room and liquid helium temperatures was measured to be about 10^3. This sample, 1.7 x 0.7 x 4.5 mm in size between the potential contacts, was used in the experiments with a current source of 100 milliamperes. The voltage across the potential contacts was amplified by a voltmeter using a chopper stabilized D.C. amplifier and the signal was displayed on a strip chart recorder while the field was swept uniformly with time.

Figure V-5 shows a partial trace up to maximum field of oscillations without bucking of the H^2 term. At zero field the voltage between the potential contacts was virtually zero on the scale of Figure V-5. It was noted that the oscillatory component of the magnetoresistance only showed up past about 15 kilogauss , whereas in dHvA experiments the oscillatory component appeared as early as from 1 to 5 kilogauss . Also, the oscillations have periods of about 5×10^{-7} gauss^{-1}, which corresponds to the Berlincourt α carriers. The β carriers were also observed at some orientations. In the trigonal-bisectrix plane there was no evidence of any long periods of about 3×10^{-5} gauss^{-1}, which are usually the dominant oscil-lations in the torque or magnetothermal dHvA experiments.
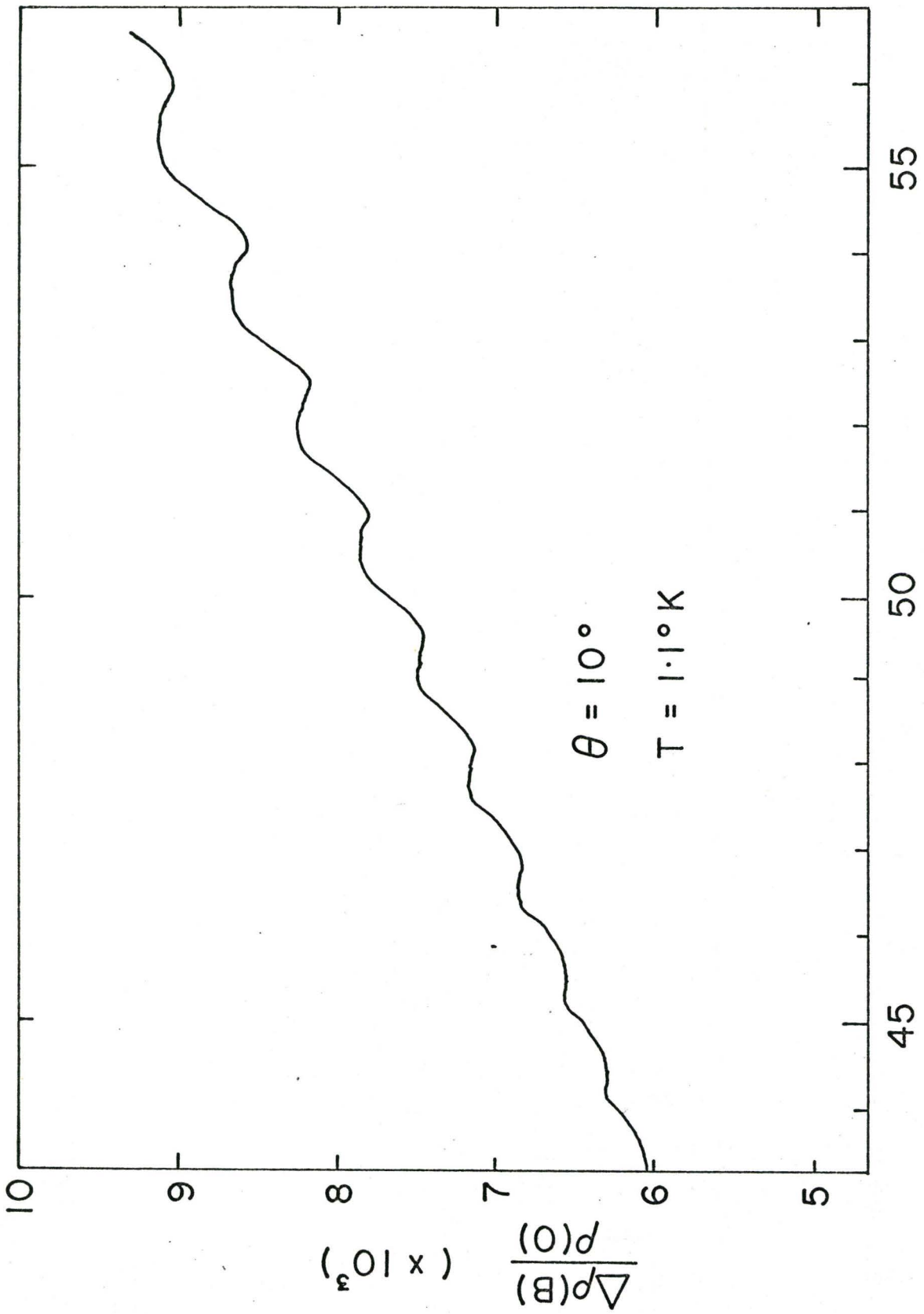
FIGURE V-5

If the oscillations in Figure V-5 are averaged, the plot of the manetoresistive voltage versus field is not adequately given by a square law. A plot of $\ln\frac{\Delta\rho}{\rho}$ versus $\ln H$ in Figure V-6 shows that the variation is well described by $\rho = k\ H^{1.8}$. The index is independent of the current which passes through the crystal and the discrepancy from the value 2 may point to some basic oversimplification in the theory of transverse magnetoresistance. This effect is also seen in other compensated metals such as Mo, Re, Pt, Fe and Pd[66]. Values of the index vary slightly for changes in orientation, and a value of 1.80 ± 0.05 describes well the general behaviour for arsenic.

The resistivity at 60 kilogauss is about an order of magnitude larger than at room temperature. It has been suggested[66] that in such cases the shorting effects of the potential contacts may cause anomalous behaviour such as indicated above. This is not likely in our case since the potential contacts were quite short compared to the length of the sample.

The absence of long period oscillations and the fact that short period oscillations only appeared for fields greater than 15 kilogauss, can indicate either that the crystal used was highly strained or that the Shubnikov-de Haas experiment gives much less data than those which depend on the free energy, such as torque or magnetothermal effects. Since
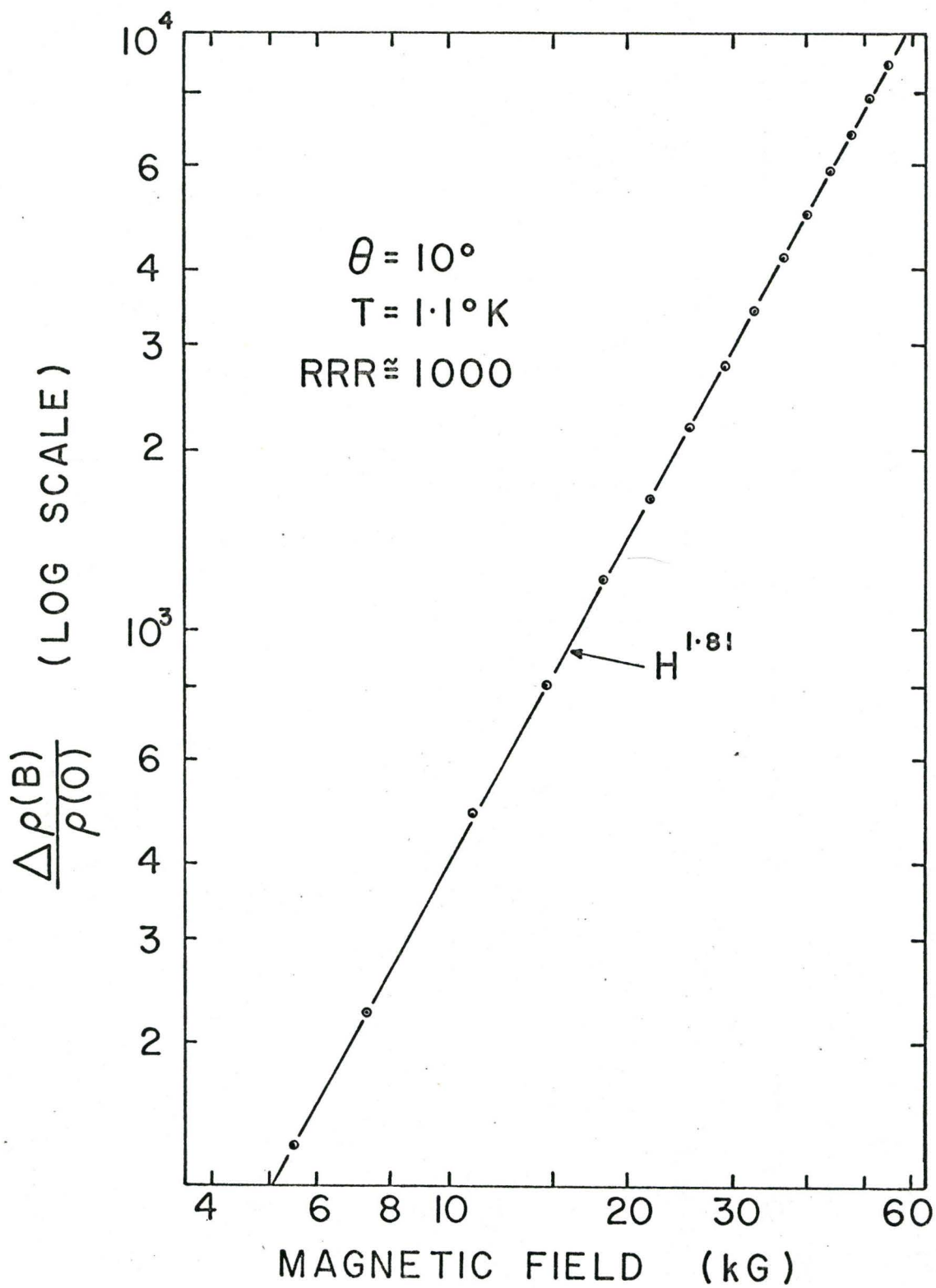
FIGURE V-6

the expression for the Shubnikov-de Haas effect is basically the same as for the other dHvA effects[24] the reduction in amplitude can be expressed as an increase in the Dingle temperature T_D. Using eqn. (V-11), a fit to the amplitude variation with field gives a Dingle temperature of about 5.6 $^{\circ}$K for the short period. This is much higher than the value obtained at the same orientation by an analysis of the torque experiments, in which values of T_D= 2.1°K were found. This trend is shown also in other magnetoresistance[64] experiments which display a T_D several times that of the more conventional dHvA experiments. The crystals used for the different experiments were of comparable quality and it must be deduced that collision processes have more effect on the Shubnikov-de Haas amplitude than the dHvA amplitude.

It is difficult to explain the absence of the long period oscillations by a simple increase in the Dingle temperature of the carriers associated with these oscillations. An increase in Dingle temperature causes less reduction in amplitude for these carriers because the value of $\beta = e\hbar/m^* c$ is about three times as large as that of the short period oscillations. Since no evidence of long period oscillations exists, it must be concluded that the cylinders have very little effect on the conductivity. This could be explained in the following way. If the period P is 3.8 x 10^{-5} G^{-1}, then the quantum limit, in which all the carriers are in the

lowest Landau level, occurs for a magnetic field of about 17.5 kilogauss. The Dingle temperature may prevent observation of the oscillations up to 17.5 kilogauss and at higher fields only a non-oscillatory behaviour would exist which would not be discernable on the large magnetoresistive background. Equation (V-11) does not contain the Fermi surface curvature $\frac{\partial^2 S}{\partial P_H^2}$ in the calculation. This term causes an additional theoretical enhancement of the long periods in the Shubnikov-de Haas effect since the density of states is multiplied by a factor $|\frac{\partial^2 S}{\partial P_H^2}|^{-1/2}$, as seen in equation (II-17).

The absolute amplitudes of the Shubnikov-de Haas effect were compared with the preditions of equation (V-11). It was found that experimental values of $\frac{\Delta\rho}{\rho}$ were generally a factor of five lower than predicted, but this is felt to be reasonable agreement since very little is known about the Fermi surface curvature, especially for the holes in arsenic. At 55 kilogauss the measured values are about $\frac{\Delta\rho}{\rho} \simeq 0.015$ and equation (V-11) predicts $\frac{\Delta\rho}{\rho} \simeq 0.075$. The absolute amplitudes of the long periods are in poor agreement since they cannot be observed but should be quite large. In this respect our results parallel those of others[65][63]. Baker and Grassie[65] measure $\frac{\Delta\rho_{11}(osc)}{\rho_{11}}$ to be at least an order of magnitude lower than our experiments. The fact that our results are closer to theoretical predictions may indicate that they have a damaged crystal.

Our results have a field dependence that is adequately described by equation (V-11), but since the exponential factors have such rapid variations, the index of an H^n factor could easily have a value different that 1/2. In conclusion it should be stated that at all observed orientations the transverse magnetoresistance did not saturate, but always had nearly an $H^{1.8}$ behaviour. This confirms that arsenic is a compensated metal or semimetal, a fact which is already well known.

CHAPTER VI

DISCUSSION OF EXPERIMENTAL RESULTS
CARRIER SIGN DETERMINATION

The dHvA oscillations cannot distinguish between hole or electron orbits, but only give the topology of the Fermi surface and its shape. Hall effect measurements differentiate between holes and electrons, but mobilities are not known so that an interpretation of the results will be difficult. Cyclotron resonance with circularly polarized radiation would give results, but to our knowledge this has not been attempted for arsenic.

Tanuma, Ishizawa and Ishiguro[67] have done dHvA experiments on arsenic doped with Si, Ge, Sn, Pb, S, Se or Te of a fraction of an atomic percent by weight. They reported that the period maximum for the principal branch of the trigonal-bisectrix plane always increased on doping, indicating that that part of the Fermi surface became smaller upon doping by either an element from group IV or group VI of the periodic table. They concluded that the effect of adding or subtracting electrons was more than offset by the shifting or warping of bands due to a change of mean lattice potential. The rigid band model[68] is thus not a good approximation for arsenic.

Berlincourt[32] also observed that his impure crystal

which had considerable amounts of the Group IV elements Si
and Pb, as well as Cu, had larger long periods near the
trigonal axis than his pure arsenic crystal. These impuri-
ties would be expected to remove electrons and thereby
lower the values of long periods, if they are holes as is
strongly indicated by the theory of Lin and Falicov[42].

The reason for the breakdown of the rigid band
model in arsenic is most likely due to the crystal structure.
In Chapter III we saw that under the assumptions made for
the pseudopotential method, the band structure was very
dependent on the internal displacement parameter u, which
is irrational for the semimetals. The shear of the rhomo-
bohedral lattice greatly affects the kinetic energy terms
and can change the relative kinetic energy of some symmetry
points with respect to others. Thus arsenic, because of its
lower symmetry, has several means whereby a small impurity
concentration can slightly change crystal parameters so
that the bands change shape and the rigid band model is
definitely not useful in predicting changes of the Fermi
surface. However, it is still not clear why the Fermi sur-
face should deform in a unilateral way with quite a variety
of dopants.

In view of the above difficulties, the sign of the
carriers will be determined by comparing the experimental
dHvA results with the theoretical predictions given by the

band structure calculations. Recent doping experiments[69] have confirmed the carrier designation as given by the band structure calculations.

PHASE OF THE LONG PERIODS

The oscillatory part of the free energy in equation (II-17) may be written in simplified notation as

$$F_{osc} = K \ \cos(\frac{2\pi F}{H} - 2\pi\gamma \pm \frac{\pi}{4}) \qquad (VI-1)$$

where K > O and is a slowly varying function of field and temperature compared to the oscillating cosine. Only the fundamental is considered here, although harmonics of the long periods are noticeable at the highest fields of our investigation. The spin splitting is assumed to be small so that cos $(\frac{\pi}{2} \frac{g}{m_e}^{*})$ is positive. Let us call the phase

$$\delta = - 2\pi\gamma \pm \frac{\pi}{4} . \qquad (VI-2)$$

The torque is given by $- (\partial F_{osc}/\partial\theta)_H$ and is

$$T = \frac{2\pi K}{H} (\frac{\partial F}{\partial\theta}) \ \sin (\frac{2\pi F}{H} + \delta). \qquad (VI-3)$$

If the sense of the torque oscillations are known, a plot of the torque maxima or minima as integers versus the 1/H values at which they appear can be extrapolated to infinite magnetic field ($\frac{1}{H} \to 0$) and the phase can be determined.

A very simple method to check the direction of the torque is to compare the oscillations with the torque due to the magnetic anisotropy. This torque varies as H^2 and is such that the trigonal axis of the crystal tries to line up with the field. This was verified in an experiment. Taylor, Bennett and Heyding[50] note this also, and point out that Berlincourt's[32] values for the anisotropy susceptibility $(\chi_{||} - \chi_{\perp})$ should be positive, not negative.

The sign of $(\frac{\partial F}{\partial \theta})$ is immediately available from the period plots $(P = \frac{1}{F})$. Thus all the signs of equation (VI-3) are known and the maximum torque will lead to either a maximum of + 1 or a minimum of - 1 for the sine function in this equation, depending on whether $\partial F/\partial \theta$ is positive or negative respectively. The plots of integers (as torque maxima if $\frac{\partial F}{\partial \theta} > 0$, and minima if $\frac{\partial F}{\partial \theta} < 0$) versus $1/H$ values intersect the integer axis in Figure IV-14 approximately at values of $n' + 3/8$, where n' is an integer. For $\theta = 80°$ and $85°$ the point of intersection is somewhat lower, but these lines do not give as accurate results. Since the sine function has its maxima at integers, then for corresponding values of $\frac{1}{H}$,

$$\frac{2\pi F}{H} + \delta = \frac{\pi}{2} + 2\pi N \qquad (VI-4)$$

where N is an integer. As $H \rightarrow \infty$, the integer N must be replaced by $n' + 3/8$, since N does not necessarily become a true integer. Therefore we have

$$\delta = \frac{\pi}{2} + 2\pi \ (n' + 3/8)$$

$$= \frac{10}{8}\pi + 2\pi n' \qquad\qquad (VI-5)$$

We shall pick $n' = -1$ to give the smallest absolute value of δ, which is most logical. Thus

$$\delta = -\frac{3}{4}\pi$$

$$= 2\pi\gamma \pm \frac{\pi}{4}$$

From the long period plots we know that the segment of the Fermi surface responsible for these periods must be long and slender. There will be very little change in energy along the segment, but an approximately parabolic dispersion relation will probably exist perpendicular to its length. Hence we expect that $\gamma \simeq 1/2$ as for free electrons, since the carrier density is quite low and electron-electron interactions are not expected to alter γ[27]. This may not be true for orbits of higher area, such as those near the bisectrix and binary axes. Then in equation (VI-1), we see that the proper choice of the factor $\pm \frac{\pi}{4}$ is $+ \frac{\pi}{4}$, which occurs for a minimum extremal area of the Fermi surface. This substantiates the claim that the long periods are connecting links between larger sections of the Fermi surface.

It is possible that γ differs from the value $1/2$ by an integer, since this would still satisfy equation (VI-5) if n' were changed. We have chosen to disregard this circumstance

in view of the otherwise excellent agreement between theory and experiment. The effects of spin splitting are also neglected. In bismuth this cannot be done, and the splitting due to spin is equal to the Landau level spacing for some orientations, resulting in a phase shift of $p\pi$ for the pth harmonic[70]. There is good reason to neglect spin splitting in arsenic since it is the lightest element of the three semi-metals Bi, Sb and As. It would be very interesting to observe the long periods in arsenic in pure crystals at very low temperatures. This would allow an analysis of the harmonics and cast light on the amount of spin splitting of carriers.

COMPARISON OF EXPERIMENTAL AND THEORETICAL FERMI SURFACE

A comparison of our results with the Fermi surface model of Lin and Falicov[42] allows us to assign the β carriers to the electron pockets and the α carriers to the pockets of the hole crown. With this assignment, there is reasonable agreement between the theoretical and experimental values of the tilt angles of the minimum areas in the trigonal-bisectrix plane. The measured angle of $86^\circ \pm 1^\circ$ for the β carrier compares well with the theoretical value of $+ 80^\circ$ since quite small changes in pseudopotential parameters can change this angle appreciably. The α carrier has a predicted tilt angle of $+ 44^\circ$ and our value is $+ 38^\circ \pm 1^\circ$. Tilt angles of the cylindrical sections of the hole surface are measured to be

$- 10^{\circ} \pm 1^{\circ}$ from our experiments and theory predicts a value of -11°.

Cross-sectional areas of the Fermi surface can also be compared. The electron Fermi surface was fitted so that the minimum area in the trigonal-bisectrix plane agreed with experiment. Our measurements of torque unfortunately give little of the electron surface, but Shapira and Williamson[38] and Priestley et al[40] give values which are in reasonable agreement with theory for areas normal to the trigonal and normal to the binary. A projected ellipsoidal fit to the data in Figures IV-9 and IV-16 indicates that the predictions are reasonable. For the α carrier there is not such satisfactory agreement between theory and experiment. The cross-sectional area of the cylinders has been chosen to agree with the experimental values. The only area which Lin and Falicov give is the area of one of the α pockets normal to the binary. In atomic units it has an area of 9.6×10^{-3}, which would cause a dHvA period of 2.7×10^{-7} G^{-1}. Figure IV-11 shows a period near the binary axis of about this value, but Priestley et al[40] have shown that this period is caused by a skew orbit between the α pockets and the joining cylinders which is not in the mirror plane perpendicular to the binary axis. For this orbit to exist the cylinders must join the α pockets not as shown pictorially in Figure III-8, but they must join the pockets closer to the points H. Equivalently, it may be argued that each α pocket has a protrusion which

sticks in between the two cylinders which join it. Hence the area normal to the binary may be expected to have a period considerably lower than 2.7×10^{-7} G^{-1}. Our period of 0.97×10^{-7} G^{-1} near the binary axis could be due to the orbit which goes around the α pocket and is in the mirror plane perpendicular to the binary axis. This is called the δ-orbit in our cyclotron resonance[57] paper and it has an effective mass of 0.50 m_o, which is somewhat higher than the largest mass of the electron Fermi surface of 0.42 m_o. The corresponding period of the electron surface is approximately 1.3×10^{-7} G^{-1}. Since the low cyclotron mass determinations of electrons and holes are so close in the binary-bisectrix plane, it is not unreasonable to expect that the α pocket will have a period near 1.3×10^{-7} G^{-1}, since its effective mass is slightly higher. It is even possible that our measured period of 0.97×10^{-7} G^{-1} is the second harmonic of a period near 2×10^{-7} G^{-1}. This would be somewhat closer to the period of 2.7×10^{-7} G^{-1} predicted at the binary axis. The theoretical results may show some deficiency here but in any event the orbit about the α pocket in the mirror plane does exist, as it must for the symmetry of the proposed Fermi surface.

Table III-1 gives a comparison of a number of features of the theoretical and experimental Fermi surface. The gross elements are in good agreement, but some details may not agree so well because spin-orbit corrections have not been carried out in the latest determination.

SYMMETRY OF THE FERMI SURFACE

The period plots of Chapter IV can be analyzed to give the multiplicities of the Fermi surface pockets and possible locations in the Brillouin zone. Figure IV-9 shows that the α carrier has three or six pockets because only two branches appear. The multiplicity of the non-principal branch will be twice that of the principal branch. There are three α carrier branches in Figure IV-10 in accord with a three or six pocket assignment. β-carrier branches in Figures IV-9, IV-10 and IV-16 are consistent with either three or six pockets. Only one branch is seen in Figure IV-9, but since it is not symmetrical about the trigonal axis, we expect another branch. In the binary-bisectrix plane Figure IV-11, we see there are three branches and hence there must be a minimum of two branches in the trigonal-bisectrix plane. It is not possible to distinguish between three or six pockets except by considering other determining factors such as carrier compensation or the joining of pockets by cylinders.

The long periods can be similarly considered. There are two branches in Figure IV-9, and three branches in Figure IV-10, which again points to the existence of three or six segments. These carriers are known to be connecting links between other sections of the Fermi surface, both from the period plots and the $+\frac{\pi}{4}$ phase factor, as mentioned earlier. The choice as to whether the α or β carriers are connected,

or both, is made from the study of the period plots. The
α carrier is reasonably well observed in the trigonal-bisectrix
and trigonal-binary planes, but hardly at all in the binary-
bisectrix plane. The β carrier is observed over a long an-
gular range in the bisectrix-binary plane but not in the
other two planes. Shapira and Williamson[38] measure one
branch of the β carrier over 180° in the trigonal-bisectrix
and trigonal-binary planes, and thus it is safe to conclude
that β carriers exist in closed pockets. Priestley et al[40]
have recently shown by their modulation techniques that the
α oscillations display very rapid changes in amplitude with
angle which they interpret as a cut-off of the orbit by the long
cylinders. Thus good evidence exists that the α carrier poc-
kets are joined by thin cylindrical sections.

It can be rigorously argued[40] that of the choices
that the cylinders join α pockets in groups of two, three or
six, only the latter choice is compatible with the data for
the following reasons. Groups of two require three such groups
and each group must possess inversion symmetry since there
is no observed tilt in the binary-bisectrix plane. This re-
stricts the centres to Γ, T, L and X points, of which only
L and X would give the required number of pockets. The α
pockets and cylindrical necks must then lie on the mirror plane.
This is contrary to the data obtained for the skew orbit of
Priestley et al .

To satisfy crystal symmetry, groups of three would require inverted pairs above and below the Γ or T point of the Brillouin zone. This would mean that the necks would have to be perpendicular to ΓT, which is not in accord with an observed tilt angle of -10°. Thus the only possible choice is that six cylinders join all six α pockets together in a single surface. This surface must have the full crystal symmetry and can only exist about the Γ or T point of the Brillouin zone. The six cylindrical necks must lie on binary axes or in mirror planes, and the latter choice is impossible for then there would have to be twelve α pockets. Thus the necks are centred on binary axes and the α pockets must lie in the mirror planes, producing a multiply connected toroidal shape.

To decide the number of β pockets we must ascertain the volumes of the α and β pockets and use the well established fact that that arsenic is a semi-metal with equal numbers of holes and electrons. If we assume an ellipsoidal approximation, it can easily be shown that the number of carriers per ellipsoid is given by

$$n = \frac{8}{3} \left[\frac{e^3}{\pi h^3 c^3 \, P_1 P_2 P_3} \right]^{1/2} \qquad \text{(VI-6)}$$

where P_1, P_2 and P_3 are the three principal periods of the ellipsoid. In Figure IV-9 one principal period of $4.70 \times 10^{-7} \, G^{-1}$

is readily available for the β-carrier. An ellipsoidal fit
to the data in Figures IV-9, IV-10 and IV-16 gives the three
principal periods as

$$
\left.
\begin{array}{l}
P_1 = 1.40 \\
P_2 = 4.70 \\
P_3 = 1.35
\end{array}
\right\} \times 10^{-7} \ G^{-1}
$$

from which the carrier density is estimated to be $n = 6.0 \times 10^{19}$
carriers cm^{-3} per ellipsoid. The α carrier is known to be
quite non-ellipsoidal, but an attempt to calculate the volume
of the pockets must be made. In Figure IV-9 there is one
principal period of $6.75 \times 10^{-7} \ G^{-1}$. At $\theta = -30^{\circ}$ we see
that the principal α carrier branch seems to pass a point of
inflection and curves upward, disappearing against the huge
background signals of the non-principal α branch and the
weaker β carrier branch (or branches) at $\theta = -35^{\circ}$. Thus it
is reasonable to assume that the minimum period would be near
$2 \times 10^{-7} \ G^{-1}$ at about $\theta = -55^{\circ}$. The third principal period
occurs at the binary axis, where we measure a period of
$0.97 \times 10^{-7} \ G^{-1}$ or possibly twice this value. If we adopt
values

$$
\begin{array}{l}
P_1 = 0.97 \times 10^{-7} \ G^{-1} \\
P_2 \cong 2 \times 10^{-7} \ G^{-1} \\
P_3 = 6.75 \times 10^{-7} \ G^{-1}
\end{array}
$$

we have $n \simeq 4.8 \times 10^{19}$ carriers cm^{-3} per ellipsoid.

If we adopt values

$$P_1 = 2.0 \times 10^{-7} \; G^{-1}$$
$$P_2 \simeq 2 \times 10^{-7} \; G^{-1}$$
$$P_3 = 6.75 \times 10^{-7} \; G^{-1}$$

we have $n \simeq 3.4 \times 10^{19}$ carriers cm^{-3} per ellipsoid. The cylinders are known to have a small volume indeed even though they are fairly long, since their cross-sectional area is two orders of magnitude lower than either the α or β carrier pockets. Therefore, the ratio of carriers in the β and α pockets should be an integer such as 1:1 2:1 or 4:1. Of these, the only reasonable one is 2:1, using the second choice of principal periods.

We conclude that since there must be six α pockets as discussed earlier, there are three β pockets, each of twice the volume of an α pocket. Thus the β-pockets can only be situated at X or L points of the Brillouin zone. As a consequence of this carrier compensation we can say with some degree of certainty that the orbit in the plane about an α pocket has a period near $2 \times 10^{-7} \; G^{-1}$. Since the pockets are quite non-ellipsoidal we must allow that this designation may be in error.

NONLINEAR EFFECTS

The nonlinear effects discussed in Chapter IV result from the angular compliance of the torque magnetometer and the oscillatory nature of the torque as a function of both the magnetic field strength and its direction. Mounts of any nature will allow some finite rotation of the specimen and all dHvA properties such as the torque magnetization and magnetothermal effect will have nonlinearities. This is true because the free energy(equation II-17) depends on the angle between a crystal axis and the magnetic field. If this angle has oscillatory variations, then all properties depending on the quantization of electrons in momentum space by the magnetic field will be affected in an identical way.

In order to obtain an estimate of the rigidity of a crystal mount, let us make some simple calculations for small beams made of nylon. This material is often used in low temperature experiments. The bending of a beam with an applied torque T is such that the curvature is given by[71]

$$\frac{d^2y}{dx^2} = \frac{T}{EI} \qquad (VI-7)$$

where E is Young's modulus for the material. I is the moment of inertia of the beam, given by

$$I = \int_A y^2 \, dA \qquad (VI-8)$$

where the area integration occurs over the cross-sectional area of the beam. For a square beam of sides W, $I = W^4/12$. A cantilever beam has one end clamped and equation (VI-7) is integrated to give the total change in slope of the beam.

$$\frac{dy}{dx} = \frac{T\ell}{EI} \qquad\qquad (VI-9)$$

where ℓ is the length of the beam. Hence since the angle through which the beam turns is $(dy/dx)_{x=\ell}$, the compliance is

$$\eta = \frac{\partial \Theta}{\partial T} = \frac{\ell}{EI} \quad . \qquad\qquad (VI-10)$$

For a nylon beam of dimensions 3 x 0.3 x 0.3 cm. we find $\eta \cong 2 \times 10^{-7}$ radian/dyne-cm. This is close to the value for which $\Gamma = 1$ in equation (IV-55), and is not an unrealistic calculation. Therefore great care must be taken in the design of experiments with large crystals, if harmonic analysis is attempted.

We believe that various torque experiments[72] in the past have been subject to nonlinearities of the type discussed in Chapter IV. Any experiment in which the nonlinear effects were ascribed to magnetic interaction should be carefully reconsidered if a crystal mount has a low compliance. In the case of pulsed high-field dHvA experiments, even small samples could exhibit the effects if the inertia of the sample is insufficient to prevent it from oscillating in position as the field is varied.

SUMMARY OF THE WORK ON ARSENIC

The first measurements of the torque dHvA effect in arsenic were reported by Berlincourt in 1955[32]. He found two sets of periods. The short period oscillations fitted into a three or six ellipsoid scheme and the long period oscillations were interpreted as a single ellipsoid of revolution. This interpretation was not complete because there was no semi-metallic carrier compensation, there were long period beats (not possible for a single ellipsoid) and the amplitude of the long period oscillations was a factor of 30 greater than expected.

The first band structure calculations of arsenic were pioneered by Cohen, Falicov and Golin[34]. They studied the energy band structure of the Group V semi-metals using pseudopotential methods and indicated that holes probably occur near T in the Brillouin zone and electrons may occur at either L or X points. Later studies more specifically for arsenic by Falicov and Golin[30] did not change the above conclusions and a correct model of the Fermi surface still was not obtained.

Shapira and Williamson[75][38] observed a new segment of the Fermi surface and it could be described by three or six equivalent ellipsoids each with a carrier density of 5.9×10^{19} cm^{-3}. There was a departure of the Berlincourt carriers from an ellipsoidal fit and the semi-metallic character of arsenic could now be explained. Ketterson and

Eckstein [76] [77] also observed the new carrier and suggested
that the Fermi surface of arsenic might be similar to that
of antimony. The Berlincourt or α carriers with 36° tilt
angle would then consist of six ellipsoids and the new
carriers, called β carriers, would represent 3 ellipsoids
with a tilt angle of 86°. The long periods are observed not
to originate from a single ellipsoid because of an observed
tilt angle, but insufficient data existed for a better
interpretation. Our own measurements [78] of cyclotron
resonance and the torque dHvA effect at first were consistent
with Berlincourt's data, but two discrepancies were soon
found. The new segment of the Fermi surface was observed
and the long period plots had several branches, excluding
the possibility of a single ellipsoid.

A proper understanding of the Fermi surface of arsenic
came from the recent band structure calculations of Lin and
Falicov [42]. A quasi-quantitative pseudopotential for
arsenic was constructed from the known potentials of Ge and
GaAs and the Fermi energies were altered slightly to fit
several dHvA extremal areas. The proposed model of the
Fermi surface consisted of a single multiply-connected hole
surface about T and 3 electron pockets at L. Previous
experimental data were not complete enough to establish the
model. Two experiments concurrent with Lin and Falicov's
work which helped to confirm the model were part of the
work of this thesis and the experiments of Priestley et al [79].

The latter were first to report a determination of the entire Fermi surface based on the theory of Lin and Falicov. They showed that the Berlincourt or α carriers deviated from an ellipsoidal model and indicated that the long period oscillations were due to cylinders joining the α carrier pockets. Our results[41] also support the Lin and Falicov model and give detailed information on the connecting cylinders of the hole surface. The data were seen by Falicov before his calculations were done and we believe they were of considerable help. The interpretation of our results according to the Lin and Falicov model was completely independent of the work of Priestley et al except for the interpretation of a period 2.9×10^{-7} G^{-1} near the binary axis. Both the results of Priestley et al[40] and our own results[25] have appeared in final form.

Other related experiments on aresnic have been reported. Specific heat measurements by Culbert[74] were used by Priestley et al[40] to show that their results gave the entire Fermi surface. Ih and Langenberg[80] have measured cyclotron masses in 3 major crystal planes and their results agree with our measurements[78] in the binary-bisectrix plane. A detailed comparison of their results with the Lin and Falicov model is not yet available. Magnetoresistance of arsenic has been studied by Baker and Grassie[65] and Sybert, Mackey and Miller[63]. The former find the amplitude of the Shubnikov-de Haas effect

is far less than theoretically expected, and do not observe
the long periods. An anomalous $H^{1.8}$ behaviour of the
steady transverse magnetoresistance also occurs. The latter
find only the short periods and little information is
available. Measurements of magnetoresistance given in this
thesis are more in accord with theory of the Shubnikov-
de Haas effect, but the long period oscillations are
anomalously not observed. In our latest cyclotron resonance
measurements[57] we have observed the entire electron
Fermi surface in the binary-bisectrix plane, as well as
a hole orbit which must of necessity exist if the Lin and
Falicov model is correct. Holes masses from other orbits
are expected to be degenerate with low electron masses.
There is a discrepancy of a factor of two between
experimental and theoretical cyclotron masses as well as
the electron Fermi energy from the bottom of the L_4 band.
Several neglected factors in the pseudopotential calculations
could explain this discrepancy. The torque dHvA effect of
doped arsenic has been studied by Tanuma et al[67]. Their
results for the carrier signs in arsenic were inconclusive
but recently they have reported[69] agreement with the Lin
and Falicov assignment. Our magnetothermal measurements
in arsenic[81] are in agreement with earlier dHvA work and
no new additional Fermi surface information is provided
by the experiments. The spin splitting zeros mentioned in
our abstract[81] are probably incorrect. Observed zeros of

amplitude may have their origin in a magnetic interaction
effect whereby oscillations from various parts of the sample
interfere destructively.   A final proof that the long
period oscillations result from necks is provided in this
thesis from an analysis of the phase of these oscillations,
indicating they arise from a minimum extremal area of the
Fermi surface.

CHAPTER VII

CONCLUSION

A torque magnetometer was employed to study the de Haas van-Alphen effect in arsenic. The modulation technique has been successfully applied to the torque method. Formulas were developed for the response as the modulation angle was varied and it was shown that a dominant signal can be eliminated by a proper choice of modulation angle allowing observation of weaker signals. A second signal can be eliminated by the choice of modulation depth, but this usually requires a value of modulation that is too high to apply to the torque magnetometer.

Compliance of the magnetometer was measured and it was shown that quantitative agreement occurred for a theory of nonlinear effects due to the compliance of the crystal mount. The equation describing the nonlinearity is formally identical to the equation describing the magnetic interaction. Both effects are compared and it is concluded that in many experimental systems the torque nonlinearity may be the dominant effect, especially in the case of torque magnetometers.

Magnetothermal experiments were performed and de Haas-van Alphen type oscillations were observed. The amplitude of short period oscillations was found to be about 10^{-3} $^{\circ}K$

at 20 kilogauss and this is in general agreement with a simple theory of the magnetothermal effect. Experimental difficulties were encountered and the oscillations were not as good as given by the torque experiments, but improvements can probably be made in experimental techniques. An effect at low magnetic fields was explained in terms of heating caused by induced eddy currents as the field was swept.

Magnetoresistance experiments were performed which displayed Shubnikov-de Haas oscillations of the magneto-resistance . The amplitude of the short period oscillations were in reasonable agreement with theory, contrary to measurements made by other researchers. Long period oscillations were not observed. A possible explanation is that the carriers responsible for these periods are in the quantum limit for H > 17.5 kilogauss. The experiments show that arsenic is a semimetal and the steady transverse magnetoresistance is shown to have an anomalous $H^{1.8}$ behaviour.

Period plots for the dHvA oscillations predict two major segments to the Fermi surface, one presumably of holes, the other electrons. The long periods are shown to be connecting cylinders between segments of the Fermi surface. Theoretical band structure calculations of Lin and Falicov, in part influenced by our experiments and those of others, are shown to give good agreement with experiment. Some quantitative details such as cyclotron masses show discrepancies

which could be caused by a neglect of spin-orbit corrections or perhaps indicate limitations of the pseudopotential band structure calculations themselves. In any event, the gross details of the band structure are without any doubt correct. The electron Fermi surface consists of three almost ellipsoidal pockets at the L points of the Brillouin zone. The hole Fermi surface consists of a crown of six pockets joined by six slender cylindrical sections. This surface is multiply connected and is situated about the T point of the Brillouin zone. The carrier density of either holes or electrons is estimated to be ~ 18×10^{19} cm^{-3}.

Berlincourt measures the amplitude of the long period oscillations to be a factor of 30 greater than expected. This is in accord with the interpretation of these oscillations as caused by long slender sections with a low curvature. (c.f. equation II-17).

BIBLIOGRAPHY

(1)   W.J. de Haas and P. M. van Alphen, Leiden Comm.
      No. 212A (1930)

(2)   L. D. Landau, Zeit. F. Phys. $\underline{64}$, 629 (1930)

(3)   R. Peierls, Zeit. F. Physick $\underline{81}$, 186 (1933)

(4)   M. Blackman, Proc. Roy. Soc. (London) $\underline{A166}$, 1 (1938)

(5)   L. D. Landau, appendix of D. Shoenberg, Proc. Roy.
      Soc. (London) $\underline{A170}$, 341 (1939)

(6)   D. Shoenberg, Phil. Trans. Roy. Soc. (London) $\underline{A245}$,
      1 (1952)

(7)   L. Onsager, Phil. Mag. $\underline{43}$, 1006 (1952).

(8)   I. M. Lifshitz, (see Soviet Physics USPEKHI $\underline{2}$, 831 (1960)

(9)   R. B. Dingle, Proc. Roy. Soc. $\underline{A211}$, 517 (1952)

(10) I. M. Lifshitz and A. M. Kosevich, Zh. Ekserm. i. Theor.
      Fiz. $\underline{29}$, 730 (1955); [English Trans: Soviet Physics
      - J.E.T.P. $\underline{2}$, 636 (1956)].

(11) M.H.Cohen and E. I. Blount, Phil. Mag. $\underline{5}$, 115 (1960)

(12) D. Shoenberg, Phil. Trans. Roy. Soc. (London) $\underline{A255}$,
      85 (1962)

(13) C. Kittel, Phys. Rev. Letters, $\underline{10}$, 339 (1963)

(14) A. B. Pippard, Proc. Roy. Soc. (London) $\underline{A272}$, 192 (1963)

(15) R. D. Plummer and W. L. Gordon, Phys. Rev. Let. $\underline{13}$, 432
      (1964)

(16) M. G. Priestley et al, Phys. Rev. 131, 617 (1963)

(17) E. I. Blount, Phys. Rev. 126, 1636 (1961)

(18) S. J. Williamson, S. Foner and R. A. Smith, Phys.
       Rev. 136, 1065 (1964)

(19) D. Shoenberg, Physica 19, 791 (1953)

(20) D. Shoenberg and P. J. Stiles, Physics Letters 4,
       274 (1963); Proc. Royal Soc. A281, 62 (1964).

(21) A. Goldstein, S. J. Williamson and S. Foner, Rev.
       Sci. Inst. 36, 1356 (1965)

(22) J. E. Kunzler, F. S. L. Hsu and W. S.Boyle, Phys. Rev.
       128, 1084 (1962)

(23) Y. Shapira and B. Lax, Phys. Rev. 138, A1191 (1965),
       and references quoted there.

(24) E. N. Adams and T. D. Holstein, Phys. Chem. Solids,
       10, 254 (1959)

(25) J. Vanderkooy and W. R. Datars, Phys. Rev. (to be
       published)

(26) e.g. C. Kittel, Quantum Theory of Solids (Wiley, 1963)
       p. 226

(27) J. M. Luttinger, Phys. Rev. 119, 1153 (1960)
                                 121, 1251 (1961)

(28) e.g. G. E.Smith, G. A. Baraff and J. M. Rowell,
       Phys. Rev. 135, A1118 (1964)

(29) R. G. W. Wyckoff, Crystal Structures (Interscience
       Publishers, Inc.,New York 1960) Vol. I.

(30) L. M. Falicov and S. Golin, Phys. Rev. 137, A871 (1965)

(31)   C. S. Barrett et al, Acta Cryst. 16, 451 (1963)

(32)   T. G. Berlincourt, Phys. Rev. 99, 1716 (1955)

(33)   Handbook of Chemistry and Physics, (Chemical Rubber
       Publishing Co., 1963)

(34)   M. H.Cohen, L. M. Falicov and S. Golin, IBM Jour.
       Research, 8, 215 (1964)

(35)   M. H. Cohen and V. Heine, Phys. Rev. 122, 1821 (1961)

(36)   J. C. Phillips and L. Kleinman, Phys. Rev. 128, 2098.
       (1962)

(37)   D. Brust, Phys. Rev. 134, A1337 (1964).

(38)   Y. Shapira and S. J. Williamson, Phys. Letters 14,
       73 (1965)

(39)   J. B. Ketterson and Y. Eckstein, Phys. Rev. 140,
       A1355 (1965)

(40)   M. G. Priestley, L. R. Windmiller, J. B. Ketterson and
       Y. Eckstein, Phys. Rev. 154, 671 (1967)

(41)   J. Vanderkooy and W. R. Datars, Physics in Canada 22,
       #2, 32 (1966)

(42)   P. J. Lin and L. M. Falicov, Phys. Rev. 142, 441 (1966)

(43)   L. M. Falicov and P. J. Lin,Phys. Rev.141, 562 (1966)

(44)   M. H. Cohen (to be published)

(45)   D. Shoenberg in Progress in Low Temperature Physics,
       edited by C. J. Gorter (North Holland Publishing Co.,
       Amsterdam, 1957), Vol. II p. 226

(46)   J. H. Condon and J. A. Marcus, Phys. Rev. 134, A446 (1964)

(47)   R. W. Gilbert, A.I.E.E. Trans. $\underline{70}$, 1121 (1951).

       Model 1411, Weston Instrument Division, Newark,

       New Jersey.

(48)   See, for example, H. G. van Bueren, Imperfections

       in Crystals, (North Holland Pub. Co. 1961)

(49)   L. R. Windmiller, Phys. Rev. $\underline{149}$, 472 (1966)

(50)   J. B. Taylor, S. L. Bennett and R. D. Heyding,

       J. Phys. Chem. Solids $\underline{26}$, 69 (1965)

(51)   D. Shoenberg, Phil. Trans. Roy. Soc. (London) $\underline{245}$,

       1 (1952)

(52)   R. J. Higgins, J. A. Marcus and D. H. Whitemore,

       Phys. Rev. 137, A1172 (1965)

(53)   For the expansion involving the Bessel functions, see

       R. V. Churchill, Fourier Series and Boundary Value

       Problems, (McGraw-Hill, 1941)

(54)   J. Vanderkooy, J. S. Moss and W. R. Datars, (submitted

       to Jour. Sci. Instrum.)

(55)   J. Vanderkooy and W. R. Datars,(submitted to Physical

       Review)

(56)   N. B. Brandt, T. F. Dolgolenko, N. N. Stupochenko,

       Zh. Eksperim. i. Teor. Fiz. $\underline{45}$, 1319 (1963)

       [English Transl: Soviet Physics JETP $\underline{18}$, 908 (1964]

(57)   W. R. Datars and J. Vanderkooy, J. Phys. Soc. Japan,

       Vol. $\underline{21}$, Supplement 657 (1966)

(58) G. K. White, <u>Experimental Techniques in Low Temperature in Low Temperature Physics</u>,(Oxford Univ. Press 1959)

(59) J. Moss, (private communication).

(60) J. R. Clement and E. H. Quinnell, Rev. Sci. Inst. <u>23</u>, 213 (1952)

(61) H. B. Callen, <u>Thermodynamics</u>, Wiley and Sons (1960)

(62) B. D. McCombe and G. Seidel, International Conference of Low Temperature Physics, IX; Colombus, Ohio, 1964 (Low Temperature Physics - LT9 Proceedings, Plenum Press, 1965.)

(63) J. R. Sybert, H. J. Mackey and R. E. Miller, Bull. Amer. Phys. Soc. <u>11</u>, 759 (1966)

(64) D. E. Soule <u>et al</u>, Phys. Rev. <u>134</u>, A453 (1964)

(65) P. R. Baker and A. D.C. Grassie, (private communication)

(66) E. Fawcett, Adv. in Physics (Phil. Mag. Supp.) <u>13</u>, No. 50, 139 (1964)

(67) S. Tamuna, Y. Ishizawa and S. Ishiguro, J. Phys. Soc. Japan <u>21</u> , Supplement, 662 (1966)

(68) C. Kittel, <u>Quantum Theory of Solids</u>, (John Wiley, 1963) p.344

(69) S. Tanuma, private communication

(70) J. S. Dhillon and D. Shoenberg, Phil. Trans. Roy. Soc. A, <u>248</u> 1 (1955)

(71) S. H. Crandall and N. C. Dahl, <u>An Introduction to the</u> <u>Mechanics of Solids</u>, (McGraw-Hill, 1959) p.363

(72) see for example, A.S. Joseph and A. C. Thorsen, Phys. Rev. <u>138</u>, A1159 (1965).

(73) H. Jones, <u>Theory of Brillouin Zones and Electronic</u> <u>States in Crystals</u>, (North Holland Publishing Co., 1960)

(74) H. V. Culbert, Bull. Amer. Phys. Soc. <u>10</u>, 1104 (1965)

(75) Y. Shapira and S. J. Williamson, Bull. Amer. Phys. Soc. <u>9</u>, 631 (1964)

(76) J. B. Ketterson and Y. Eckstein, Bull. Amer. Phys. Soc. <u>9</u>, 632 (1964)

(77) J. B. Ketterson and Y. Eckstein, Phys. Rev. <u>140</u>, A1355 (1965)

(78) W. R. Datars and J. Vanderkooy, Bull. Amer. Phys. Soc. <u>10</u>, 110 (1965)

(79) M. G. Priestley, L. R. Windmiller, J. B. Ketterson and Y. Eckstein, Bull. Amer. Phys. Soc. <u>10</u>, 1089 (1965)

(80) C. S. Ih and D.N. Langenberg, Bull. Amer. Phys. Soc. <u>11</u> , 402 (1966)

(81) J. Vanderkooy and W. R. Datars, Bull. Amer. Phys. Soc. <u>12</u>, 286 (1967)